Tectonics®

RESEARCH ARTICLE
10.1029/2022TC007386

**Key Points:**

- We quantify the pre-drift extension in the NE Atlantic margins using crustal structure data and forward basin modeling
- We quantify the incremental crustal stretching factors and extension for each of the main rifting phases
- We restore and establish a full-fit palinspastic plate kinematic model for the NE Atlantic since the mid-Permian

**Correspondence to:**

M. M. Abdelmalak,
m.m.abdelmalak@geo.uio.no;
abdelmalak_mansour@yahoo.fr

**Citation:**

Abdelmalak, M. M., Gac, S., Faleide, J. I., Shephard, G. E., Tsikalas, F., Polteau, S., et al. (2023). Quantification and restoration of the pre-drift extension across the NE Atlantic conjugate margins during the mid-Permian-early Cenozoic multi-rifting phases. *Tectonics*, *42*, e2022TC007386. https://doi.org/10.1029/2022TC007386

Received 4 MAY 2022
Accepted 14 DEC 2022

**Author Contributions:**

**Investigation:** Sébastien Gac
**Methodology:** Sébastien Gac, Jan Inge Faleide
**Writing – review & editing:** Sébastien Gac, Jan Inge Faleide, Grace E. Shephard, Filippos Tsikalas, Stéphane Polteau, Dmitry Zastrozhnov, Trond H. Torsvik



# Quantification and Restoration of the Pre-Drift Extension Across the NE Atlantic Conjugate Margins During the Mid-Permian-Early Cenozoic Multi-Rifting Phases

**Mansour M. Abdelmalak[1,2], Sébastien Gac[1], Jan Inge Faleide[1,2], Grace E. Shephard[1], Filippos Tsikalas[1,3], Stéphane Polteau[4], Dmitry Zastrozhnov[5,6,7], and Trond H. Torsvik[1,8]**

[1]Department of Geosciences, Centre for Earth Evolution and Dynamics (CEED), University of Oslo, Oslo, Norway, [2]Research Centre for Arctic Petroleum Exploration (ARCEx), University of Tromsø, Tromsø, Norway, [3]Vår Energi ASA, Stavanger, Norway, [4]Institute for Energy Technology (IFE), Halden, Norway, [5]A.P. Karpinsky Russian Geological Research Institute (VSEGEI), Saint-Petersburg, Russian Federation, [6]Institute of Earth Sciences, Saint Petersburg State University, Saint-Petersburg, Russian Federation, [7]Volcanic Basin Energy Research (VBER), Oslo, Norway, [8]School of Geosciences, University of Witwatersrand, Johannesburg, South Africa

**Abstract** The formation of the NE Atlantic conjugate margins is the result of multiple rifting phases spanning from the Late Paleozoic and culminating in the early Eocene when breakup was accompanied with intense magmatic activity. The pre-breakup configuration of the NE Atlantic continental margins is controlled by crustal extension, magmatism, and sub-lithospheric processes, all of which need to be quantified for the pre-breakup architecture to be restored. Key parameters that need to be extracted from the analysis of crustal structures and sediment record include stretching factors, timing of rifting phases, and nature of the deep crustal structures. The aim of this study is to quantify the pre-drift extension of the NE Atlantic conjugate margins using interpreted crustal structure and forward basin modeling. We use a set of eight 2D conjugate crustal transects and corresponding stratigraphic models, constrained from an integrated analysis of 2D and 3D seismic and well data. The geometry and thickness of the present-day crust is compared to a reference thickness which has experienced limited or no crustal extension since Permian time allowing the quantification of crustal stretching. Based on the eight conjugate crustal transects, the total pre-drift extension is estimated to range between 181 and 390 km with an average of 270–295 km. These estimates are supported by the results of forward basin modeling, which predict total extension between 173 and 325 km, averaging 264 km. The cumulative pre-drift extension estimates derived from basin modeling are in turn used to calculate the incremental crustal stretching factors at each of the three main rifting phases between the conjugate Greenland-Norwegian margins. The mid-Permian early Triassic rifting phase represents 32% of the total extension, while the equivalent values are 41% for the mid-Jurassic to mid-Cretaceous and 27% for the Late Cretaceous-Paleocene rifting phases. These values are used to establish and present at first, a full-fit palinspastic plate kinematic model for the NE Atlantic since the mid-Permian and will be the base for future work on more elaborated models in order to build accurate paleogeographic and tectonic maps.

**Plain Language Summary** Restoring the effect of the multi-rifting phases is challenging because it is always difficult to quantify their contribution in the total extension. This is mainly due to the lack of extensive data coverage and trustful stratigraphic interpretation. In our contribution we use an extensive amount of seismic reflection and refraction data covering the NE Atlantic to build a set of eight conjugate crustal transects and their corresponding stratigraphic models. The observed crustal thickness is used to quantify the cumulative pre-drift extension since the mid-Permian. Forward basin modeling is used to calculate the incremental crustal stretching factors for each of the main rifting phases. The results are used to establish and present at first, a full-fit palinspastic plate kinematic model for the NE Atlantic since the mid-Permian and will be the base for future work on more elaborated models in order to build accurate paleogeographic and tectonic maps.

## 1. Introduction

Continental rifting is associated with successive extensional phases, often leading to final continental breakup and initiation of oceanic spreading. Within the context of global plate tectonics, rifting is a fundamental process starting continent dispersal (Wilson, 1966), but instead paleogeographic models or plate reconstructions generally focus on post-breakup times. The main reason is that ocean spreading typically renders well constrained key

input data in global plate kinematic models, such as oceanic magnetic anomalies and fracture zones (Domeier & Torsvik, 2014; Seton et al., 2012). On the other hand, pre-breakup deformation during the rifting of continental regions lacks obvious information to constrain the timing and structures, resulting in uncertain and often disputed pre-drift restorations of continental margins (Barnett-Moore et al., 2018; Hosseinpour et al., 2016; Neres et al., 2013; Nirrengarten et al., 2018; Torsvik and Cocks, 2016). Determining the amount and timing of crustal extension in pre-drift plate configurations is crucial for building accurate paleogeographic reconstructions and tectonic maps (e.g., Ady & Whittaker, 2019). Rifted margins around the world show significant variations in terms of crustal architecture, the extent of volcanism, and sedimentation patterns (e.g., Brune et al., 2017). Several end-member rift models have been proposed, such as magma-rich and magma-poor margins (Doré & Lundin, 2015; Geoffroy, 2005; Gernigon et al., 2004; Haupert et al., 2016; Menzies et al., 2002; Péron-Pinvidic and Manatschal, 2008; Tugend et al., 2018), wide and narrow rifts (Brun, 1999; Buck, 1991), rifts with symmetric and asymmetric crustal architectures (Lister and Kerr, 1991; Ranero and Pérez-Gussinyé, 2010), and rifts with spatially overlapping rifting domains (e.g., Gac et al., 2021).

In this study, we focus on the NE branch of the North Atlantic, between the Greenland and the Norwegian margins. The area encompasses passive margins that are variable in width, and a central deep oceanic domain transected by active and extinct mid-ocean ridges. A multitude of studies over the last decades, driven by both industry and academic interests and high-quality large data sets, have led to an unprecedented understanding of the processes governing continental breakup and the evolution of continental margins and their basins through successive stages of rifting. However, there still remains the task of integrating the vast, spatially and temporally disparate data sets into a consistent plate reconstruction model for the entire NE Atlantic realm that extends back to the earliest phases of the margin formation.

The aim of this study is to quantify the amount of stretching leading to the breakup of the NE Atlantic conjugate continental margins. Our strategy is to reconstruct the extensional evolution of the margin along a series of 2D conjugate crustal transects using the observed crustal structure and a forward basin modeling approach. The results allow us to characterize the tectonic history related to the multiple rifting phases of the NE Atlantic conjugate margins from the mid-Permian to early Eocene breakup. In addition, forward basin modeling allows us to quantify the pre-drift extension of the different rifting phases, and to evaluate the implications of different structural and stratigraphic interpretations obtained from seismo-stratigraphy. The temporal and spatial results of this study can be used to constrain plate reconstruction models with finite rotations.

## 2. Geological Setting of the NE Atlantic

The bathymetry map of the NE Atlantic (Figure 1a) shows considerable width and steepness variations of the continental shelves located between the mainland and the oceanic domains. The mid-Norwegian margin, including the Møre, Vøring, and Lofoten-Vesterålen margin (LVM) segments evolved in conjunction with the North Sea and Faroe-Shetland margin farther south. The conjugate continental margins of the NE Atlantic region have recorded a long and complex history of multiple rifting phases since the early Devonian collapse of the Caledonian orogeny at around 390–380 Ma, which have resulted in a complex mosaic of inherited basement terranes and structures (Figure 1b) (Faleide et al., 2008; Gernigon et al., 2020; Skogseid et al., 2000; Tsikalas et al., 2012). If the Caledonian orogenic collapse is considered as mainly a syn-orogenic phenomenon, then it can be assumed that rifting in response to lithospheric extension between Eurasia and Greenland was initiated at a later stage during late Paleozoic time (ca. 270–260 Ma) (e.g., Brekke et al., 2001; Skogseid et al., 2000). In this context, the main post Devonian lithospheric extension occurred in mid-Permian-Triassic (~264–250 Ma) (e.g., Skogseid et al., 2000), mid-Jurassic-Early/mid-Cretaceous (~166–140, and/or 125–110 Ma), and Late Cretaceous-Paleocene times (80–56 Ma) (Brekke et al., 2001; Gac et al., 2021; Lundin and Doré, 2005).

The location and structural expression of the late Paleozoic NE Atlantic rift system within the Caledonian orogenic domain was influenced by Caledonian, and possibly pre-Caledonian, structures (Gernigon et al., 2020; Schiffer et al., 2020). The early post-orogenic basins developed as large, intra-continental, half-graben systems, controlled by reactivated low-angle detachments onshore NE Greenland (Fossen, 2010) and offshore in the Barents Sea (e.g., Faleide et al., 2008; Fossen, 2010; Gernigon et al., 2018; Gresseth et al., 2022), the mid-Norwegian margin within the Trøndelag Platform and the Halten Terrace (Braathen et al., 2002; Breivik et al., 2011; Osmundsen et al., 2021), and in the Danmarkshavn Basin offshore NE Greenland (Voss and Jokat, 2007). The late Jurassic-early Cretaceous interval (160–140 Ma) marks a profound kinematic and paleogeographic change

10.1029/2022TC007386

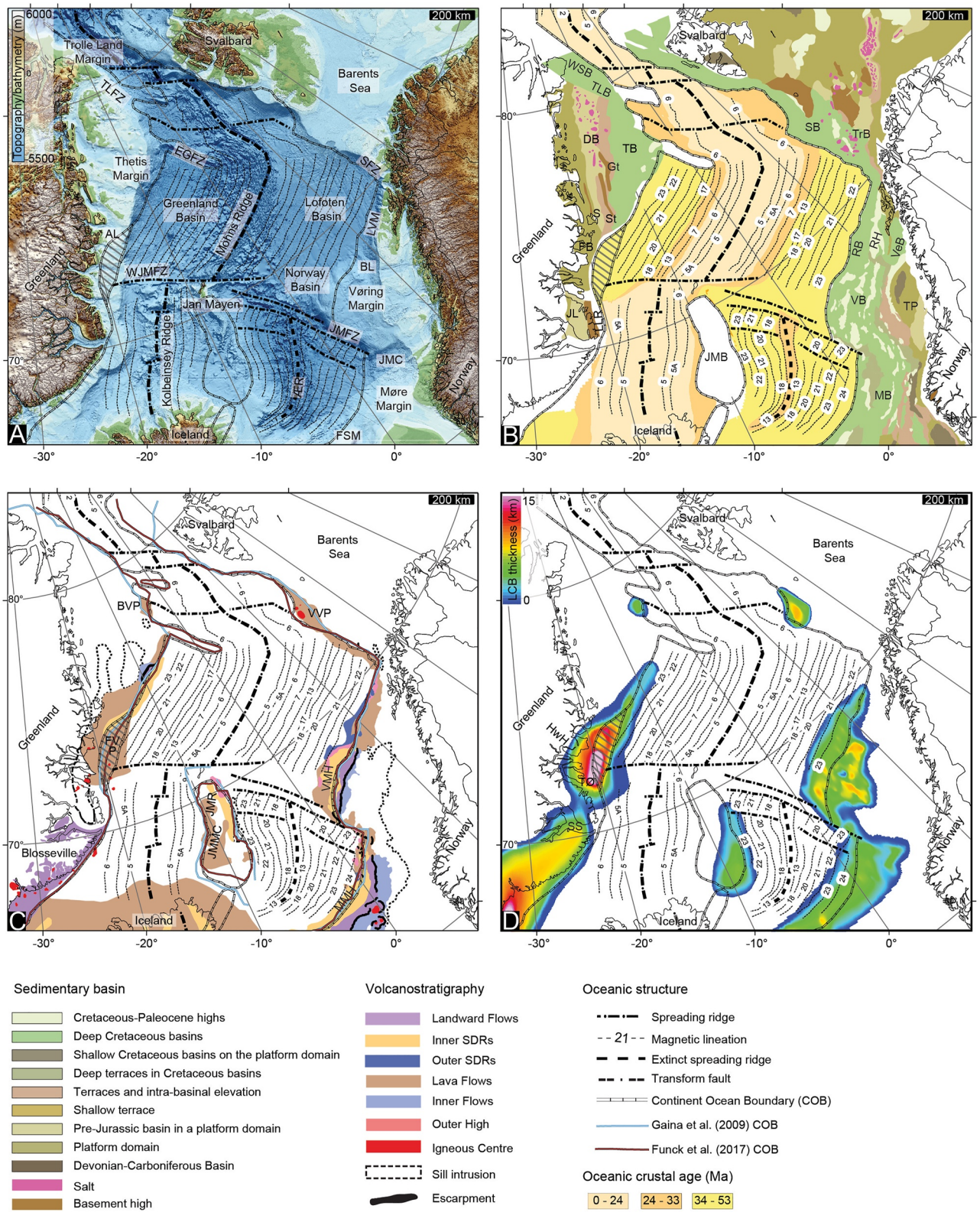


Sedimentary basin

- Cretaceous-Paleocene highs
- Deep Cretaceous basins
- Shallow Cretaceous basins on the platform domain
- Deep terraces in Cretaceous basins
- Terraces and intra-basinal elevation
- Shallow terrace
- Pre-Jurassic basin in a platform domain
- Platform domain
- Devonian-Carboniferous Basin
- Salt
- Basement high

Volcanostratigraphy

- Landward Flows
- Inner SDRs
- Outer SDRs
- Lava Flows
- Inner Flows
- Outer High
- Igneous Centre
- Sill intrusion
- Escarpment

Oceanic structure

- Spreading ridge
- 21 Magnetic lineation
- Extinct spreading ridge
- Transform fault
- Continent Ocean Boundary (COB)
- Gaina et al. (2009) COB
- Funck et al. (2017) COB

Oceanic crustal age (Ma)

0 - 24 | 24 - 33 | 34 - 53

**Figure 1.**

throughout the entire NE Atlantic region (Lundin and Doré, 2011; Nirrengarten et al., 2018) with extensional directions switching from E-W to WNW-ESE (Gernigon et al., 2020). During this period, deep sedimentary basins formed in the NE Atlantic as a result of the mid-Jurassic-early Cretaceous extensional episode. Subsidence was especially important during the Cretaceous, allowing the accumulation of up to 8 km of sediments in local depocentres in the Vøring and Møre basins (Blystad et al., 1995; Brekke, 2000; Scheck-Wenderoth et al., 2007; Zastrozhnov et al., 2020) and up to 10 km in the Thetis Basin offshore NE Greenland (Fyhn and Hopper, 2021; Hamann et al., 2005; Tsikalas, Faleide, Eldholm, & Wilson, 2005). Ongoing extension prevailed and possibly migrated to the northern Vøring Basin (Zastrozhnov et al., 2018) and LVM during the mid-late Albian-? to Turonian (Meza-Cala et al., 2021; Tsikalas et al., 2022). Early Cretaceous and mid-Albian deformation were also reported in NE Greenland (Hamann et al., 2005; Tsikalas, Eldholm, & Faleide, 2005). During the Late Cretaceous-Paleocene (80–65 Ma), a renewed phase of widespread rifting predominantly affected the distal parts of the Norway-Greenland rift system. The locus of extension migrated oceanward toward the zone of the future continental separation (Skogseid et al., 2000). This rift episode formed a zone wider than 300 km associated with lithospheric thinning (Skogseid, 1994). In the Møre, Vøring and LVM segments, the late Campanian-Paleocene rifting phase is relatively well constrained by boreholes and seismic data (Doré et al., 1999; Gernigon et al., 2003; Ren et al., 2003; Tsikalas et al., 2001), resulting in a period of simultaneous extension on both, east and west, sides of Greenland (Hosseinpour et al., 2013; Skogseid et al., 2000).

Final continental breakup in the NE Atlantic occurred at the early Eocene (~56–55 Ma) and was associated with a 2–3 Myr period of massive extrusive and intrusive volcanic activity (Eldholm & Grue, 1994) within the adjacent sedimentary basins and pre-existing continental crust along the more than 2,600 km long new plate boundary (Figures 1c and 1d) forming the North Atlantic Igneous Province (Abdelmalak, Meyer, et al., 2016; Breivik et al., 2014; Eldhom & Coffin, 2000; Planke et al., 2005). The post-breakup evolution of the NE Atlantic was dominated by thermal cooling and regional subsidence (Brekke, 2000; Faleide et al., 2008). However episodic Cenozoic compressional episodes induced by ridge-push, spreading reorganization, far-field orogenic stress (Gac et al., 2016; Lundin and Doré, 2002), mantle drag (Mosar et al., 2002) and/or gravitational and horizontal stresses from the Iceland insular margin (Doré et al., 2008) are thought to have contributed to the formation of inversion structures (domes/arches, reverse faults, etc.). The recent development of the NE Atlantic is closely linked to the Northern Hemisphere glaciation events, when large Plio-Pleistocene clinothems prograded across the continental margin (Eidvin et al., 2007; Løseth et al., 2017; Ottesen et al., 2005; Rise et al., 2005).

## 3. Data and Methods

### 3.1. Data

In this contribution, we had access to a dense grid of 2D seismic reflection data covering the entire Norwegian margin segments; from the northern North Sea to the Barents Sea, through Møre, Vøring and Lofoten-Vesterålen margins and with line-spacing ranging from 0.2 to 2 km (Figure 2). In detail, the seismic reflection database at our disposal comprises new (MNR-11 seismic survey acquired in 2011 by TGS and Fugro) and reprocessed (e.g., the series of CFI-MNR04 to CFI-MNR11 surveys obtaining in consecutive years, late reprocessing of the original MNR surveys) high-quality seismic reflection data. Our database also comprises previous long-offset seismic surveys including the VMT-95, VBT-94, and GMNR-94 surveys, which were recorded to 11–14 s (two-way travel time). All seismic data have been interpreted alongside released and revised biostratigraphy (e.g., Zastrozhnov et al., 2018, 2020). The seismic line spacing was tight enough to laterally correlate the different seismic horizons

**Figure 1.** (a) Topographic and bathymetric map of the NE Atlantic (IBCAO bathymetry; Jakobsson et al., 2020) showing the main physiographic features of the area; (b) simplified map of the NE Atlantic showing the main sedimentary and structural elements; (c) volcanic seismic facies units indicating the extent of the extrusive breakup volcanism and the sill intrusions and; (d) the Lower Crustal Body thickness map distribution in the NE Atlantic compiled from available seismic refraction data (see Figure 2). All panels show oceanic features such as mid-ocean ridges, magnetic anomalies and respective chrons. The nature of the crust below the Foster Volcanic Province (hatched area) is debated and is interpreted as transitional crust situated between an interpreted landward and oceanward COBs. The continent-ocean boundary (COB) of Funck, Geissler, et al. (2017) and Gaina et al. (2009) are indicated in map C. A: Andøya; AL: Ardencaple Lineament; BL: Bivrost Lineament; BVP: Boreas Volcanic Province; DB: Danmarkshavn Basin; EGFZ: East Greenland Fracture Zone; FB: Foster Basin; FMS: Faroe-Shetland Margin; FVP: Foster Volcanic Province; Gt: Germania Terrace; HwH: Hold with Hope; JL: Jamson Land; JMB: Jan Mayen Basin; JMC: Jan Mayen Corridor; JMFZ: Jan Mayen Fracture Zone; JMMC: Jan Mayen Micro-Continent; JMR: Jan Mayen Ridge; LLR: Liverpool Land Ridge; LVM: Lofoten-Vesterålen Margin; MB: Møre Basin; RB: MMH: Møre Marginal High; Røst Basin; RH: Røst High; S: Shannon; SB: Sørvestsnaget Basin; SFZ: Senja Fracture Zone; SS: Scoresby Sound; St: Shannon Terrace; TB: Thetis Basin; TLB: Trolle Land Basin; TLFZ: Trolle Land Fracture Zone; TP: Trøndelag Platform; TrB: Tromsø Basin; TØ: Traill Ø; VB: Vøring Basin; VeB: Vestfjorden Basin; VMH: Vøring Marginal High; VVP: Vestbakken Volcanic Province; WJMFZ: West Jan Mayen Fracture Zone; WSB: Wandel Sea Basin.

10.1029/2022TC007386



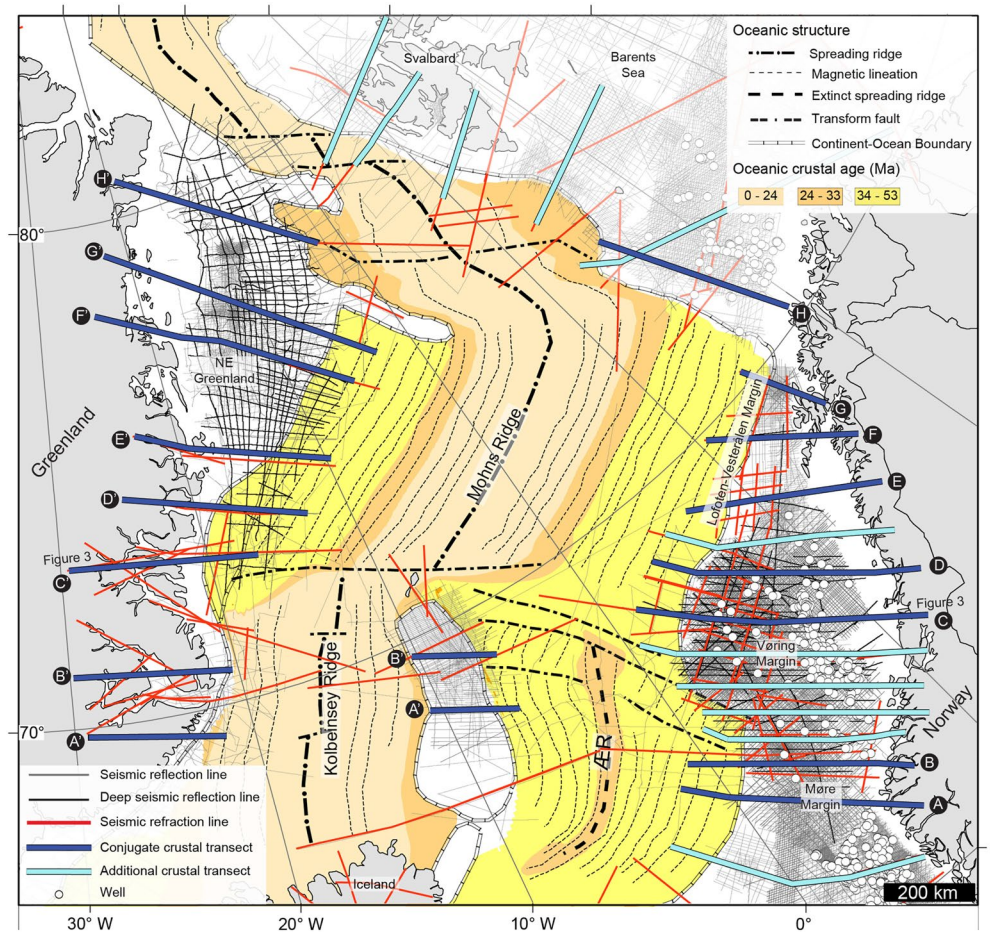


**Figure 2.** Database for the NE Atlantic area. Each crustal transect are generated from refraction and deep seismic reflection (for the crustal configuration) and reflection lines combined with well data (for the stratigraphic model). The eight sets of different conjugate crustal transects (dark blue lines) used in this study are indicated in the map. Additional crustal transects (light blue lines) were built to supplement understanding but are not discussed in detail in this paper.

and generate grids. We selected representative seismic lines in the mid-Norwegian margin that were subsequently depth-converted using a composite high-quality seismic velocity cube covering the entire mid-Norwegian Margin (e.g., Abdelmalak et al., 2017) (Table 1). The velocity cube has been compiled from 536 seismic stacking velocity data sets and 230 check shots from wells and vertical seismic profile data resulting in precise depth conversion within the sedimentary basin.

For NE Greenland, we used available published depth-migrated seismic reflection data (Dinkelman et al., 2010; Granath et al., 2011; Hamann et al., 2005; Helwig et al., 2012; Jackson et al., 2013) combined with our in-house unpublished seismic interpretation and the new tectono-sedimentary elements in the area (Fyhn and Hopper, 2021; Fyhn et al., 2021) (Table 1). For the deeper crustal part of the margins, we compiled the available 2D refraction data on the NE Atlantic area from the Møre, Vøring, and LVMs (e.g., Breivik et al., 2009; 2014; Mjelde et al., 1996, 2005, 2007; Mjelde, Raum, et al., 2009; Raum et al., 2002, 2006), the West Barents Sea (Breivik et al., 2005; Clark et al., 2013; Czuba et al., 2005; Libak et al., 2012; Ritzmann et al., 2004), refraction profiles from the NE Greenland margin (e.g., Hermann, 2013; Schlindwein and Jokat, 1999; Schmidt-Aursch and Jokat, 2005; Voss and Jokat, 2007; Voss et al., 2009; Weigel et al., 1995), and Jan Mayen (e.g., Breivik et al., 2012) (Figure 2).

The diverse data density, resolution, and availability make the selection and construction of the conjugate crustal transects challenging. For example, the type and coverage of data on the NE Greenland margin is limited. However, the Møre and Vøring margin segments of the mid-Norwegian margin are well studied by geophysical methods courtesy of the extensive amount of both seismic reflection and refraction data available. These seismic

**Table 1**
*Data Used in the Buildup of the Crustal Transects and Stratigraphic Models*

| Crustal transect | Seismic reflection lines | Seismic refraction data | Stratigraphic horizons and crustal compilation | Gravity inversion data | References and comments |
|---|---|---|---|---|---|
| Profile A | GMNR-94-102; GMNR-94-102R | None | In-house data | None | Stratigraphy modified from Zastrozhnov et al. (2020) and Gernigon et al. (2021), Moho and LCB from Abdelmalak et al. (2017) |
| Profile A' (Jan Mayen) | IS-JMR-01-0060 | None | In-house and published data | Published data | Stratigraphy modified from Blischke et al. (2017) and Polteau et al. (2019), crustal boundaries from Peron-Pinvidic et al. (2012b), LCB from Abdelmalak et al. (2017) |
| Profile A' (Greenland) | None | None | Published data | Published data | Crustal boundaries from Funck, Geissler, et al. (2017), Haase et al. (2017), and Lebedeva-Ivanova et al. (2019), LCB from Abdelmalak et al. (2017) |
| Profile B | MNR11-90277 | Profiles 1-99 and 1-00 | In-house and published data | Published data | Stratigraphy modified from Theissen-Krah et al. (2017), Zastrozhnov et al. (2020) and Gernigon et al. (2021), crustal boundaries from Breivik et al. (2006) and Mjelde, Raum, et al. (2009), LCB from Abdelmalak et al. (2017) |
| Profile B' (Jan Mayen) | NPD 1220-0101 | Profile 5-95 | In-house and published data | Published data | Stratigraphy modified from Blischke et al. (2017), crustal boundaries from Kodaira et al. (1998) and Peron-Pinvidic et al. (2012b), LCB from Abdelmalak et al. (2017) |
| Profile B' (Greenland) | Published data | None | Published data | Published data | Stratigraphy modified from Skogseid et al. (2000), Hamann et al. (2005) and Guarnieri et al. (2017), crustal boundaries from Kodaira et al. (1998) and Kvarven et al. (2016), LCB from Abdelmalak et al. (2017) |
| Profile C | MNR11-90518 | Profiles 4-03 | In-house data | None | Stratigraphy modified from Zastrozhnov et al. (2020) and Gernigon et al. (2021), crustal boundaries from Faleide et al. (2008) and Breivik et al. (2011), LCB from Abdelmalak et al. (2017) |
| Profile C' | None | Profile AWI-20030500 | Published data | In-house data | Stratigraphy modified from Salomon et al. (2020), crustal boundaries from Voss and Jokat (2007) and Voss and Jokat (2009) |
| Profile D | MNR11-90698 | None | In-house data | In-house data | Stratigraphy modified from Zastrozhnov et al. (2020) and Gernigon et al. (2021), crustal boundaries from Faleide et al. (2008) and Zastrozhnov et al. (2018), LCB from Abdelmalak et al. (2017) |
| Profile D' | Published data | Profile AWI-20030400 | Published data | In-house data | Stratigraphy modified from Franke et al. (2019) and Salomon et al. (2020), and crustal boundaries from Voss and Jokat (2007) |
| Profile E | GMNR-94-108 | Profile 3-88 | In-house data | In-house data | Stratigraphy modified from Tsikalas et al. (2001), Bergh et al. (2007), Hansen et al. (2011), Henstra et al. (2017), and Tsikalas et al. (2019), crustal boundaries from Mjelde et al. (1993) and Tsikalas, Eldholm, and Faleide (2005), Moho and LCB from Abdelmalak et al. (2017) |
| Profile E' | Published data | Profiles AWI 20030300 and AWI 94300 | Published data | In-house data | Stratigraphy modified from Tsikalas, Faleide, Eldholm, and Wilson (2005), Dinkelman et al. (2010), Granath et al. (2011) Helwig et al. (2012), Tsikalas et al. (2012) and Jackson et al. (2013), crustal boundaries from Voss et al. (2009) |
| Profile F | GMNR-94-109 | Profile 6-03 | In-house data | In-house data | Stratigraphy modified from Tsikalas et al. (2001), Bergh et al. (2007), Hansen et al. (2011) and Meza-Cala et al. (2021), crustal boundaries from Breivik et al. (2017) |

**Table 1**
*Continued*

| Crustal transect | Seismic reflection lines | Seismic refraction data | Stratigraphic horizons and crustal compilation | Gravity inversion data | References and comments |
|---|---|---|---|---|---|
| Profile F' | Published data | Profile AWI-20030200 | Published data | Published data | Stratigraphy modified from Hamann et al. (2005), Tsikalas, Faleide, Eldholm, and Wilson (2005), Dinkelman et al. (2010), Granath et al. (2011), Helwig et al. (2012), Tsikalas et al. (2012), Jackson et al. (2013) and Fyhn et al. (2021), crustal boundaries from Voss et al. (2009) |
| Profile G | LO-88-48 | Unpublished profile 5-03 | In-house data | In-house data | Stratigraphy modified from Meza-Cala et al. (2021), crustal boundaries from Tsikalas, Eldholm, and Faleide (2005) |
| Profile G' | Published data | None | Published data | Published data | Stratigraphy modified from Hamann et al. (2005), Tsikalas, Eldholm, and Faleide (2005), Dinkelman et al. (2010), Granath et al. (2011), Helwig et al. (2012), Tsikalas et al. (2012), Jackson et al. (2013) and Fyhn et al. (2021), crustal boundaries from Granath et al. (2010) and Funck, Geissler, et al. (2017) |
| Profile H | NBR-20-224944, BSS01 | None | In-house data | In-house data | In-house stratigraphy, crustal boundaries from Ritzmann and Faleide (2007), Klitzke et al. (2015) and Funck, Erlendsson, et al. (2017), Funck, Geissler, et al. (2017) |
| Profile H' | Published data | Profile AWI-20090200 | Published data | Published data | Stratigraphy modified from Granath et al. (2010), crustal boundaries from Granath et al. (2010) and Funck, Geissler, et al. (2017) |

data served as the foundations for the final crustal transects, and we further prioritized the refraction profiles that cover our crustal model domain, but we used seismic compilations of Moho and top-to-basement depths to complete the missing areas (e.g., Funck, Geissler, et al., 2017; Granath et al., 2011). We compared the data set to inverse modeling of gravity data in the NE Atlantic area (Haase et al., 2017; Lebedeva-Ivanova et al., 2019; Petrov et al., 2016) to verify the reliability of the deep crustal levels. The seismic data have been combined with regional public grids of satellite gravity data (Sandwell and Smith, 2009), magnetic compilations (Maus et al., 2009; Verhoef et al., 1996), and bathymetry (IBCAO, International Bathymetric Chart of the Arctic Ocean; Jakobsson et al., 2020). The gravity data have been Bouguer-corrected using a correction density of 2,200 kg/m$^3$ for sediments. Both the gravity and magnetic grids have been high-pass filtered with cut-off wavelengths of 50, 100, 200, and 400 km.

### 3.2. Methods

In order to reconstruct the basin evolution and paleogeographic/tectonic maps, we quantified the pre-drift extension in both time and space by analyzing a set of eight pairs of representative conjugate crustal transects. These 16 transects (8 conjugate pairs) were selected from a wider series of 28 available crustal transects (Figure 2). The transects were built based on an integrated analysis of all relevant in-house and published geophysical and geological data in the NE Atlantic area as described below. The eight crustal transect pairs are described as conjugate, however, with the restoration to break-up times they can be more accurately described as "near conjugate" due to variable data availability between the two conjugate margins of the North Atlantic.

#### 3.2.1. Conjugate Profile Construction: Moho and Basement, Lower Crustal Body, and Tectono-Stratigraphy

The deep crustal boundaries, such as the depth to basement and the depth to Moho are drawn for each crustal transect. The Moho, representing the crust-mantle boundary, is defined where the *P*-wave ($V_p$) velocities increase from 6 to 6.8 km/s to values of 7.9–8 km/s in the oceanic domain, and to 8.0–8.3 km/s in the continental domain (e.g., Mjelde et al., 2005). The top basement is defined as the top of the igneous crust in the oceanic domain and the top of the crystalline crust in the continental domain where the *P*-wave velocities change from <5.5 km/s to values >6 km/s that are typical of continental crystalline rocks (e.g., Mjelde et al., 2005; Raum et al., 2002). In

order to better constrain the top basement depth, we used seismic refraction data and complemented them with the deep depth-converted seismic reflection data. We, then compared the top basement depth with available seismic compilations and deep crustal boundaries (crustal thickness, depth to basement, and depth to Moho) derived from inverse gravity modeling in the NE Atlantic area (e.g., Haase et al., 2017; Lebedeva-Ivanova et al., 2019; Petrov et al., 2016). Deeply buried and metamorphosed sediments with petrophysical properties similar to crystalline rocks may be included in the basement. In the NE Atlantic, wide-angle seismic surveying across most of the conjugate volcanic margins revealed high-velocity layers at the base of the crust that are commonly referred to as lower crustal bodies (LCB) located in the outer part of the margins (Holbrook et al., 2001; Mjelde et al., 2007; Mjelde, Faleide, et al., 2009; Voss and Jokat, 2007; Voss et al., 2009) (Figures 1d and 3). These are usually interpreted as underplated magmatic bodies (Holbrook et al., 2001; White et al., 1987) or highly intruded lower crust (Abdelmalak et al., 2017; White et al., 2008). LCBs are characterized by *P*-wave velocities of 7.1–7.7 km/s and $V_p/V_s$ (*P*-wave/*S*-wave) ratios ranging between 1.8 and 1.9 (e.g., Mjelde et al., 2003). They are often interpreted along the continent-ocean transition (COT) but can extend continent-ward outside the identified volcanic province. The outer limit of the LCB is located where "normal" oceanic crust (6–8 km thickness) is clearly identified at the location of magnetic chrons C22–C23 that are evidenced by magnetic data (Figure 3).

On the mid-Norwegian margin, we used the interpreted stratigraphic horizons from Zastrozhnov et al. (2018, 2020) where well-tied seismic data allowed for a confident interpretation of the different Mesozoic-Cenozoic time horizons and unconformities. The base Cretaceous unconformity (BCU) is a key regional marker often used to constrain the spatial and temporal rift climax activity of the major late Jurassic-early Cretaceous extensional phase. The BCU is particularly well imaged landward of the extruded basalts, together with pre-Cretaceous strata down to Jurassic and Triassic horizons in the inner part of the margin within the Trøndelag Platform. Pre-Cretaceous sequences are hard to interpret in the deeper parts of the Vøring and Møre basins, and cannot be traced confidently to the west below thin basalt flows in the volcanic domain. On the NE Greenland margin, the main horizons used for the construction of the profiles are based on available published data (Dinkelman et al., 2010; Granath et al., 2011; Hamann et al., 2005; Helwig et al., 2012; Jackson et al., 2013; Tsikalas, Faleide, Eldholm, & Wilson, 2005; Tsikalas et al., 2012). With reference to the geological history of the NE Atlantic, we subdivide the sedimentary succession in the crustal transects into five mega-sequences (Figure 3). An orogenic extensional collapse mega-sequence is defined for the Devonian to mid-Permian age. This sedimentary package is characterized by thick successions of mainly intermontane continental deposits. Three mega-sequences are defined with reference to the rifting history related to lithospheric extension: (a) mid-Permian to late Jurassic/earliest Cretaceous (BCU), (b) BCU to mid-Campanian, and (c) mid-Campanian to earliest Eocene. The mega-sequence bounding horizons, which correspond to major hiatuses or condensed levels on the basin flanks,

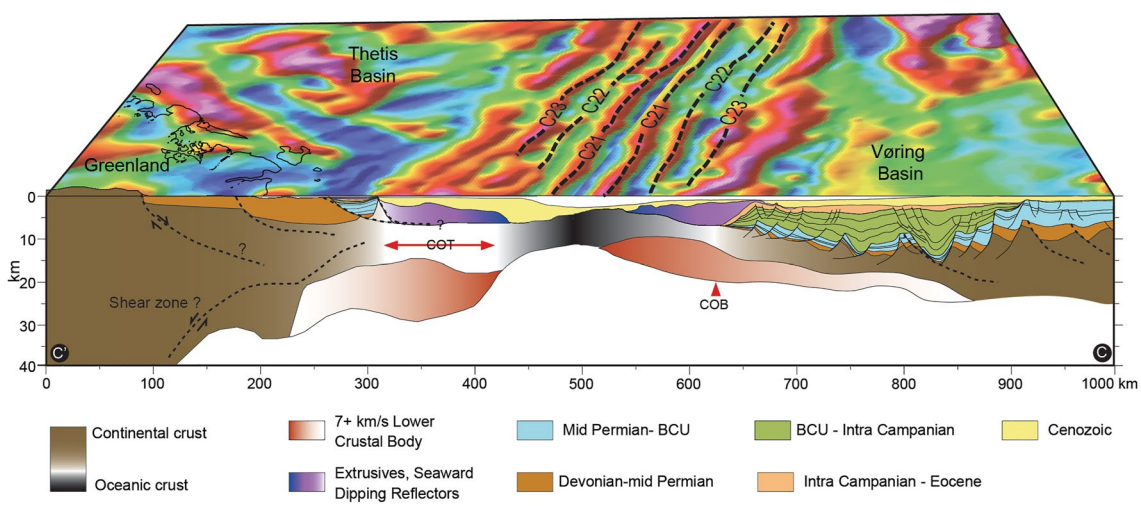


**Figure 3.** A 3D reconstruction at post-breakup times, C21 (~47 Ma), of the crustal structure across the Vøring Margin and its conjugate Greenland margin in the Thetis Basin (Schlindwein and Jokat, 1999; Voss and Jokat, 2007). The magnetic anomalies are defined using released magnetic data EMAG2 (Maus et al., 2009). The continent–ocean boundary is indicated for Central Vøring transect (profile C), however on the conjugate margin (profile C') it consist of a continent ocean transition. The lower crustal body along the conjugate profiles extends to magnetic chrons C22–C23. Dashed black lines in the crustal transects indicate the location of the interpreted shear zones. This figure corresponds to conjugate profile C-C'.

may be found within thick sedimentary units reflecting rapid differential subsidence in the deepest basins. Finally, the post-breakup mega-sequence is related to the margin subsidence, continental uplift of Fennoscandia and associated glacial erosion, and comprises sediments from early Eocene to the seafloor, including the large Plio-Pleistocene sedimentary wedge.

#### 3.2.2. Crustal Stretching From Observations and Relation to LCB Nature

In order to quantify the rift-related deformation along the rifted margins it is first necessary to define the spatial extent of the stretched crust. This involves identifying the limit of the unstretched continental crust (UCC) and the oceanward limit of the stretched continental crust (or continent-ocean boundary, COB) In the NE Atlantic area, the UCC limit is located close to the shoreline where the crust has experienced limited or no extension since mid-Permian time.

The boundary from oceanic lithosphere to continental lithosphere can form a distinct narrow band (COB) or a diffuse zone of varying width (alternatively the COT). At magma-poor margins, the nature of the crust in the transition zone is controversial, with models ranging from thinned and disrupted continental crust to exhumed mantle or ultra-slow spreading oceanic crust (e.g., Peron-Pinvidic et al., 2013). At magma-rich margins such as most of the NE Atlantic margin segments, the interpretation of the COT becomes even more complicated as remnants of thinned continental crust may become indistinguishable from oceanic crust due to the breakup-related magmatic overprint.

However, confidence in mapping the COB, outboard of which pure oceanic crust is present, is key to deriving realistic estimates of the pre-drift extension for plate kinematic reconstructions (e.g., Gaina et al., 2017). We mapped the COB based on the location of the first well-defined seafloor spreading magnetic anomalies in the oceanic crust and the landward limit of undisputed oceanic crust on seismic refraction profiles. Further refinements were implemented using potential field data and seismic reflection/refraction data. Along the NE Atlantic volcanic margins, the COB is frequently masked by thick volcanic sequences formed during breakup (Berndt et al., 2001; Eldholm et al., 2000), significantly complicating its along-margin identification. Seismic refraction data show that the COB is characterized by sudden lateral velocity changes at mid-crustal and lower crustal levels related to clear density contrasts near the inner edge of the seaward dipping reflectors (SDRs) (e.g., Breivik et al., 2014; White and Smith, 2009). Using these different criterias, we mapped out the COB and compared the outline with previously published COBs from the NE Greenland (Geissler et al., 2016; Hamann et al., 2005; Tsikalas, Faleide, Eldholm, & Wilson, 2005; Voss et al., 2009); the SW Barents Sea (Breivik et al., 1999); mid Norwegian margins (Breivik et al., 2009; Gernigon et al., 2015); and the entre NE Atlantic region (Funck, Erlendsson, et al., 2017; Gaina et al., 2009, 2017).

On the mid-Norwegian side, the COB is well-defined on several data sets and its location is generally agreed upon. A dense 2D seismic grid reveals a well-developed volcanic extrusive complex including SDRs. In addition, several deep seismic profiles from ocean bottom seismic (OBS) reveal significant crustal velocity and density contrasts across the COB. Along the Barents Sea, Svalbard, Wandel Sea, Boreas Basin, and East Greenland margins, we interpret the COB based on a combined interpretation of gravity and magnetic data and commercial seismic surveys. In general, our COB mapping is in good accordance with the published COB in the regions where there is the best and most comprehensive data coverage. However, on the Central East Greenland the location of the COB is difficult to be defined because of the occurrence of thick breakup volcanics that mask clear magnetic lineation. In this case, the COB is interpreted either landward (Scott, 2000) or oceanward (Voss and Jokat, 2007) (Figure 1).

In the case of the Jan Mayen microcontinent (JMMC), the definition of the COB is of primary importance as it allows to constrain the extent of the microcontinent itself. In that case also, the various published COB outlines differ quite substantially (Funck, Erlendsson, et al., 2017; Gaina et al., 2009; Peron-Pinvidic et al., 2012a). In the central part of the JMMC, the COB definition was constrained by both seismic reflection and refraction data, together with potential field maps (e.g., Blischke et al., 2017; Breivik et al., 2012; Gernigon et al., 2009). The definitions there are mostly consistent with each other. On the other hand, the northern and southern limits are very much debated. The northern limit of the microcontinent has been defined based on seismic refraction profiles (Kandilarov et al., 2012). The southern limit is still more vague and could consist of a transitional continental crust north-east of the Icelandic shelf (Brandsdóttir et al., 2015). Continental crust beneath southeast Iceland was proposed as part of ~350-km-long and 70-km-wide extension of the JMMC (Torsvik et al., 2015).

As a consequence, the definition of the COB is extended farther south to the east of Iceland based on inversion of gravity anomaly data (crustal thickness), analysis of regional magnetic data, and plate reconstructions (Torsvik et al., 2015). However, no seismic data are available to constrain confidently the southern extent of continental crust between Jan Mayen and Iceland.

The stretching factor is the ratio between a reference crustal thickness and the present-day crustal thickness, with the latter constrained by direct geological observations. The stretching factor calculated from observed crustal thickness can only be used to highlight variations along the constructed transect because the original (pre-drift) thickness was unlikely uniform. In standard basin analysis, a typical 30–35 km thick reference crystalline crust with densities between 2,700 and 2,900 kg/m$^3$, and a 120–130 km thick lithosphere, are assumed to be balanced at sea level (e.g., Gac et al., 2021; McKenzie, 1978; Skogseid et al., 2000; Theissen-Krah et al., 2017). In this study, we consider an initial crustal reference thickness of 35 km. For the orogenic and early post-orogenic evolution, the reference crustal thickness cannot be defined precisely, and standard assumptions applied in basin modeling are considered not applicable. In addition, sediments may become indistinguishable from the uppermost crystalline crust where the deepest and metamorphosed sedimentary rocks have *P*-wave velocities in excess of 5.5 km/s. As a consequence, the crustal thickness may be overestimated in places, and the stretching factor underestimated.

Unraveling the nature of the LCB is crucial to understand the deep structure and tectonic evolution of the volcanic margins, and to understand its implications for crustal stretching, heat flow, and vertical motion. Geochemical analyses of a sill intrusion on the Vøring margin demonstrated that the LCB can be explained as an heterogeneous mixture of cumulates associated with breakup-related magmatism and less dense rocks such as old continental basement (Neumann et al., 2013). Wangen et al. (2011) suggested that an unrealistic amount of extension is required to generate a LCB of 100% underplated magmatic material. Therefore, the LCB likely represents a complex mixture of pre- to syn-breakup mafic and ultramafic rocks (cumulates and sills) and high-grade metamorphic rocks such as granulites and eclogites (Abdelmalak et al., 2017). Taking into consideration the effect of LCB for the calculation of the stretching factor, we considered three different scenarios with different amount of magma addition (0%, 50%, and 100%). For the 0% magma addition, the LCB could be considered as fully crustal rock. For the 100% magma addition, the LCB is considered as 100% magma underplating, while for the 50% magma addition model as a mixture of breakup-related magma and crustal rocks. Hence, the crustal thickness estimates change along the extent of the LCB depending on the magma addition. By considering different magma addition within the LCB, we define end members as well as the intermediate values of the crustal stretching along the crustal transect where the LCB is mapped (Figure 4).

### 3.2.3. Crustal Restoration Approach Deduced From Observations

From the calculated stretching factor inferred from the observed crustal structure (Figure 4), we quantified the total extension by restoring the COB back to its estimated pre-drift position in the different transects. A case example of restoration workflow along the Northern Vøring margin segment is illustrated in Figure 5. A total extension of 335 km (for 50% magma addition in the LCB) is generally estimated from the stretching factor averaged along the transect (average $\beta = 3.01$, Table 2). However, this value may be an underestimation because the average stretching factor does not capture the thickness variations along the transect. The solution is to divide the crustal transect into $n$ columns, each characterized by an average stretching factor. The pre-drift column widths are computed then added in order to obtain the total extension and the initial width of the entire transect. The greater the number $n$ of columns, the better the crustal thickness variations are captured, hence the more accurate the total extension is estimated. The results of this exercise show that the estimate of total extension decreases when increasing the number $n$ of columns, reaching a constant value for $n > 20$. In our work, each transect is divided into regular 1-km wide columns. In the Northern Vøring margin case example, the total extension is 246 km (for a 0% magma addition), 253 km (for a 50% magma addition), and 261 km (for a 100% magma addition) (Table 2). Margin asymmetry does not affect the restoration since the stretching factor is derived only from the crustal thickness. However, it is important to note that the restoration process assumes that the extension direction is parallel to the orientation of the transect. Any implemented deviations to extension direction, for example, in digital plate reconstructions, should consider these estimates accordingly.

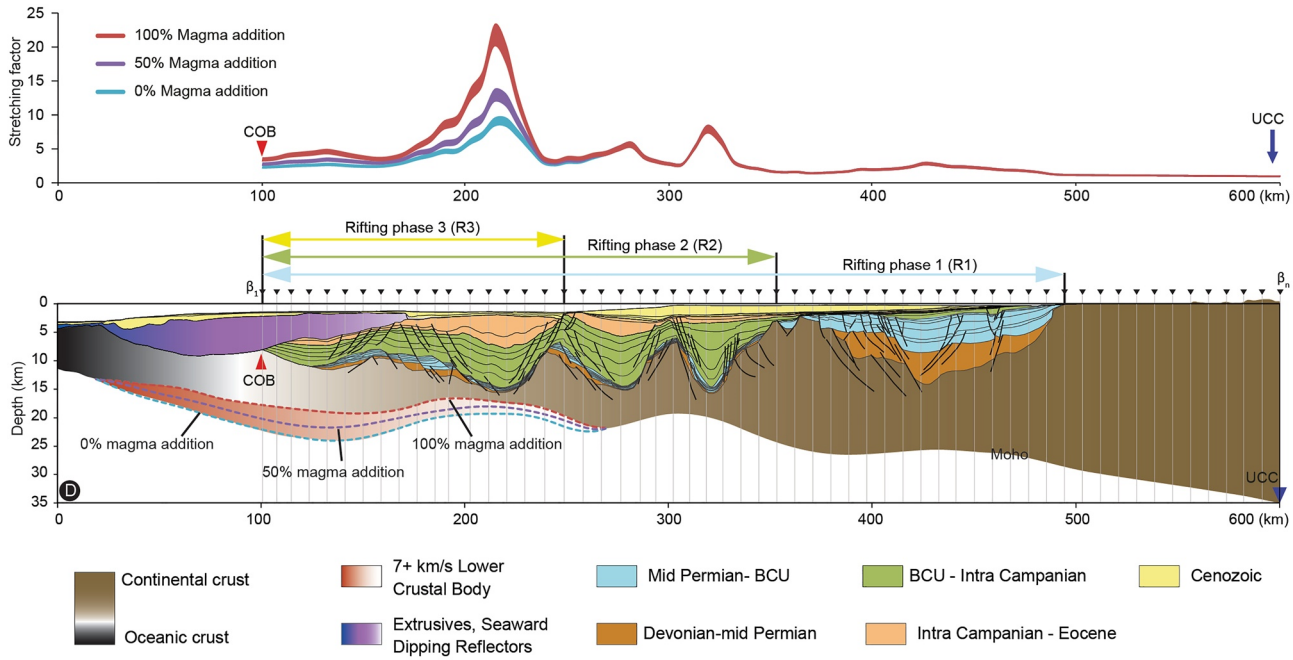


**Figure 4.** Example of the Northern Vøring crustal transect (profile D) constrained using interpreted seismic data. Stretching factors are calculated from observed crustal thickness assuming an initial thickness of 35 km. The crustal stretching factor or beta ($\beta$) factor is calculated along the entire profile in different location ($\beta_1$ to $\beta_n$) with a regular spacing. The higher number of "$n$" measurements implies a better-constrained stretching factor curve along the crustal transect. The stretching factor curve was calculated for the different amounts of magma addition (0%, 50%, and 100%). With reference to the geologic history of the NE Atlantic, we subdivide the sedimentary succession in the crustal transects into five mega-sequences. Three extension phases are shown for reference. COB: Continent-Ocean Boundary; UCC: unstretched continental crust.

### 3.2.4. Restoration of Multiphase Rifting

The restoration process is applied to a margin that experienced multiple rifting phases and migration of the main locus of deformation toward the (future) COB. The behavior of the locus of extension during such multiple phases of rifting falls into two broad categories: the "rift jump" and the "rift focus" categories (Figure 6). For each category we need to define the stretching factors of the different extensional episodes, the tectonic hinge lines which delineate the area along the transect that was affected during a given extensional episode, and the extensional directions. We start the restoration by estimating first the pre-rift width of the section that experienced the last rifting episode before continental breakup. We subsequently restore the margin sections that experienced older rifting phases to obtain the full pre-rift width of the margin.

In the rift jump case, the main locus of extension shifts with time, leading to a succession of well-defined parallel sedimentary basins. The migration of the locus of extension is the consequence of multiple stretching phases separated by periods during which the lithosphere is not under tensile stress and cools down to strengthen again. In this scenario, the subsequent phase of deformation jumps to a margin section where the lithosphere is weaker (e.g., Kusznir and Park, 1987; Van Wijk and Cloetingh, 2002). The hinge lines delineate the margin sections affected by a single extensional episode, and the full pre-drift margin width can be estimated by adding the pre-drift width of each margin section (Figure 6a). The restoration process is more challenging in the case of the rift focus case where the deformation across the conjugate margins incrementally converges toward the COB (Figure 6b). In the rift-focus case, hinge lines cannot be precisely defined since all margin sections are involved in several extensional episodes where rifting domains overlap.

### 3.2.5. Basin Modeling

A basin modeling approach using TecMod2D software is applied in order to restore the multi-rift margin evolution (Rüpke et al., 2008). This approach allows to quantify both the amount and distribution of extension during the different extensional episodes, but also the intermediate paleo-positions of the "restored COB" back through time. Hence, the outputs from the basin modeling allow minimization of the overlap and underlap

10.1029/2022TC007386

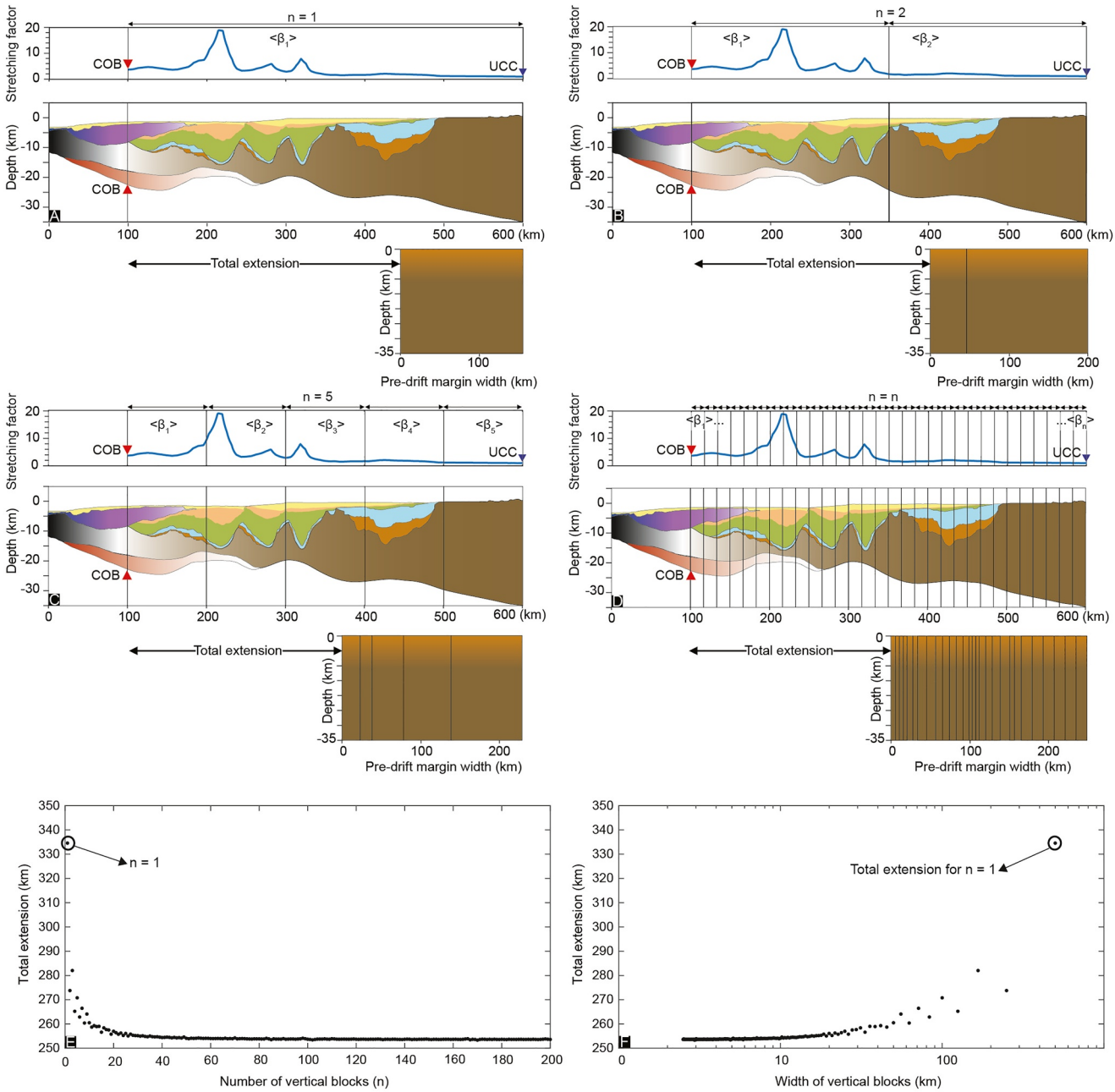


**Figure 5.** Example of restoration of the pre-drift margin width for the Northern Vøring transect (Profile D; see also Figures 3 and 4) using a crustal stretching curve with 50% magma addition. The upper left panels (A), shows the estimated crustal stretching factors, which are averaged along the transect and used for restoring the Continent-Ocean Boundary back to its estimated pre-rift position closer to the assumed unstretched continental crust limit. However, the beta factor averaged along the transect may be an underestimation because it does not capture the crustal thickness variations along the transect. Therefore, we instead divide the crustal transect into n columns (B–D), each with an averaged beta factor. The pre-drift width of each column is computed and then added in order to obtain the initial width of the entire transect. A greater n number of columns captures the crustal thickness variations, hence the estimation of the pre-rift margin width is more accurate. The estimate of pre-drift margin width increases when increasing the number $n$ (E) of columns and decreasing their width (F), reaching a constant value for $n > 20$. This workflow allows the calculation of the total extension from the observed crustal structure.

at intermediate stages leading to the establishment of palinspastic deformable margin plate kinematic models. TecMod2D automates sedimentary basin and passive margin reconstruction in 2D, and is based on an algorithm that couples a forward lithosphere extension model to an inverse scheme which automatically updates the crustal and mantle stretching factors, and the paleobathymetry until the input stratigraphy fits to the desired accuracy

**Table 2**
*Calculated Values of the Average Stretching Factor and Total Extension (km) for Each of the Eight Conjugate Profile Transects (A/A'–H/H'), Listed From North to South*

| | Observed crustal structure | | | | | | | | Basin modeling | |
|---|---|---|---|---|---|---|---|---|---|---|
| | Average stretching factor | | | | Total extension (km) | | | | | |
| Profile | 0% | 100% | 50% | Std | 0% | 100% | 50% | Std | Average stretching factor | Total extension (km) |
| H-SW Barents Sea | 2.63 | 3.67 | 2.96 | 0.53 | 233 | 244 | 238 | 6 | 2.79 | 257 |
| H'-Northern NE Greenland | 2.37 | 2.78 | 2.52 | 0.20 | 213 | 219 | 215 | 3 | 1.79 | 165 |
| G-Northern Lofoten Andøya | 1.87 | 1.87 | 1.87 | 0.00 | 40 | 40 | 40 | 0 | 1.30 | 21 |
| G'-NE Greenland Thetis | 2.19 | 2.19 | 2.19 | 0.00 | 226 | 226 | 226 | 0 | 1.92 | 204 |
| F-Northern Lofoten | 1.90 | 2.16 | 2.00 | 0.13 | 63 | 66 | 61 | 3 | 1.93 | 71 |
| F'-NE Greenland | 1.84 | 1.87 | 1.83 | 0.02 | 170 | 171 | 160 | 6 | 1.68 | 160 |
| E-Southern Lofoten | 1.91 | 2.35 | 2.06 | 0.23 | 92 | 95 | 92 | 1 | 2.14 | 98 |
| E'-NE Greenland Shannon | 1.69 | 2.06 | 1.79 | 0.19 | 91 | 96 | 88 | 4 | 1.46 | 75 |
| D-Northern Vøring | 2.72 | 3.54 | 3.02 | 0.41 | 246 | 261 | 253 | 8 | 3.10 | 245 |
| D'-NE Greenland Foster | 1.17–1.51 | 1.42–2.51 | 1.22-182 | 0.13–0.51 | 29–89 | 49–145 | 33–111 | 10–28 | 1.25 | 36 |
| C-Central Vøring | 2.44 | 3.45 | 2.79 | 0.51 | 273 | 297 | 284 | 12 | 3.04 | 276 |
| C'-CE Greenland Traill Ø | 1.12–1.32 | 1.34–1.95 | 1.22–1.82 | 0.1–0.3 | 28–87 | 49–134 | 38–106 | 10–24 | 1.19 | 36 |
| B-Central More | 3.31 | 2.55 | 2.87 | 0.38 | 203 | 184 | 194 | 9 | 3.43 | 214 |
| B'-Jameson Land/Jan Mayen | 1.63 | 1.70 | 1.62 | 0.04 | 109 | 118 | 98 | 10 | 1.23 | 59 |
| A-Southern Møre | 2.13 | 2.89 | 2.43 | 0.38 | 171 | 191 | 181 | 10 | 3.47 | 205 |
| A'-Blosseville/Jan Mayen | 2.30 | 2.69 | 2.44 | 0.15 | 168 | 204 | 185 | 15 | 1.56 | 120 |

*Note.* Estimates are made for different magma addition into the lower crust (0%, 50%, and 100% additions) based on the observed crustal structure. For the profiles C' and D' we considered two scenarios using the oceanward and the landward interpreted COB to calculate the stretching factor and total extension. The standard deviations (Std) from the mean crustal stretching and total extensions document the effect of magma addition. The average stretching factor and the total extension values for each crustal transect, computed from basin modeling (via TecMod2D), are also indicated. For both methods, we assumed a reference crustal thickness of 35 km. The 50% magma addition scenario is used in Table 3.

(generally within 5%–10% error) (Rüpke et al., 2008). The 2D forward model based on pure shear kinematics and coupled with thermal evolution modeling of the lithosphere (McKenzie, 1978) allows for multiple rifting phases of finite duration (e.g., Theissen-Krah et al., 2017).

The effects of flexural isostasy and depth of necking are included (Braun & Beaumont, 1989; Watts et al., 1982). The velocity field derived from pure shear kinematics and crustal flexure is used to advect the temperature field. The time-dependent heat-transport equation includes advection and diffusion and is solved in the entire modeling domain. Crustal radiogenic heat production is assumed to decrease exponentially with depth (Turcotte and Schubert, 2002). Water and sediments are included into the thermal solver to account for the effects of sediment blanketing (Theissen and Rüpke, 2010). Sedimentation is controlled by sedimentation rates determined by the inversion scheme. The deposited sediments are compacted using empirical compaction laws (Royden and Keen, 1980). The boundary conditions for the thermal solver are fixed temperatures at the base and top of the numerical domain and zero horizontal heat flow at the sides. In the absence of metamorphic phase transitions, density changes are computed from a reference density and the thermal expansion factor (McKenzie, 1978).

TecMod2D allows for additional lithosphere processes that may accompany extension to be implemented (e.g., Gac et al., 2021), such as melt generation based on a simple parameterization of melting as well as melt retention and extraction. Melt production starts once the lithosphere/asthenosphere boundary rises above 90 km depth and achieves maximum value at 20 km depth. Melt fractions are linearly interpolated between these two reference points. A specified fraction of melt is emplaced as a magmatic underplate, characterized by a crustal density higher than normal (3,100 kg $m^{-3}$). During the post-rift, melt is extracted from the asthenosphere at a specified rate. TecMod2D also allows during extension and under varying pressure and temperature conditions for the phase transitions of dry mantle peridotites (Kaus et al., 2005; Simon and Podladchikov, 2008) that can experi-

10.1029/2022TC007386

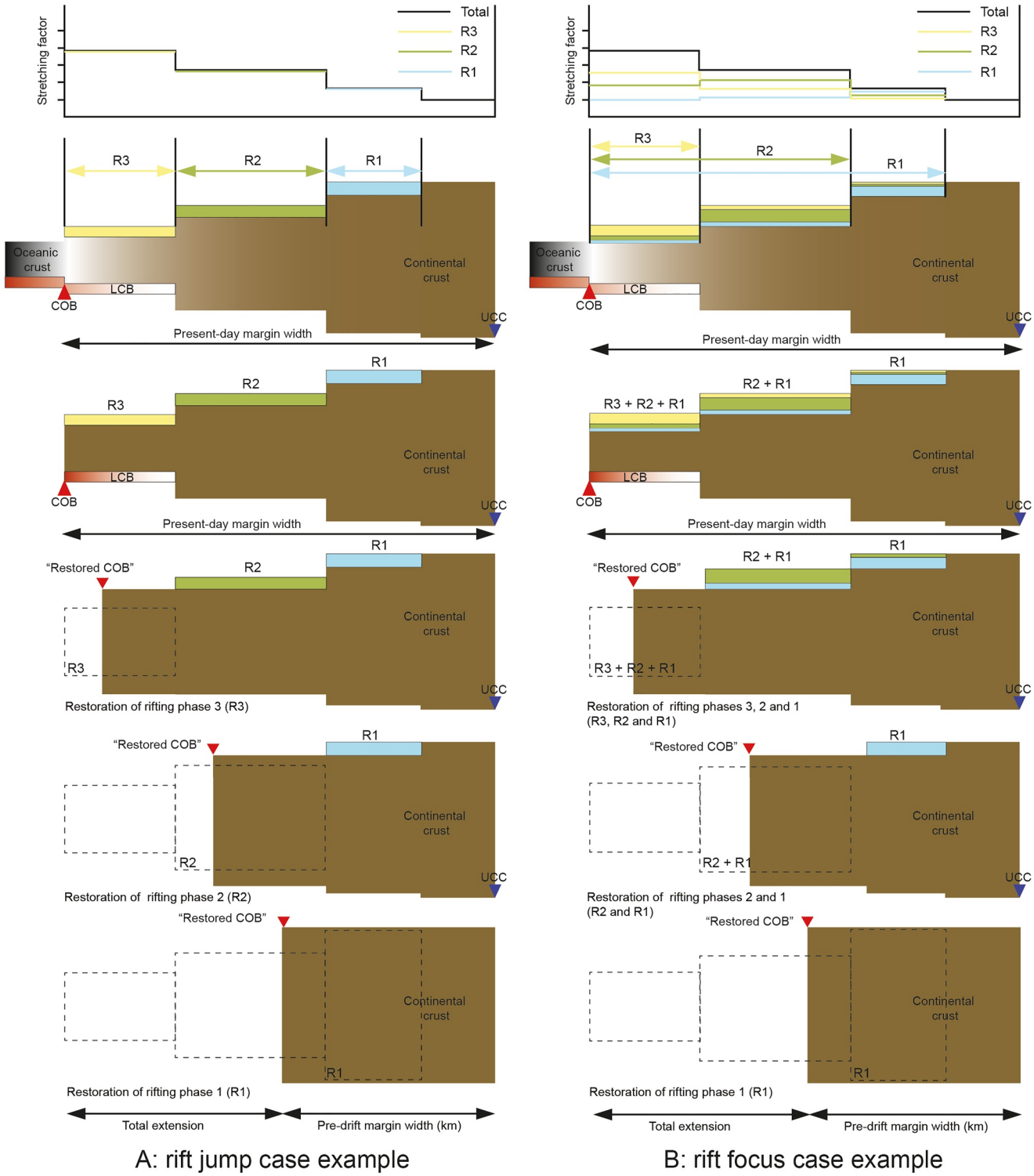


**Figure 6.** Schematic explaining the restoration of multiphase rifting phases. The behavior of the locus of extension during multiple phases of rifting can be described into two main categories: the "rift jump" (A) and the "rift focus" (B). The figure shows the process from present-day through each successive rifting phase, going backwards in time. For each category tectonic hinge lines are delineating the margin segment that have been affected during the extensional episode, and the extensional directions. In the rift jump case, each margin segment is affected by one rifting phase "R." Restoring the pre-rift margin width is the result of restoring individual segment delineated by well-defined hinge lines. The restoration process is more challenging in the case of the rift focus case whereby the deformation across the conjugate margins incrementally converges toward the Continent-Ocean Boundary. In this case, hinge lines cannot be precisely defined since all margin sections are involved in several rifting phases, leading to overlap of rifting domains. In this case, a basin modeling approach is needed to define the pre-rift margin width.

ence garnet-spinel, plagioclase-in phase transitions associated with significant density jumps. TecMod provides thermodynamic tables of mantle densities based on mantle phase transition models from Kaus et al. (2005) and Simon and Podladchikov (2008) for various mantle compositions (Hartz et al., 2017).

The stratigraphic model of each crustal transect is loaded into the TecMod2D software. Rock properties are assigned to each stratigraphic layer (see Gac et al., 2021 for more details). Assumptions regarding the lithology of each unit were made, choosing either the dominant lithology (e.g., sandstone) or mixtures (e.g., 50% sand, 50% shale). Similarly, porosity-depth trends linked to mechanical compaction during burial were applied to each sedimentary unit based on the assumed dominant lithology, while sand-shale mixtures were linearly interpolated based on their ratios. Due to their minor influence, chemical compaction, diagenesis, and low-grade metamorphism were neglected.

The number and timing of each rift episode are set as input. We assume that rifting in response to lithospheric extension between Eurasia and Greenland was initiated at mid Permian time (270–260 Ma). Hence, four main rifting phases are defined in our model setup: mid-Permian-early Triassic (264–247 Ma), mid-Jurassic-early Cretaceous (166–140 Ma), mid-Cretaceous (125–110 Ma), and late Cretaceous-Paleocene (80–56 Ma) (e.g., Gac et al., 2021). The distinction between mid-Jurassic-early Cretaceous and mid-Cretaceous rifting phases is sometime challenging this is why we combined them in one single rifting episode in some figures.

For each model, a flexural isostasy is applied through an effective elastic thickness (Te) of 2 km and a corresponding necking depth of 15 km. These values are difficult to constrain and vary spatially and temporally but are consistent with other published models for the Viking Graben and Vøring Basin (Fjeldskaar et al., 2009; Rüpke et al., 2008; Theissen and Rüpke, 2010). Post-Caledonian crust and lithosphere varied in thickness along the profiles before rift initiation. Constant initial crustal thickness of 35 km (17.5 km upper crust, 17.5 km lower crust) and a total lithospheric thickness of 120 km are therefore used for most of our models (Clark et al., 2014; Gac et al., 2021). Other main forward model parameters include temperature boundary conditions of 0°C at the seafloor, and 1,300°C at the lithosphere-asthenosphere boundary (LAB) and a 2 $\mu W/m^3$ radiogenic heat production in the crust. The numerical resolution of the finite element mesh is set at $nx = 100$ and $ny = 100$ (see Gac et al., 2021 for details).

Reference models are first run (M0) whereby only lithospheric extensional processes are accounted (e.g., McKenzie, 1978). Such models are often proposed to account for the development of passive margins, but do not satisfactorily explain the outer parts of volcanic passive margins of the NE Atlantic region. They often fail to reproduce key observations such as: (a) the observed stratigraphy, (b) the observed stretching factors along the transect calculated from observed crustal thickness, (c) the breakup volcanism and magma additions into the lower crust, and (d) the vertical motions and paleobathymetric observations (e.g., Gac et al., 2021). Additional processes are hence required to fit all geological observations. Excess magmatism and uplift may be related to sub-lithospheric mantle processes such as the arrival of the hot Icelandic mantle "plume" (Skogseid et al., 2000) or small-scale convection processes (Van Wijk et al., 2001). Melt retention in the asthenosphere (Quirk and Rüpke, 2018) accompanying these sub-lithospheric processes, as well as mantle phase transitions during extension (Simon and Podladchikov, 2008) may enhance the magnitude of uplift.

In the case of the NE Atlantic region, the breakup time is characterized by excess magmatism, uplift and subaerial conditions in the outer margins such as in the Vøring and Møre marginal highs. Basin modeling along a transect crossing the Northern Vøring Margin (Gac et al., 2021) shows the hot Icelandic mantle plume (Skogseid et al., 2000), magmatic underplating, melt retention in the asthenosphere and mantle phase transitions during extension satisfactorily reproduce key observations at both the inner and outer margins (see Gac et al., 2021 for more details).

## 4. Results

### 4.1. Conjugate Crustal Transects

The results from the sixteen (eight conjugate) profiles are described below, first for the Norwegian margin and then for the Greenland margin (Figures 7–10). Each of the pairs are labeled with A–H lettering from south-to-north where, for example, A is the Norwegian conjugate and the A' is the Greenlandic conjugate. All profiles from

10.1029/2022TC007386

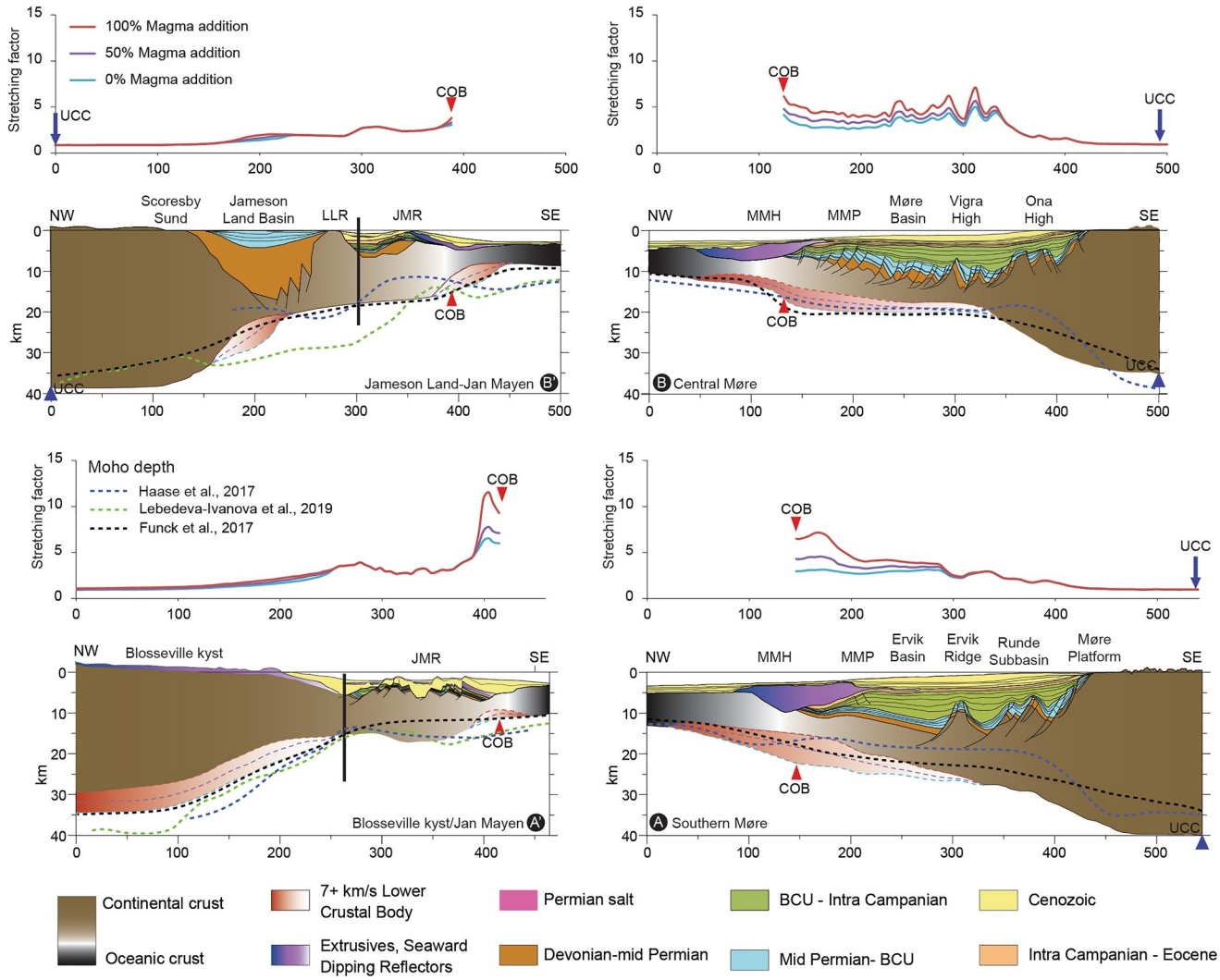


**Figure 7.** Conjugate crustal transects across Southern Møre and Blosseville-Jan Mayen (A-A') and Central Møre-Jameson land margin (B-B'). The crustal stretching factors curve for the different amount of magma addition (0%, 50%, and 100%) are drawn above each crustal transect. For the crustal transects A' and B', the central East Greenland crustal structure and the Jan Mayen crustal structure are linked together at the vertical black line. See panels for corresponding features. JMR: Jan Mayen Ridge; LLR: Liverpool Land Ridge; MMH: Møre Marginal High; MMP: Møre Marginal Plateau. See Table 1 for more information about the crustal transect build up.

the Norwegian side trend in a NW-SE direction, whereas the Greenland profiles vary from E-W to NW-SE in orientation at present-day.

### 4.1.1. Møre Margin

The two key profiles (A and B) across the Møre margin, shown in Figure 7, run from the continent to the oceanic crust through the Møre Platform, the Møre Basin, and the Møre Marginal High. The main tectonic features are well imaged by the seismic data and include several intra-basinal highs and ridges (Vigra High, Ona High, Ervik Ridge) that separate narrow and deep sub-basins (Figure 7). In the Southern Møre profile (A), the BCU lies at 0.5–1 km depth on the western flank of the Møre Platform and deepens to locally reach 12–13 km in the Runde Sub-basin. The BCU level in the outer Møre Basin is shallower and the elevated part is defined as the Møre Marginal Plateau. The eastern flank of the Møre Marginal Plateau represents a large east-dipping monocline. West-dipping detachment faults controlling the sub-basin evolution are interpreted in the Møre Basin (e.g., Ervik Basin).

10.1029/2022TC007386

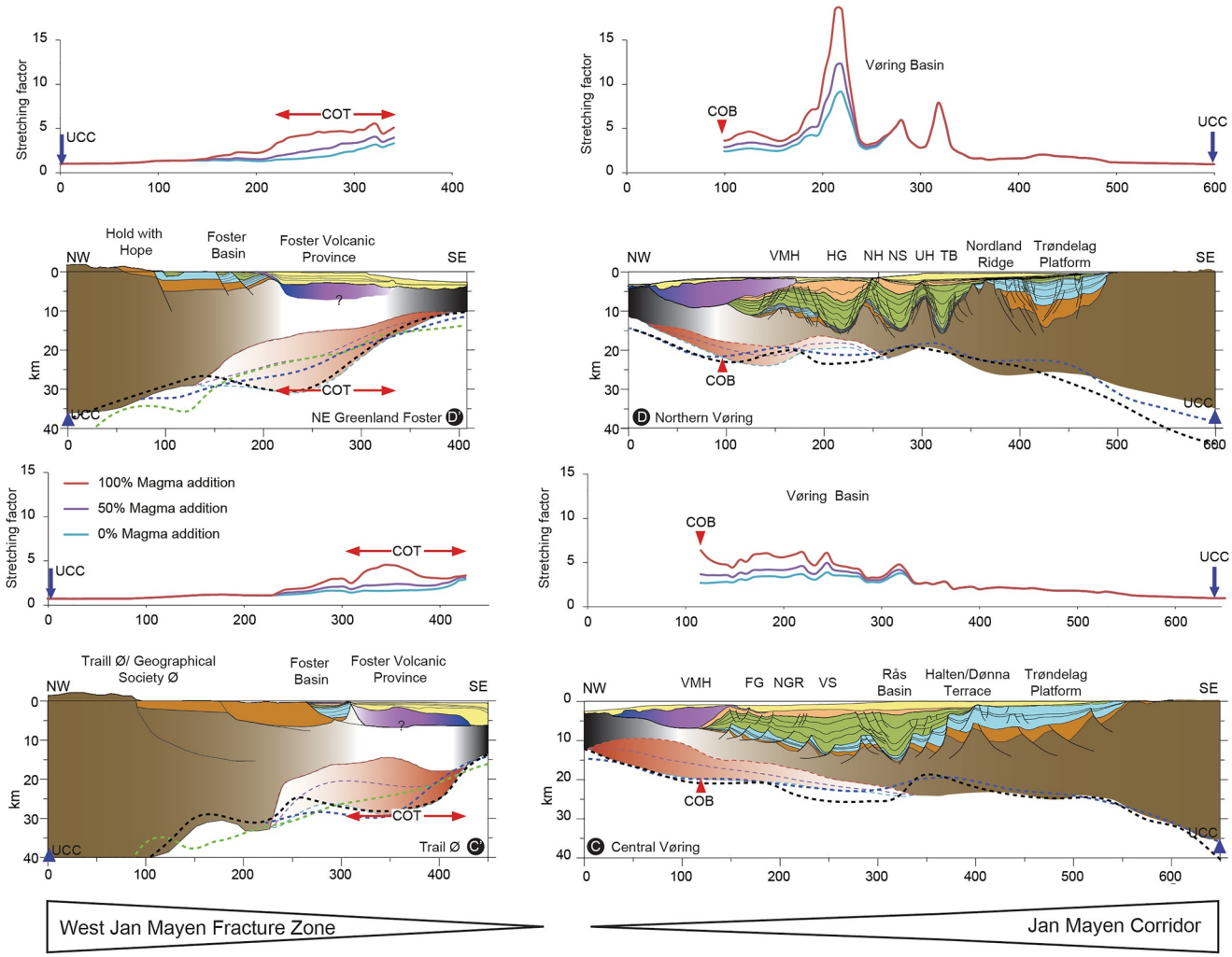


**Figure 8.** Conjugate crustal transects across the Vøring and the Central East Greenland conjugate margin segments (C-C' and D-D'). The crustal stretching factor curve for the different amounts of magma addition (0%, 50%, and 100%) are drawn above each crustal transect. The Vøring and its conjugate margin segments are separated from the Møre and its conjugate margin segments by the Jan Mayen corridor on the Norwegian side and the West Jan Mayen Fracture zone on the Greenland side. FG: Fenris Graben; HG: Hel Graben; NH: Nyk High; NGR: North Gjallar Ridge; NS: Någrind Syncline; TB: Træne Basin; UH: Utgard High; VMH: Vøring Marginal High. See Table 1 for more information about the crustal transect build up.

The Moho depth beneath the Møre Platform and coastal areas varies between 30 km below the shelf edge to 40 km onshore (Figure 7). The Moho is shallower in the oceanic domain and is identified between 11 and 13 km depth. Beneath the Møre Basin the Moho is 20–25 km deep, while the continental crystalline crust is locally thinned to <10 km and is underlain in its outer parts by ~4 km-thick LCB that extends to magnetic chrons C22–C23. Low crustal stretching values are characteristic of the Møre Platform where the crustal thickness is close to the assumed 35 km reference thickness. High crustal stretching occurs at the deepest depocenters (e.g., on either side of the Vigra High) where thinner crystalline crust is observed. In the outer part, the interpretation of the LCB nature (magmatic or not) influences the stretching factor. The thicker the LCB is the wider the difference between the observed crustal stretching between 0% and 100% magma addition.

### 4.1.2. Vøring Margin

Two key profiles (C and D) across the central and northern parts of the Vøring margin are shown in Figure 8. To the south, the Vøring Basin is connected to the Møre Basin through a broad regional transfer zone called the Jan Mayen Corridor (Figures 1 and 8). The Trøndelag Platform is much broader than the platform domain of the Møre margin. Across most of the Trøndelag Platform, the Upper Paleozoic-Lower Triassic basinal succession can reach

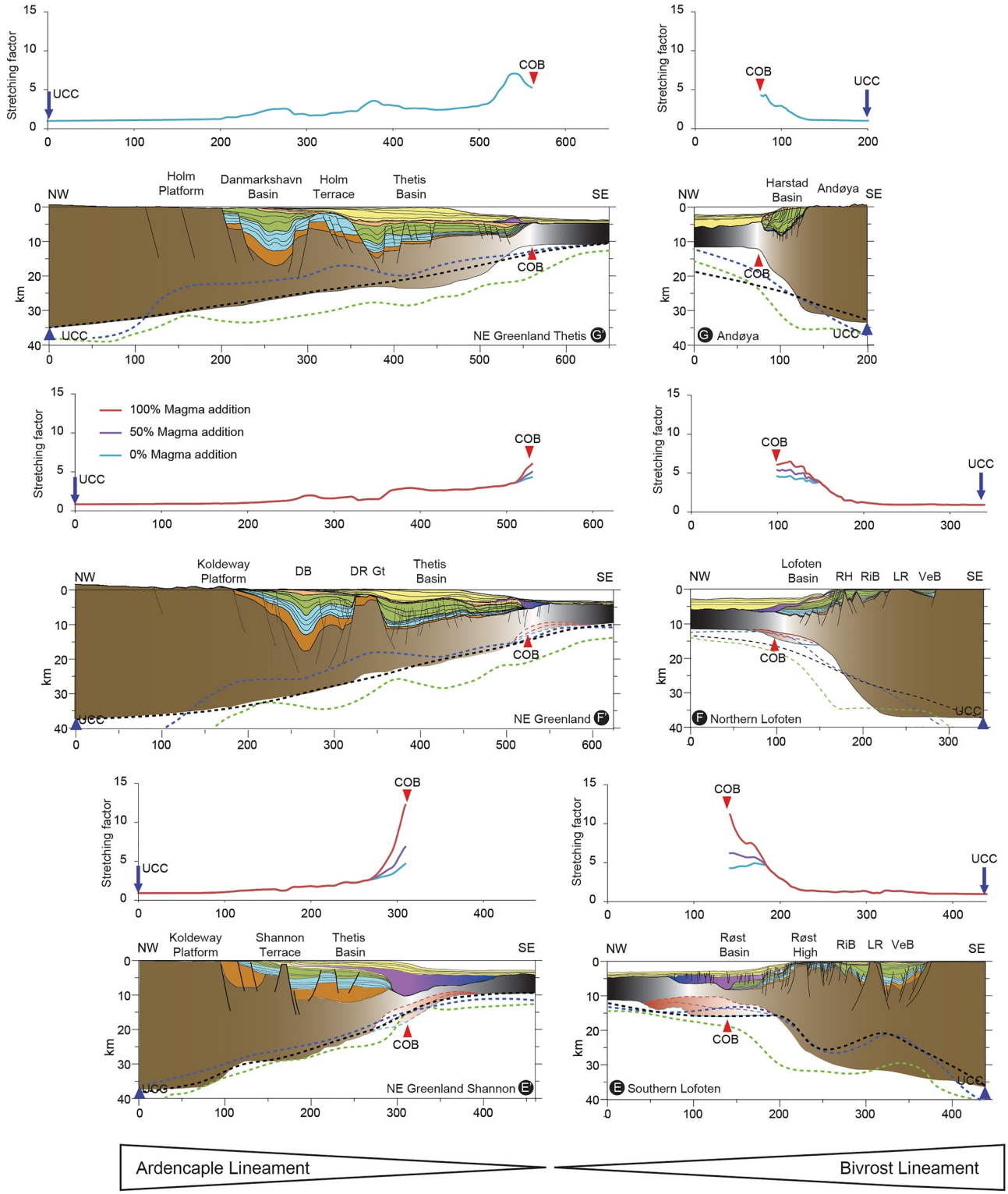


**Figure 9.** Conjugate crustal transects across the Lofoten-Vesterålen and NE Greenland conjugate margin segments (E-E', F-F', and G-G'). The crustal stretching factor curve for the different amounts of magma addition (0%, 50%, and 100%) are drawn above each crustal transect. No Lower Crustal Body is recorded for the conjugate crustal transect G-G'. The Lofoten-Vesterålen and its conjugate margin segment are separated from the Vøring and its conjugate margin segments by the Bivrost Leneament on the Norwegian side and the Ardencaple Lineament on the Greenland side. DB: Danmarkshavn Basin; DR: Danmarkshavn Ridge; Gt: Germania Terrace LR: Lofoten Ridge; RiB: Ribban BasinVB: RH: Røst High; VeB: Vestfjorden Basin. See Table 1 for more information about the crustal transect build up.

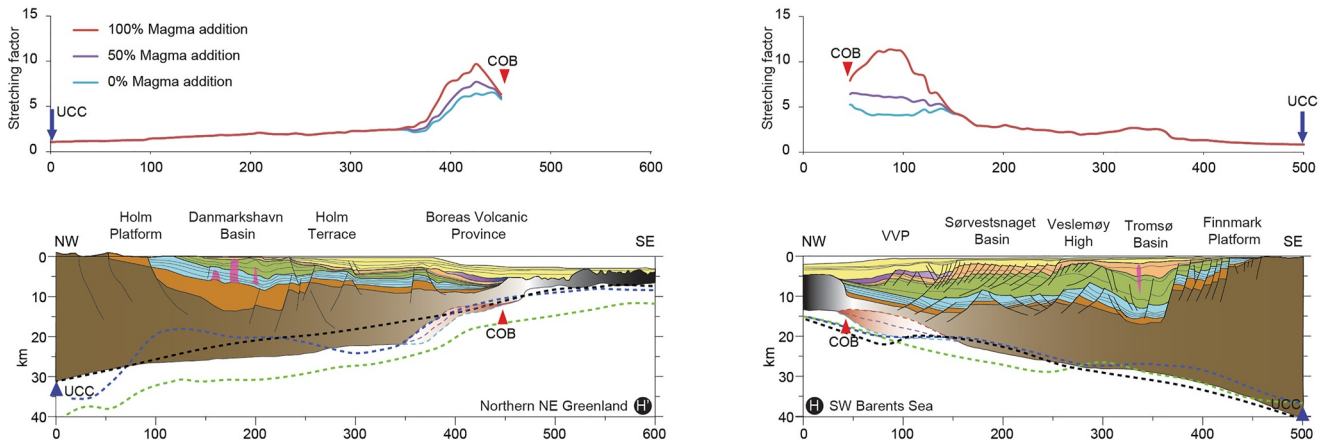


**Figure 10.** Conjugate crustal transects (H-H') across the SW Barents Sea and the Northern NE Greenland conjugate margin segments. The crustal stretching factor curve for the different amounts of magma addition (0%, 50%, and 100%) are drawn above each crustal transect. The transect on conjugate sides crosses salt structure. The sedimentary basins in these two profiles are highly affected by the strike slip movement that affected these areas during the long extensional processes. See Table 1 for more information about the crustal transect build up.

thicknesses of 6–7 km locally, whereas the Middle Triassic to Jurassic sequences show relatively uniform thickness (5 km on average) with a gradual thinning toward the SE border. In the central Vøring transect (Figure 8, profile C), the late Paleozoic rift system forms a series of half-grabens mostly controlled by major east-dipping faults. The BCU is much deeper in the Vøring Basin and reaches a maximum depth at around 13–15 km in the Træna and Rås basins. The average BCU depth along the structural highs ranges between 6 and 10 km, with the shallowest depths interpreted in the Northern Vøring profile at the Utgard High and toward the Vøring Marginal High.

The Moho depth beneath the Trøndelag Platform and coastal areas varies between 30 and 35 km (Figure 8). The Vøring Basin is underlain by continental crystalline crust characterized by $V_p$ of ~6.0–6.9 km/s and a thickness of 5–10 km. A LCB is clearly identified in the Outer Vøring Basin but is limited or absent in the eastern part of the Vøring Basin (Figure 8). The COT across the Vøring Marginal High shows a thick crust of 20–25 km, and the LCB extends oceanward until magnetic chrons C22–C23. Low values of crustal stretching are calculated for the inland and along the platform domain. Elevated crustal stretching occurs at the deepest depocenters (e.g., Træna Basin, Rås Basin, Vigrid Syncline and Hel Graben) where a thin continental crystalline crust is interpreted. Similarly to the Møre margin transects, the interpretation of the LCB nature (magmatic or not) influences the calculated crustal stretching/thinning.

### 4.1.3. Lofoten-Vesterålen Margin

Three profiles across the LVM segment (profiles E–G) are shown in Figure 9. The widest portion of LVM (~150 km in south Lofoten margin) is positioned just north of the Bivrost Lineament and close to the Vøring Margin, while the LVM narrows toward the north (~35 km offshore Andøya) when approaching the Senja Fracture Zone in the vicinity of the SW Barents Sea (Figures 1 and 9). A striking feature of the continental shelf along the LVM is the relatively thin sequence of Jurassic-Triassic sediments. The occurrence of older sedimentary rocks is uncertain, though Paleozoic strata might be present in the deepest parts of the area (Figure 9). The narrow, NE-SW-trending Ribban and Vestfjorden basins contain thick Cretaceous sequences. Pre-Cretaceous and Cretaceous structural levels in the Røst Basin to the west are interpreted below the breakup-related intrusives and extrusives.

The Moho depth along the LVM varies from 35 to 40 km beneath the coastal areas to 11 km in the outer part of the margin domain (Figure 9). The depth to basement varies from <1 km to >10–12 km in the Vestfjorden Basin. Along the LVM, the LCB has a very limited extent with a rapid decrease in thickness toward the oceanic domain where it disappears at the location of magnetic chron C23. The thicker LCB (~4 km) is situated along the COB in the Røst Basin, whereas a thinner LCB is interpreted farther north beneath the inner part of the Lofoten Basin. The LCB is absent farther north in the northern part of the LVM. Low crustal stretching values are calculated

inland and along the coastal domain. A regular increase of the stretching factor toward the COB is noticed in the crustal transects of the LVM. The effect of the LCB on the crustal stretching decreases northward due to the decrease of its thickness (Figure 9). No LCB is interpreted in the Andøya profile (profile G).

#### 4.1.4. SW Barents Sea Margin

A profile (H) crossing the SW Barents Sea is shown in Figure 10. The profile comprises different structural provinces along strike, including the Finnmark Platform, the Tromsø Basin, the Veslemøy High, the Sørvestsnaget Basin, and the Vestbakken Volcanic Province. Therefore, the profile includes a wide range of lithological units of different ages, from Proterozoic craton to late Paleozoic early Cenozoic rift basins; and volcanics related to the Eocene continental breakup from Greenland. The inner part of the profile is characterized by thick sequences of Upper Paleozoic sedimentary strata, whereas thick Cretaceous strata characterize the Tromsø Basin and the Sørvestsnaget Basin where the BCU reaches 10–13 km depth. The transect shows a laterally complex architecture of the crystalline crust with thicknesses ranging from 40 km toward the continent to 12 km beneath the deep Cretaceous basins. Assuming an original/reference, post-Caledonide, crustal thickness of 35 km in the offshore area, the cumulative crustal stretching along the inner part of the profile is less than 1.5. Local crustal stretching values approach 3 in the area where the Tromsø and Sørvestsnaget basins reach depths of more than 15 km. An increase of crustal stretching in the Vestbakken Volcanic Province is correlated with the thinning of the crust and the occurrence of LCB toward the oceanic domain.

#### 4.1.5. Central-East and Northeast Greenland Margins

Several profiles across the Central-East and the NE Greenland margins (A'–H') are shown in Figures 7–10. The Blosseville-Jan Mayen (A') and the Jameson Land-Jan Mayen (B') profile are a merged and composite profiles of the Central-East Greenland and the JMMC. In the profile A', extrusives are lying directly above the basement in the Blosseville area (Figure 7). However the deep crustal structure is less known since there is no onshore/offshore seismic reflection/refraction data in the area. Most of the crustal constraints are based on seismic compilation (Funck, Erlendsson, et al., 2017) and gravity inversion data (Haase et al., 2017; Lebedeva-Ivanova et al., 2019). The profile B' is characterized by a 15 km deep Devonian-lower Mesozoic sedimentary basin that is bounded to the east by the Liverpool Land Ridge (Figure 7). To the north of the West Jan Mayen Fracture Zone (Figure 1), thick Devonian to Cretaceous sedimentary strata are found in Traill Ø, Geographical Society Ø, and Hold with Hope area (Figure 8). This area is characterized by the occurrence of the Foster Volcanic Province, where thick volcanic layers (2–4 km) are draped by Eocene and younger sediments (profiles C' and D'). The nature of the crust below the Foster Volcanic Province is debated and is interpreted as basalt and synrift sediment (Voss and Jokat, 2007) or oceanic crust. However the limited amount of seismic reflection data combined with the sub-basalt imaging problem, makes the determination of the nature of this transition area challenging. The Foster Basin is interpreted as the seaward extension of the Late Paleozoic to Mesozoic onshore basins. The Foster Basin may continue northward across the East Greenland shelf into the Danmarkshavn Basin.

Offshore NE Greenland (profiles E'–H'), the Danmarkshavn and Thetis basins are the two main sedimentary basins, which are separated by the Danmarkshavn Ridge (Figure 9). The Danmarkshavn Basin is a 15–17 km deep Paleozoic and Mesozoic sedimentary basin that broadens to the north where Carboniferous-Lower Permian salt diapiric structures appear to be similar to those in the SW Barents Sea. The Danmarkshavn Ridge may be divided into a southern and northern segment that are offset dextrally (Figure 1b). The northern segment separates the Danmarkshavn Basin from the Germania Terrace, whereas the southern segment separates the Shannon Terrace from the Thetis Basin. The Thetis Basin developed during the late Jurassic-early Cretaceous and late Cretaceous-Paleocene rifting phase. The basin is widest in the north and narrows to the south where it terminates against the COB. The basin is up to 10 km deep and heavily influenced by sill intrusion complexes. In the north, the Wandel Sea Basin (80°N–83°N) is dominated by widespread marine Carboniferous-Triassic sediments, overlain by Mesozoic sediments that were deposited in pull-apart basins formed along the Trolle Land Fault Zone (Figure 1). The Trolle Land Basin in the north is believed to have been initiated during Late Cretaceous to Early Paleocene rifting and evolved into a shear margin along Greenland and Svalbard since the initial breakup in the early Eocene.

Integrated geophysical and geological studies have revealed pronounced along-strike differences in the crustal architecture of the East and NE Greenland margin. To summarize the above, on the East Greenland margin

segment, the Moho shallows from ~40 km onshore of the Scoresby Sound to 25 km below the Jameson Land Basin. The Moho depth in the NE Greenland margin varies from 35 km to 11–14 km near the oceanic crust. The thicker part (12–16 km) of the LCB is situated below the Foster Volcanic Province. Along the Thetis margin, the thickness of the LCB does not exceed 4 km. Similarly to the mid-Norwegian margin, the LCB thickness decreases at magnetic chrons C23–C22 and merges into oceanic layer 3. Low crustal stretching values (stretching factor close to 1) are calculated inland and along the platform domain, whereas high crustal stretching (stretching factor up to 4) occurs oceanwards. If we consider that the Foster Volcanic Province is an oceanic plateau, most of the LCB is mapped on the oceanic domain and appears to not affect much the crustal stretching along each transect.

#### 4.1.6. Jan Mayen Microcontinent

Two profiles across the JMMC are shown in Figure 7A' and 7B'. The Jan Mayen profile (A') represents the southern region of the microcontinent. The JMMC includes continental fragments that were part of the pre-breakup rifted system located between the Faroe Plateau, the outer Vøring Basin and Greenland prior to continental breakup at the earliest Eocene. The separation of the JMMC from Greenland took place in the earliest Miocene at around 22 Ma (Polteau et al., 2019). The main structural and tectonic features are well imaged by the seismic data, including the Jan Mayen Ridge (JMR) and the Jan Mayen Basin. Upper Paleozoic sedimentary strata are interpreted in the deeper part of the Jan Mayen Basin underlying the Cenozoic sediments. On the JMMC, the Moho depth is at around 18–20 km below the JMR and shallows on both sides toward the COB. The main part of the JMR is underlain by 15–16 km thick continental crust. From recent seismic data (Blischke et al., 2019; Peron-Pinvidic et al., 2012b), a LCB was recorded at the base of the crust at the central-eastern part of the JMMC passive margin (e.g., Breivik et al., 2012). The crustal stretching along the JMMC ranges between 2 and 3 and increases toward the COB to more than 5.

### 4.2. Total Pre-Drift Margin Extension Inferred From Observations

The average crustal stretching and the total pre-drift extension calculated from the observed crustal geometries along the conjugate transects of the NE Atlantic margin are indicated in Figure 11. These values are calculated for a reference initial crustal thickness of 35 km and proportion of magma addition of 0%, 50%, and 100% to the LCB (Table 2). The standard deviations from the mean crustal stretching and total extensions are computed for each transect and they document the effect of the proportion of magma addition in the LCB. On the Norwegian side, the average crustal stretching factor ranges between 1.87 in the Andøya transect to 3.01 for the Northern Vøring transect. The Vøring margin segment records the highest average crustal stretching followed by the Møre margin segment. The lowest average crustal stretching is calculated for the LVM segment. On the Greenland side, the calculated average crustal stretching ranges between 1.12 and 2.52. The lowest average crustal stretching is calculated for the Central-East segment (profiles B'–D'), whereas the highest crustal stretching is found in the NE Greenland margin segment where the average crustal stretching increases northward as a consequence of the widening of the margin. In the Blosseville area (profile A'), the crustal structure is not well constrained because of the limited coverage of seismic data, resulting in increasing the uncertainties in building and accurate crustal transect and in crustal stretching values. In the Central East Greenland margin segment, the crustal nature of the COT is not well constrained (profiles C' and D'), and therefore the crustal stretching values are even more uncertain there. The conjugate H-H' profiles record crustal stretching factors of 2.96 and 2.52, respectively. Unlike the other profiles, which are sub-orthogonal to the COB, the H-H' profiles are actually oblique to the COB along the SW Barents Sea and the Northern NE Greenland segments. Hence, the sedimentary basins in these two profiles are highly affected by strike-slip movement. As a consequence of this, the stretching factors calculated in theses transect could be overestimated.

The total extension values correspond to the total extension of the margin since the mid-Permian and represent the cumulative effect of the successive rifting phases until the time of breakup (Figures 11 and 12; Table 2). On the Norwegian side, the total extension values range between 40 and 284 km. The lowest total extension is calculated for the LVM segment across the Andøya crustal transect (G), while the highest total extension value is found in the central Vøring transect (C). On the Greenland side, the total extension values range from 33 to 226 km. The lowest total extension is calculated for the Central-East Greenland, while the widest total extension value is found in the NE Greenland segment (Figure 12A). Note that assuming the COT as continental for the central East Greenland results in a larger total extension in the area. The Møre and Vøring margin segments experienced much more extension than the Central-East Greenland. On the contrary, farther north, most of the extension is

10.1029/2022TC007386

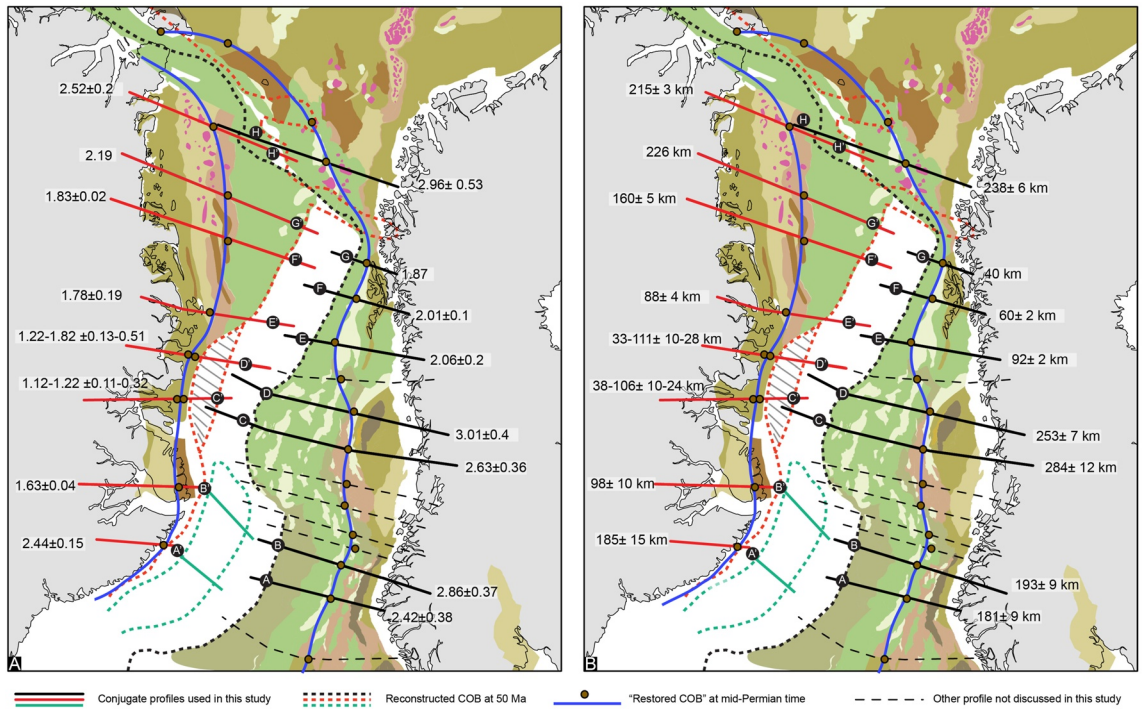


**Figure 11.** (A) average crustal stretching factor calculated from observed crustal structure along the eight conjugate profiles. (B) the total extension along the conjugate profile calculated from observed crustal structure. This allows to "restore" the continent-ocean boundary (COB) at its position at the mid-Permian time. The standard deviations from the mean crustal stretching and total extensions are computed for each transect and they document the effect of the proportion of magma addition in the Lower Crustal Body. For the profiles (C') and (D') we used the oceanward and the landward interpreted COB to calculate the total extension. However both version give a close result for the "restored" COB. The margins are reconstructed to an approximate post-breakup time (~50 Ma).

focused on the NE Greenland margin, whereas the least extension occurred in the LVM segment. The results show an asymmetric distribution of the total extension between the different conjugate parts of the NE Atlantic (Figures 11 and 12). Along the conjugate profiles H-H' the total extension is 238 and 215 km, respectively. These values represent an overestimation probably related to the strike-slip component of the two transects since they present high obliquity to the COB. Assuming a continental nature for the transition crust in profiles C' and D', the sum of the total pre-breakup extension along the NE Atlantic conjugate crustal transects ranges between 181 and 328–390 km with an average of 270–295 km (Table 3 and Figure 12B). Similarly, the sum of the total extension along the SW Barents Sea and the Northern NE Greenland conjugate crustal transects is 454 km (Table 3).

### 4.3. Reconstruction of Multi-Rift Phases

The reconstructed pre-breakup tectonic and thermal history of the 16 conjugate transects is based on the assumption that the margin evolution is controlled by lithosphere extension. For each conjugate transect, we run various extensional models incorporating or not geological complexities. Models incorporating late Paleocene-early Eocene mantle thinning, simulating the arrival of the hot Icelandic mantle "plume," and taking into account magmatic processes (melt retention and magmatic underplate) and mantle phase transitions satisfactorily reproduce the specific observations of the outer volcanic margin (Gac et al., 2021). The total extension values calculated from TecMod for the best-fit models (M2) are compared to the total extension inferred from observations (Tables 2–3 and Figures 12A, 12B, and 13).

#### 4.3.1. Blosseville-Jan Mayen and Southern Møre Transects (Lines A-A')

The modeled present day cumulative total extension since mid-Permian time is ~120 km for the Jan Mayen transect and 205 km for the conjugate Southern Møre transect (Tables 2–3, Figure 12A and Figures 13A and 13A'). The cumulative crustal stretching is mild (~2) and evenly distributed along the Blosseville-Jan Mayen transect. Most of the extension takes place during the final Late Cretaceous-Paleocene rifting phase (Figures 14A

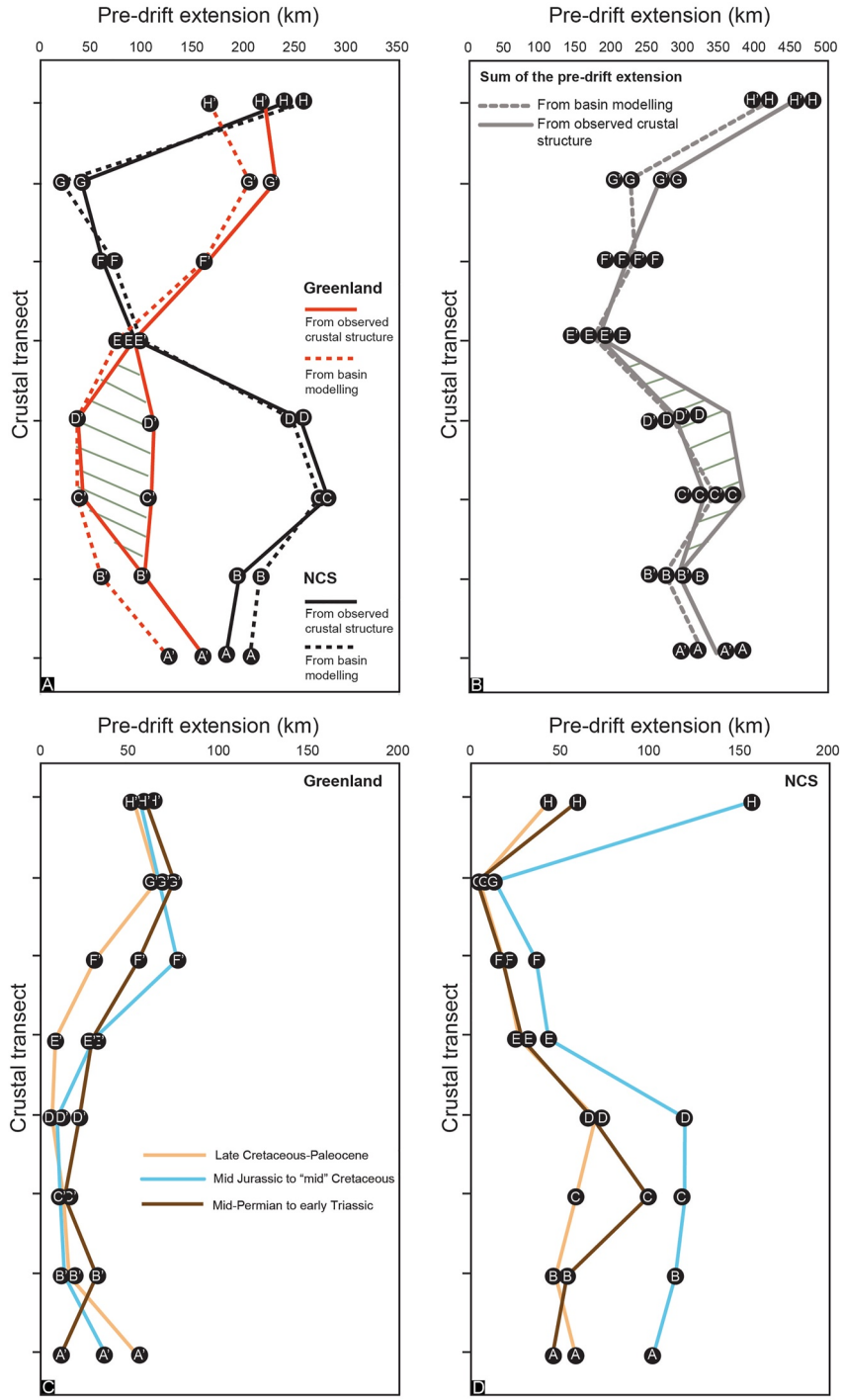


**Figure 12.** (A) pre-drift extension value for each crustal transect along the Norwegian Continental Shelf and Greenland calculated from observed crustal structure and basin modeling. Profiles run from south (A/A') to north (H/H'). (B) sum of the total pre-breakup extension along the NE Atlantic conjugate crustal transects Greenland calculated from observed crustal structure and basin modeling. The hatched area indicate the uncertainties related to the nature of the transition crust situated in the Central East Greenland. (C) pre-drift extension for the main extensional episodes on the Greenland calculated from basin modeling. (D) pre-drift extension for the main extensional episode on the Norwegian Continental Shelf calculated from basin modeling.

**Table 3**
*Sum of the Total Extension (km) Deduced From Observed Crustal Structure (Magma Addition 50%; Table 2) and Basin Modeling for Each of the Conjugate Profiles (A/A'–H/H'), Listed in North to South Order*

| | Observed crustal structure (50% magma addition) | | Basin modeling | |
|---|---|---|---|---|
| Profile | Total extension (km) | Sum (km) | Total extension (km) | Sum (km) |
| | SW Barents Sea and Northern NE Greenland conjugate margin profiles | | | |
| H-SW Barents Sea | 238 | 454 | 257 | 421 |
| H'-Northern NE Greenland | 215 | | 165 | |
| Average | 227 | | 211 | |
| | NE Atlantic conjugate margin profiles | | | |
| G-Northern Lofoten Andøya | 40 | 266 | 21 | 225 |
| G'-NE Greenland Thetis | 226 | | 204 | |
| F-Northern Lofoten | 61 | 221 | 71 | 231 |
| F'-NE Greenland | 160 | | 160 | |
| E-Southern Lofoten | 92 | 181 | 98 | 173 |
| E'-NE Greenland Shannon | 88 | | 75 | |
| D-Northern Vøring | 253 | 287–364 | 245 | 281 |
| D'-NE Greenland Foster | 33–111 | | 36 | |
| C-Central Vøring | 284 | 328–390 | 276 | 312 |
| C'-CE Greenland Traill Ø | 38–106 | | 36 | |
| B-Central More | 194 | 292 | 214 | 273 |
| B'-Jameson Land/Jan Mayen | 98 | | 59 | |
| A-Southern Møre | 181 | 366 | 205 | 325 |
| A'-Blosseville/Jan Mayen | 185 | | 120 | |
| Average | 138–149 | 270–295 | 132 | 264 |

*Note.* Uncertainties related to the location of the continent-ocean boundary (profile C' and D') could trigger some variation in the amount of the total extension. Fortunately, the results show comparable estimates between the two methods.

and 14A'). On the conjugate wider southern Møre margin, the extension is more pronounced. A maximum cumulative crustal stretching of more than 3 is modeled over the distal margin. The mid-Permian, mid-Jurassic-early Cretaceous and Cretaceous rifting phases are mild and focus on the intermediate margin (Figures 14A and 14A'). Extension during the late Cretaceous-Paleocene rifting phase is much more modest at the intermediate and distal margins but very large toward the COB.

#### 4.3.2. Jameson Land-Jan Mayen and Central Møre Transects (Lines B-B')

The modeled present day cumulative total extension since mid-Permian time is ~59 km for the Jameson Land-Jan Mayen transect and 214 km for the conjugate Central Møre transect (Tables 1–2, Figure 12A and Figures 13B and 13B'). The cumulative crustal stretching ranges between 1 and 2 along the entire Jameson Land-Jan Mayen transect, indicating negligible extension except during the initial and modest mid-Permian rifting phase in the Jameson Land Basin (Figures 14B and 14B'). On the conjugate Central Møre margin, the extension is more pronounced with a maximum cumulative stretching factor of 4 modeled over the Vigra High where the rifting phases focused during the mid-Permian, late Jurassic-Early Cretaceous and mid-Cretaceous. Extension during the late Cretaceous-Paleocene rifting phase is more modest and focusses toward the COB.

#### 4.3.3. Trail Ø and Central Vøring Transects (Lines C-C')

In the COT area of the Central East Greenland Margin we did not build a stratigraphic model because of the large uncertainties driven by limited data and poor imaging below the thick lava pile (profile C' and D'). Since the "restored" COB in the area using observed crustal structure and considering the landward and oceanward

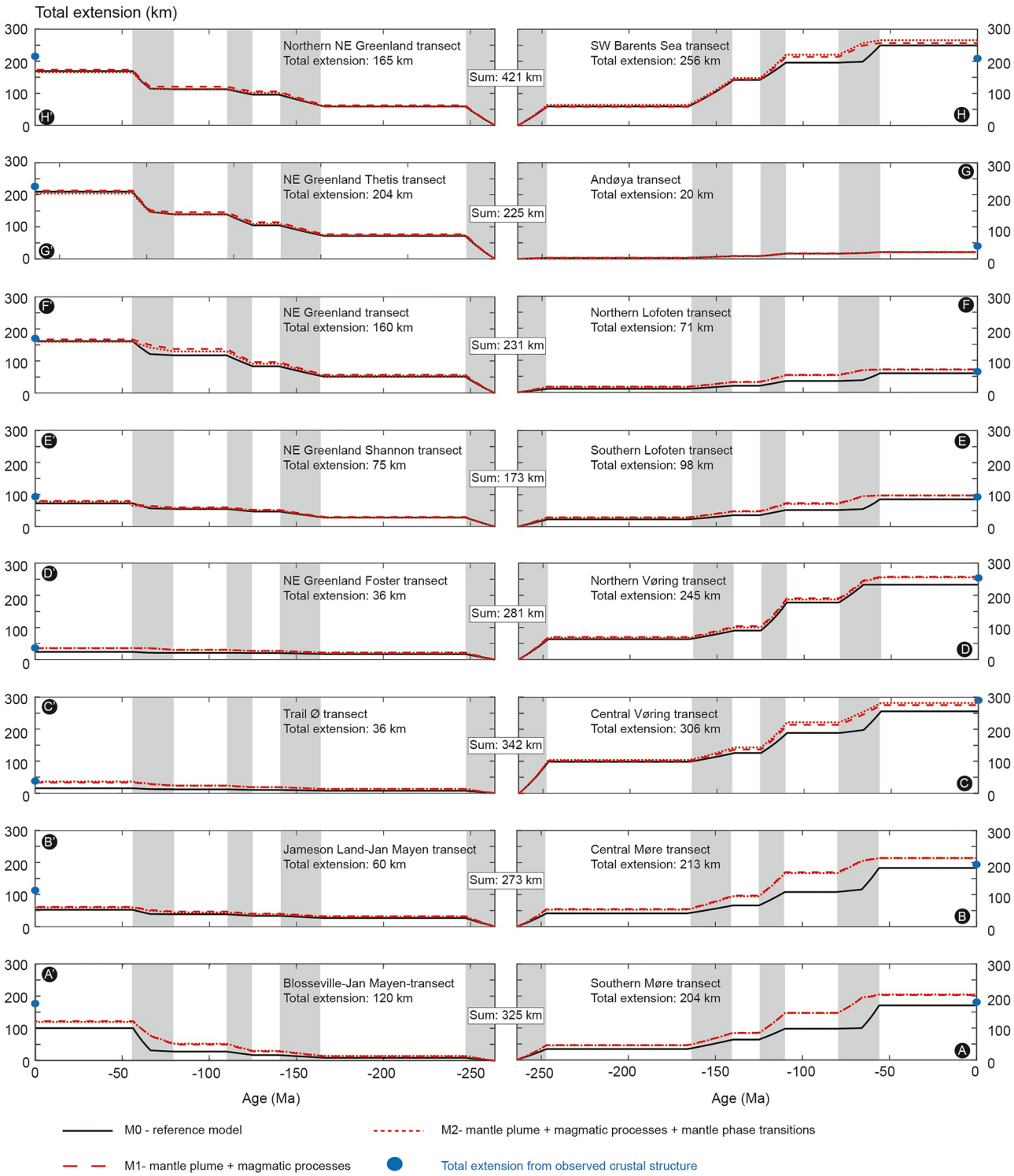


**Figure 13.** Modeled pre-drift margin widths through time for the eight conjugate profiles. The different extensional phases are indicated by the gray area. The blue dots represent the pre-drift margin widths estimated from the observed stretching factors for a 50% magma addition in the Lower Crustal Body. The pre-drift margin width is calculated for a reference model M0 before introducing more processes to satisfy the geological observation. M1 models involve mantle plume and account for magmatic processes such as melt retention and magmatic underplate. M2 Models are similar to M1 model but in addition, we account for the mantle phase transitions during extension.

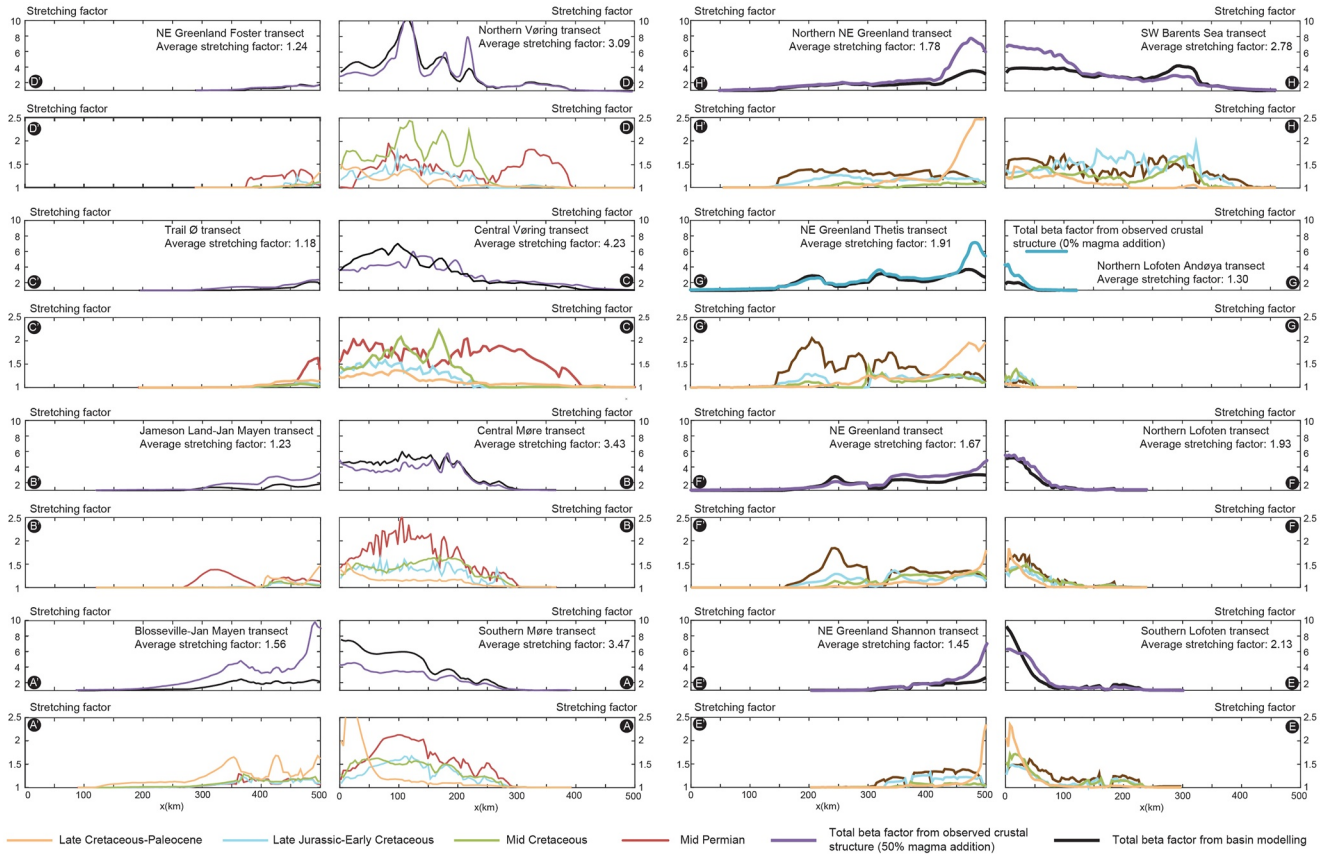


**Figure 14.** (In two parts) Modeled total crustal stretching factors curve calculated along the eight conjugate profiles from north (H/H') to south (A/A'). Results are extracted from forward basin modeling for the best-fit model M2. For the sake of comparison, we plot in the same graph the crustal stretching factors curve defined from observed crustal structure with a 50% magma addition in the Lower Crustal Body. From the basin modeling, we extract the stretching factors for the individual rift phases.

COB scenarios give comparable location (Figure 11), we used the landward COB for the modeling. However, we should keep in mind that the total extension calculated along profile C' and D' may be underestimated. The present day cumulative total extension since mid-Permian time is ~36 km for the Traill Ø transect and 276 km for the conjugate Central Vøring transect (Tables 2–3, Figure 12A and Figures 13C and 13C'). The cumulative crustal stretching ranges between 1 and 2 along the entire Trail Ø transect indicating low extension values, with the exception of the observed modest extension during the initial mid-Permian rifting phase (Figure 14C'). On the conjugate Vøring margin, the extension is much more pronounced with a maximum cumulative crustal stretching of five modeled over the Vigrid Syncline. A regional trend can be seen in the stretching factor distributions, with the main axis of extension roughly migrating westward until the Eocene. Again, the extension is maximum during the first modeled mid-Permian rifting phase, and during the mid-Cretaceous phase but milder during the late Jurassic and the final late Cretaceous-Paleocene rifting phases.

### 4.3.4. NE Greenland Foster and Northern Vøring Transects (Lines D-D')

The present day cumulative total extension since mid-Permian time is ~36 km for the NE Greenland Foster transect, while it is much larger (~245 km) for the conjugate Northern Vøring transect (Tables 2–3, Figure 12A, and Figures 13D and 13D'). Across the narrow NE Greenland margin (Figures 13D and 13D'), the cumulative crustal stretching ranges between 1 and 2 along the entire transect, indicating negligible extension except for the observed modest extension during the initial mid-Permian rifting phase. On the conjugate Northern Vøring margin, the extension is much more pronounced. A maximum crustal stretching of 9 is modeled over the deep Hel Graben (Figure 14D). Maximum stretching occurred during the mid-Cretaceous rifting phase when the stretching was the highest over the Hel Graben, Någrind Syncline and Træna Basin, but absent farther east. In contrast,

extension is modest during the mid-Permian, late Jurassic-early Cretaceous and late Cretaceous-Paleocene rifting phases. A regional trend can be seen in the stretching factor distributions, with the main axis of extension roughly migrating westward until the Eocene. The Trøndelag Platform was the main focus of extension during the mid-Permian time (e.g., Bunkholt et al., 2021). The extension is maximum during the modeled mid-Cretaceous rifting phase and modest during the mid-Permian, Late Jurassic-Early Cretaceous and Late Cretaceous-Paleocene rifting phases (Figure 14D).

#### 4.3.5. NE Greenland Shannon and Southern Lofoten Transects (Lines E-E')

The present day cumulative total extension since mid-Permian time is almost evenly distributed between the two conjugate margins with ~75 km for the NE Greenland Shannon transect and ~98 km for the conjugate Southern Lofoten transect (Tables 2–3, Figure 12A, and Figures 13E and 13E'). Along the NE Greenland Shannon transect, the cumulative crustal stretching is generally low but tends to increase eastward, and it reaches a maximum value of ~2 at the COB (Figures 14E and 14E'). The mid-Permian, mid-Jurassic-early Cretaceous and mid-Cretaceous rifting phase are evenly distributed on the eastern half of the margin, with extension being the highest for the oldest rifting phases. The crustal stretching strongly focusses at the COB in the late Cretaceous-Paleocene rifting phase, where it reaches a value of ~2. For the conjugate Southern Lofoten transect, the maximum cumulative stretching factor is ~4 near the COB. The extension is maximum during the modeled mid-Permian and late Cretaceous-Paleocene rifting events and focuses toward the COB during the final late Cretaceous-Paleocene rifting phase.

#### 4.3.6. NE Greenland and Northern Lofoten Transects (Lines F-F')

The modeled present day cumulative total extension since mid-Permian time is ~160 km for the NE Greenland transect at the expense of only ~71 km for the Northern Lofoten transect (Tables 2–3, Figure 12A, and Figures 13F and 13F'). The cumulative crustal stretching is evenly spread along the NE Greenland margin with an average value of 2 (Figures 14F and 14F'). Extension was strongest during the mid-Permian rifting phase, and the crustal stretching reaches almost 2 at the Danmarkshavn Basin. Extension at later rifting phases is more modest, varying between 1 and 1.5. During the late Cretaceous-Paleocene rifting phase, the extension focused close to the COB region where crustal stretching reaches a value above 2. Along the conjugate Northern Lofoten transect, the cumulative crustal stretching concentrated on the western side of the transect to reach a maximum value of 5 at the COB. The individual crustal stretching factors are evenly distributed across the Lofoten Basin at the mid-Permian, mid-Jurassic-early Cretaceous and mid-Cretaceous rifting phases, but converge to the COB during the late Cretaceous-Paleocene rifting phase. The extension is maximum during the modeled mid-Permian and late Cretaceous-Paleocene rifting phases.

#### 4.3.7. NE Greenland Thetis and Lofoten Andøya Transects (Lines G-G')

The modeled present day cumulative total extension since mid-Permian time is ~204 km for the NE Greenland Thetis transect while it is only 21 km for the conjugate Andøya transect (Tables 2–3, Figure 12A and Figures 13G and 13G'). The cumulative crustal stretching on the North-East Greenland margin has two peaks, each reaching a value of ~3 that correlate with the formation of the Danmarkshavn and Thetis basins. The cumulative crustal stretching reaches a maximum value of 4 near the NE Greenland COB (Figures 14G and 14G'). The individual crustal stretching factors are distributed evenly along the entire transect. Extension was the strongest during the mid-Permian rifting phase with stretching factor values of ~2 in the Danmarkshavn Basin. Extension at later rifting phases is more modest, varying between 1 and 1.5. During the late Cretaceous-Paleocene rifting phase, the extension dramatically focusses close to the COB region where crustal stretching factor reaches a value of 2. The conjugate Andøya Transect, situated in the northern Lofoten-Vesterålen margin, is only ~50 km wide versus a ~300 km wide conjugate NE Greenland Thetis Margin. The cumulative stretching factor achieves a maximum value of ~2 near the COB. The individual crustal stretching factors are, in general, evenly distributed along the full transect at the mid-Permian, mid-Jurassic-early Cretaceous and mid-Cretaceous rifting phases, but is concentrated close to the COB during the late Cretaceous-Paleocene rifting phase. Similar to the other transects, the extension is maximum during the modeled mid-Permian and late Cretaceous-Paleocene rifting phase.

#### 4.3.8. Northern NE Greenland and SW Barents Sea Conjugate Transects (Lines H-H')

The present day cumulative total extension since mid-Permian time is ~165 km for the Northern NE Greenland transect, and 257 km for the SW Barents Sea conjugate transect (Tables 2–3, Figure 12A, and Figures 13H

and 13H'). Along the Northern NE Greenland transect the cumulative crustal stretching is ~2 along most of the transect and reaches a maximum value of 4 over the COB (Figures 14H and 14H'). The stretching factors of the individual rifting episodes are distributed evenly along the full transect on the Northern NE Greenland Margin. The amplitude of the stretching factor generally decreases from ~1.5 for the oldest mid-Permian phase, to almost 1 for the youngest late Cretaceous-Paleocene rifting phase. However, the final extension phase converges on the COB whereby crustal stretching reaches a high value of 2.5. Along the conjugate SW Barents Sea transect, the cumulative stretching factor has a sub-constant value of ~4 across the deep Cretaceous sedimentary basins but it is reduced to 1 over the Finnmark Platform. The stretching factors for the mid-Permian, mid-Jurassic-early Cretaceous and mid-Cretaceous rifting phases are, in general, distributed evenly along the full transect. The late Cretaceous-Paleocene rifting phase is almost non-existent toward the Finnmark Platform and is only recorded toward the Vestbakken Volcanic province to the NW (Figure 14H and 14H'). Similar to the other transects, the extension is maximum during the modeled mid-Permian and late Cretaceous-Paleocene rifting phases.

## 5. Discussion

Despite the time and effort spent studying the NE Atlantic geology, there remains the task of integrating the vast, spatially and temporally disparate data sets into a consistent plate reconstruction model for the entire NE Atlantic realm that also extends back to the earliest phases of the passive margin's formation. Initial plate configurations and syn-extensional reconstructions are frequently overlooked for the NE Atlantic area. Difficulties in quantifying time-dependent crustal stretching histories have led to a variety of permissible kinematic scenarios, usually with spatial or temporal limitations. Early iterations included restorations based on a static time and a single rotation (e.g., Bullard et al., 1965) and others have used a basic backstripping approach which accounts for variations of the stretching factors in time and space. For example, Skogseid et al. (2000) estimated the crustal extension along crustal transects crossing various margin segments of the Norwegian margins for the late Jurassic-Cretaceous and Maastrichtian-Paleocene rifting episodes. More recently, using a simple geometric crustal restoration approach, Barnett-Moore et al. (2018) estimated the amount of extension experienced by the North Atlantic conjugate margins since the earliest Jurassic. However, the existing reconstructions are problematic from several points of view as they include, but are not limited to: (a) high uncertainties due to derivations of approximate stretching factors (i.e., assumptions about initial crustal thickness being uniform along the margin); (b) inaccurate geometry of the sedimentary basin and associated crustal thickness; (c) often the studies are refined for a given region of the North Atlantic, and may cause overlaps and gaps in the restoration; (d) the Euler pole rotations are not consistently included; (e) difficulties in identifying the continent-ocean boundaries (COBs); (f) identification of the location of sequential rift hinges related to discrete rift episodes; (g) assumptions on the spatial distribution of rifting (e.g., depth-dependent localization); (h) controversial interpretations related to LCBs (i.e., whether magmatic origin, intruded continental origin, and to what degree) leading to over- or under-estimation of the crustal stretching. These common issues are further compounded by large uncertainties inherent to the used methods.

### 5.1. Deformable Plate Margins

In conventional paleogeographic reconstructions, major plates are assumed to be rigid with boundaries that can vary through time from being divergent, convergent and transform. Deformable plate kinematic models attempt to go a step beyond conventional paleogeographic reconstructions by restoring quantitatively the crustal deformation history of plate margins instead of using rigid plates with fixed geometries (Ady & Whittaker, 2019; Nirrengarten et al., 2018; Peace et al., 2019). In this study, we quantify the amount of pre-drift extension experienced by the NE Atlantic margins to restore the deformed continental margins. Our workflow is based on the classification of Ady and Whittaker (2019) who defined different approaches such as the averaged deformable margin and palinspastic deformable margin to restore the pre-drift margin geometry.

For the averaged deformable margin plate approach, the pre-drift extension is quantified by restoring the COB and the enclosed basins to their unstretched positions (assumed to be at the mid-Permian time) by using the stretching factors calculated from observed crustal thickness averaged along the transects. For the NE Atlantic conjugate transects the total extension is ranging between 181 and 328–390 km with an average of 270–295 km (Table 2 and Figure 12B). An averaged deformable margin plate model can produce good restoration results that

fit geological and geophysical constraints except in wide hyperextended margins (e.g., Nirrengarten et al., 2018). Unfortunately, an averaged deformable margin approach can provide neither the amount of extension caused by each individual rift phase nor the architecture of the sedimentary basins through time. In addition, this method incorrectly assumes that the deformation is distributed evenly in the direction of plate movement over the deformable part of the margin.

The palinspastic deformable margin approach can restore quantitatively the history of crustal deformation during multiple rifting phases and further accommodate asymmetry at continent margins, and is valid even for hyperextended margins (e.g., Ady & Whittaker, 2019). This approach allows to track the changes in stretching factor from the proximal to the distal parts of the margin through time along with the corresponding amount of extension for each rifting phase. In our study, the stretching factors of each rifting phase are provided by forward thermal-kinematic modeling along the conjugate 2D transects. The corresponding stretching factors provide a total extension ranging between 173 and 325 km with an average of 264 km (Table 2 and Figure 12B). Our modeling takes into consideration magma additions to the crust during the breakup time, but does not implement fault motions. The cumulative stretching factors and the pre-drift extension estimates, inferred from present-day crustal structure, successfully compare to the forward basin modeling values. The forward basin modeling can then be confidently used as a base to reconstruct the geometrical evolution and the isostatic response of the margin through time.

The main limitation in our method is that the 2D transects are not constrained by data of the same quality and resolution across the entire length of the conjugate NE Atlantic margins. Therefore, the accuracy of the stratigraphic model is highly dependent on the confidence in the interpretation of the sedimentary sequences in seismic reflection data. In addition, we used a reference crustal thickness of 35 km assumed to represent the unstretched crustal limit even for the areas where refraction data in the proximal domain show small variation with values ranging between 37 and 33 km. In the case of the mid-Norway rifted margin, the initial rifts were superposed on structures inherited from the Caledonian continental collisions. The structural, thermal and rheological conditions of the lithosphere at the onset of rifting must therefore have been highly heterogeneous, including mixtures of lithologies, suture zones, nappe stacks and thickened lithosphere (e.g., Peron-Pinvidic et al., 2020). Fortunately, sensitivity tests indicate that these small variations in crustal thickness have little effect on the results. Similarly, the presence of LCB, which complicates the quantification of the amount of extension, appears to affect our results only within small error bars/uncertainties.

Uncertainties related to the location of the COB could also induce some variation in the amount of the total extension. In this study, these uncertainties were minimized by picking the COB consistently using all available geophysical data. Furthermore the outline of our COB is well supported by the most relevant published COBs in NE Atlantic area region (e.g., Funck, Erlendsson, et al., 2017; Gaina et al., 2009). Palinspastic deformable margin plate kinematic models are relatively insensitive to picks in the COB (e.g., Ady & Whittaker, 2019). For example, an error of as much as 10 km with a beta factor of 10 at the plate margins would be reduced to 1 km, which is well within the resolution of a regional or global plate kinematic model. At last, the total extension along the Northern NE Greenland and the SW Barents Sea is over-estimated in these areas because of the higher obliquity of these transects and resulting strike-slip component during the long-term extensional processes. However, the cumulative total extension can give an upper limit of the overlap between these segments during the restoration process of the NE Atlantic.

### 5.2. NE Atlantic Margin Geometry

The crustal transects along the NE Atlantic margins (Figure 15) highlight the important changes in the dip direction of the major extensional faults on opposite conjugate margins. South of the Jan Mayen Fracture JMFZ, the architecture of the Møre margin is dominated by west-dipping crustal faults controlling the development of the deep Møre Basin (transects B'-B). On the conjugate side, the Jameson Land and Liverpool Land structures are characterized by an important extensional fault system dipping to the west (Figure 15). Seismic data along the JMMC also show dominantly west-dipping normal faults (Figure 15). In contrast, the major faults are east-dipping especially in the Northern Vøring area farther north along transect D'-D (Figure 15) (e.g., Gernigon et al., 2021). The deposition of the Paleozoic succession identified in the Trøndelag Platform is controlled by these east-dipping detachment faults that were most likely active since the post-Caledonian collapse. The Central-East Greenland conjugate margin is dominated by east-dipping extensional normal faults that participated in the development of

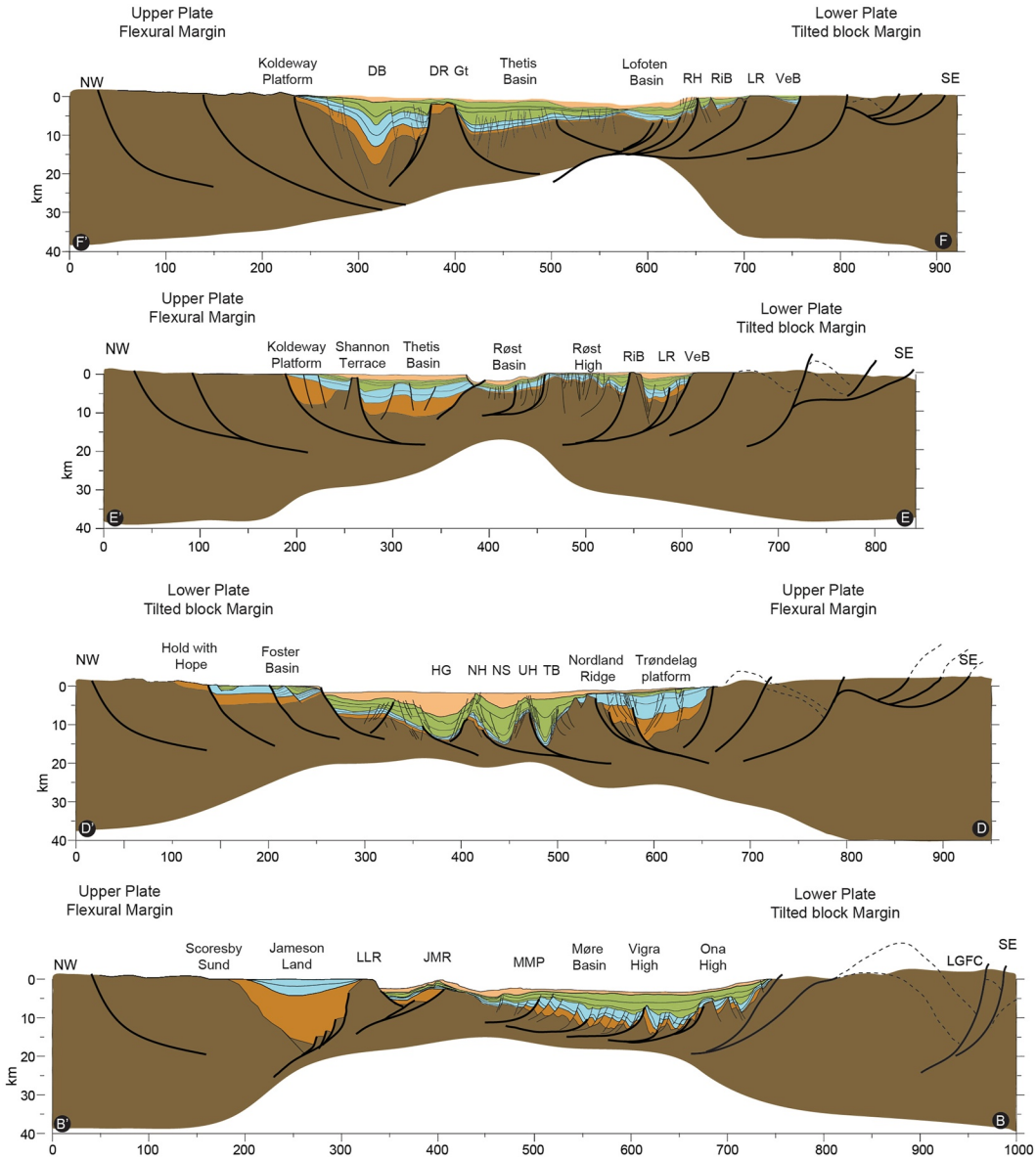


**Figure 15.** Restored conjugate crustal-scale cross-sections along the NE Atlantic (F-F', E-E', D-D', B-B').The Lofoten-Vesterålen (and conjugate) transect (F-F') shown with lower plate—tilted block geometry and all the major extensional faults dipping to the west. The NE Greenland conjugate transect (E-E') shows with an upper plate geometry with the important extensional faults dipping to the east. The Northern Vøring crustal transect (D-D') shows an upper plate geometry with the important extensional faults dipping to the east. The Møre (B-B') crustal transect shows a lower plate—tilted block geometry with all the major extensional faults dipping to the west. Onshore faults are recognized from surface structures (Braathen et al., 2002; Fossen et al., 2017; Mandler and Jokat, 1998). The profiles are extended landward in order to include Caledonian orogenic structures. DB: Danmarkshavn Basin; DR: Danmarkshavn Ridge; Gt: Germania Terrace; HG: Hel Graben; JMR: Jan Mayen Ridge; LGFC: Lærdal-Gjende Fault Complex; LLR: Liverpool Land Ridge; LR: Lofoten Ridge; MMP: Møre Marginal Plateau; NH: Nyk High; NS: Någrind Syncline; TB: Træne Basin; UH: Utgard High; RiB: Ribban BasinVB: RH: Røst High; VeB: Vestfjorden Basin. See Figure 17E for the location of the profiles.

important basins since the Permian (e.g., Surlyk, 1991) in agreement with geophysical studies (e.g., Schlindwein and Jokat, 2000). Along strike, major basin-bounding faults form relay-ramp structures such as in the Hold with Hope area (Peacock et al., 2000). On the LVM several west-dipping detachment faults are mapped and involved in the development of the sedimentary basins and the evolution of the margin (transects E-E' and F'F). The conjugate NE Greenland margin is controlled by east-dipping detachment faults.

The rifted margins offshore NE Greenland and mid-Norway show a structural asymmetry, which can be described in terms of upper-plate geometry or flexural margin vs. lower-plate geometry or tilted-block margin. The presence of listric faults and the configuration of a conjugate detachment system can control the resulting asymmetric rift geometry observed in the study area. The architecture of the conjugate crustal transects suggests that: (a) the asymmetry of the passive margin in the Møre Margin is of lower-plate or tilted-block margin type (e.g., Mosar et al., 2002), (b) the central Vøring Margin exhibits an upper-plate or flexural margin geometry, and (c) the LVM is of lower-plate or tilted-block margin type (e.g., Meza-Cala et al., 2021). The geometries of the margin segments and the detachment faults indicate a shift from a lower-plate to an upper-plate geometry between the Møre and the Central/Northern Vøring margin segments. On the contrary, a shift from upper- to lower-plate geometry is observed between the Central/Northern Vøring and the Lofoten-Vesterålen margin segments.

### 5.3. Palinspatic Reconstructions on a Selected 2D Conjugate Crustal Transect

We performed a detailed 2D palinspastic reconstruction at selected time-steps along the conjugate transect crossing the Lofoten margin and its NE Greenland conjugate (Figure 16). The 2D palinspastic reconstruction is based on the results of the forward basin model reconstruction of transect E-E'. However, the basin modeling approach

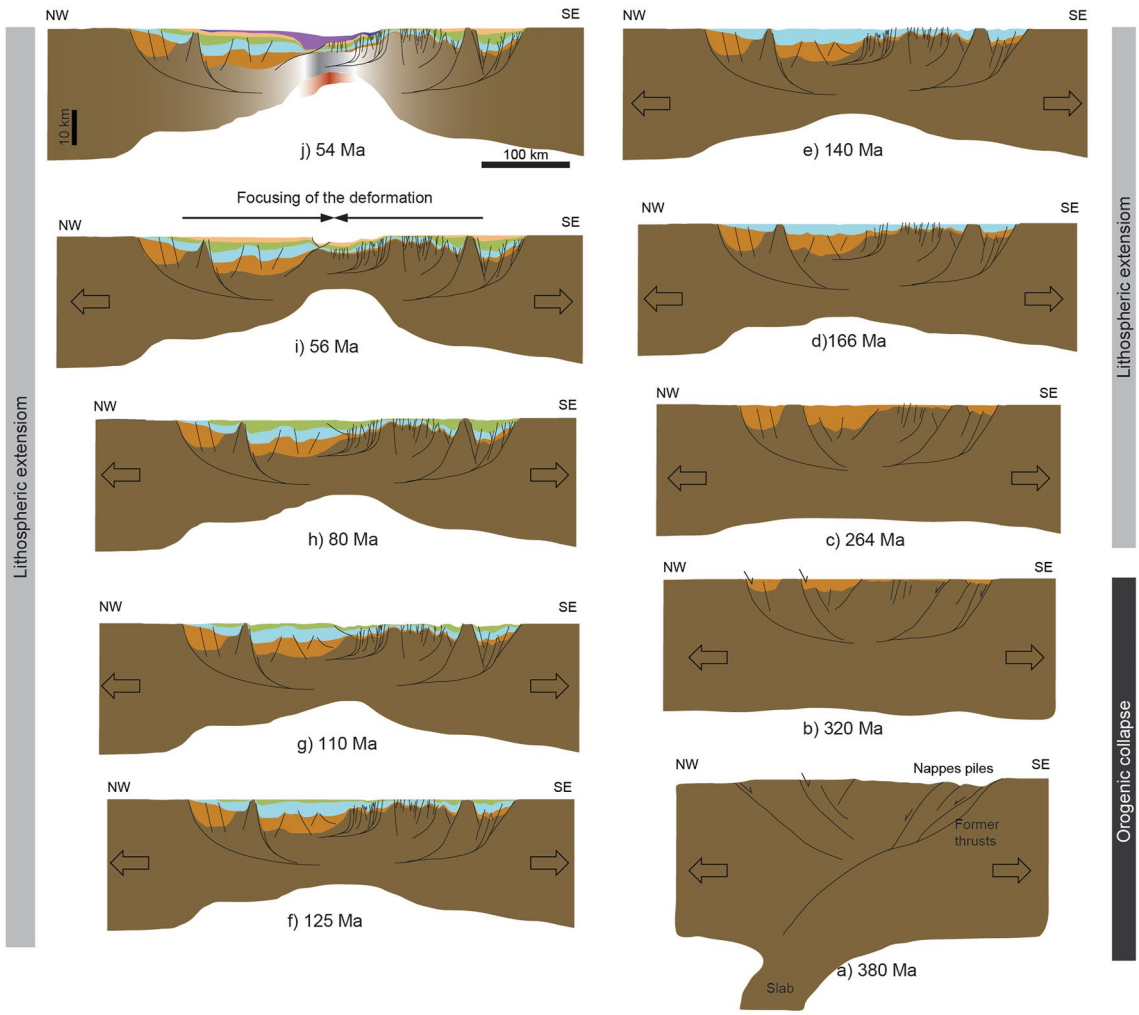


**Figure 16.** 2D palinspastic reconstruction of a selected conjugate transect (profile E-E') crossing the Lofoten margin and NE Greenland. The 2D palinspastic reconstruction is based on the results of the forward basin model reconstruction of transect E-E'. The basin modeling approach does not incorporate faulting, it does not allow for structural restoration and isostatic adjustments related to faults. Here we use the present-day structures and tentatively draw the different fault structures guided by the basin modeling restoration and geologic observation. On both margins, the initial rifts were superimposed on structures inherited from continental collisions of the Caledonian orogeny. The lithospheric structural, thermal and rheological conditions at the onset of rifting must therefore have been highly heterogeneous, including mixtures of lithologies, suture zones, nappe stacks and thickened lithosphere.

does not incorporate faulting and hence does not allow for structural restoration and isostatic adjustments related to faults. Therefore, we use the present-day structures to complete the 2D palinspastic reconstruction and tentatively draw the different fault structures guided by the basin modeling restoration and geological observations. The total extension is extracted from the forward basin model at each time step. In addition, the basin model provides the isostatic adjustment caused by the decompaction and removal of the corresponding sedimentary unit. The total extension for each time-step is determined backwards from the breakup time (~54–55 Ma) to the mid-Permian time (Figures 16c–16j). For the steps prior to mid-Permian, where the extension is mostly controlled by the post-Caledonian orogenic collapse (Figures 16a and 16b), the crustal configuration is speculative and based on geological observations (e.g., Peron-Pinvidic et al., 2020). Our palinspastic reconstruction shows both the locations of depocenters and exposed structural highs during the different time steps. This approach gives a first order indication on the crustal and the sedimentary basin architecture.

The fact that the pre-drift extension inferred from the present-day crustal structure compares well with the forward basin modeling values indicates that our approach is valid and useful. Structurally, the Lofoten margin is characterized by west-dipping major faults and acts as lower plate whereas the NE Greenland margin is marked by east-dipping major faults and acts as upper plate. The next step would be to combine the basin reconstructions modeled by TecMod2D with structural fault restoration provided by other modeling tools. This task, which is beyond the scope of this contribution, would allow more refined restorations that could include balancing and isostatic adjustments related to faults and faulting.

### 5.4. Manual Palinspatic Reconstructions for the NE Atlantic

We applied the same restoration approach, as for the selected transect in Figure 16, to all conjugate transects in order to derive palinspastic plate reconstruction maps of the NE Atlantic realm from breakup until the mid-Permian time (Figure 17). For this purpose we used the pre-drift extension values for the individual rift phases in order to restore the conjugate NE Atlantic conjugate margins. For each time step, the pre-drift margin width defines the incremental "restored COB" that are used to generate intermediate paleogeographic position. As a first step, we establish a manual restoration by fitting the incremental "restored COB" following the extensional direction for the different rifting phases and by minimizing the overlap and the underlap between "restored COBs" at incremental stages. The path of Greenland will give an indication of the regional extension at incremental steps back in time (Figure 17A). On the restored maps, we draw the location of the depocenters and structural highs defined by the basin modeling tool and the main structural features defined by seismic interpretation such as the salt structure and pre-Permian basins. A fully consistent digital plate restoration with Euler poles and finite rotations is the subject of an additional future paper.

#### 5.4.1. Devonian—Caledonian Collapse

The stage of orogenic collapse extends from 380 Ma until the mid-Permian time around 264 Ma (Figures 16a and 16b). Following continent-ocean subduction, Laurentia collided with Baltica during the Caledonian orogeny to form a thick crustal root during the Silurian (e.g., Roberts and Gee, 1985). The gravitational instability of the thickened crust eventually led to collapse and crustal thinning during the Devonian, mainly by reactivation of the original thrusts by normal slip, ductile to brittle crust deformation and important basement thinning with exhumation of deeply buried rocks toward shallow crustal levels (Andersen et al., 1994). The collapse is suggested to have initiated the formation of a series of large Devonian half-graben basins along major faults inherited from the Caledonian orogenic belt. These basins, which are deeper on the Greenland than the Norwegian side, were subsequently filled with thick successions of mainly intra-continental molasse deposits (e.g., Braathen et al., 2002; Hartz and Andresen, 1995; Osmundsen et al., 2002). The extent of gravitational collapse and syn-orogenic extension remain speculative since the mid-Permian-Devonian crustal thickness is difficult to assess with the current available data.

#### 5.4.2. Mid-Permian–Early Triassic

The plate restoration to the mid-Permian shows a good fit between the restored "COB" on the Norwegian and Greenland sides (Figure 17B). NE Atlantic rifting was initiated at mid-Permian following an E-W extensional direction (e.g., Brekke, 2000; Lundin and Doré, 1997). The mid-Permian-early Triassic rifting phase accounts for a total extension ranging between 3 and 113 km with an average of ~40 km. This extensional episode represents

10.1029/2022TC007386

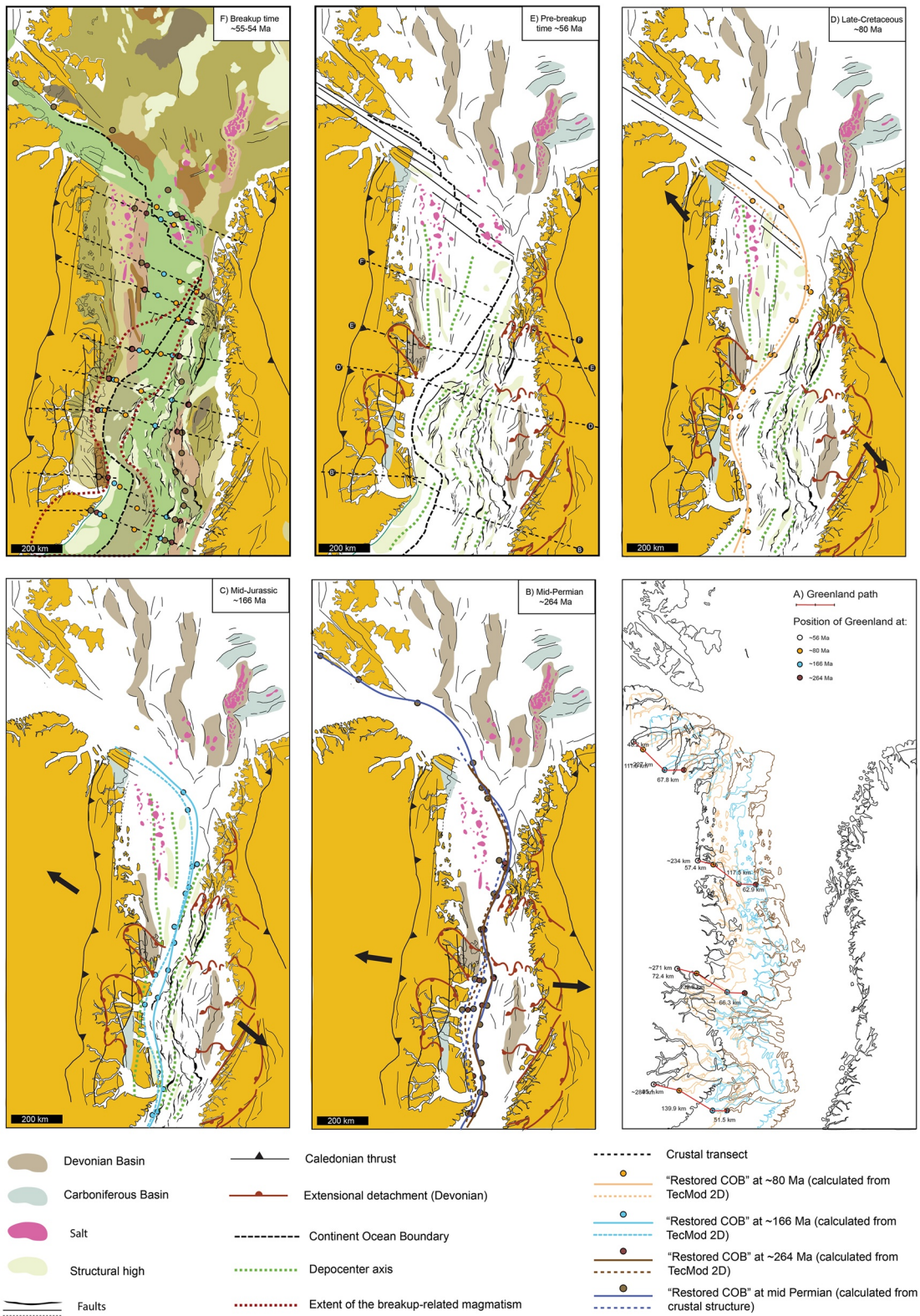


**Figure 17.** Palinspastic plate reconstruction maps of the NE Atlantic realm from breakup until the mid-Permian time. For this manual fitting, we use the pre-drift extension values for the individual rift phases to restore the conjugate NE Atlantic margins. This allows for minimized overlaps and underlaps between "restored continent-ocean boundary" in incremental stages. For each time step we draw the location of the depocenters and structural highs defined by the basin modeling tool and we draw the main structural feature defined by seismic interpretation such as the salt structure and pre-Permian basins.

~32% of the total extension of the NE Atlantic area (Table 4). Most of the mid-Permian extension is located in the Møre/Vøring margin in the south and the NE Greenland margin in the north (Figures 12C and 12D). The location and structural expression of the late Paleozoic NE Atlantic rift system is influenced by Caledonian, and possibly pre-Caledonian structures (e.g., Braathen et al., 2002; Doré et al., 1997). Between Norway and Greenland the rift system followed the NE-oriented Caledonides into the SW Barents Sea, where north-trending structures suggest a structural connection to the Arctic rift system (e.g., Roberts et al., 1999; Skogseid et al., 2000). At the northern NE Greenland and SW Barents Sea areas, several salt diapirs penetrate Mesozoic and Cenozoic layers. The diapirs reach diameters of ~10–15 km and are believed to originate from thick late Paleozoic evaporite sequences like the ones deposited in the deepest parts of the ~8–10-km-deep Sørvestsnaget, Tromsø and Nordkapp basins in the SW Barents Sea (Faleide et al., 1993; Hassaan et al., 2021). The salt diapirs along the NE Greenland and the SW Barents Sea belong to the same large composite basin prior to the mid-Permian extensional episode. Our mid-Permian plate restoration shows a small misfit between the Central East Greenland and the Vøring Margin segments. This could indicate that the COT area in the Central East Greenland margin could comprise continental crust and sedimentary units that unfortunately could not be mapped and characterized precisely.

### 5.4.3. Mid-Jurassic–Mid-Cretaceous

The mid-Jurassic to mid-Cretaceous rifting phase is characterized by NW-SE extensional stress field reflecting the northward propagation of the Central Atlantic spreading during the early Cretaceous. The mid-Jurassic (~166 Ma) plate restoration compensates for the amount of extension derived for this extensional episode (166–110 Ma). The width of the sedimentary basins has, thus, been extended by ~9–138 km with an average of 57 km. This

**Table 4**
*Extension Values (km) and Their Relative Contribution to Three Individual Rift Phases (in Percentage %) for Each Crustal Transect, Computed From Basin Modeling (TecMod2D)*

| Profile | Breakup to mid-Cretaceous extension (km) | Percentage (%) of individual rift phases | Mid-Cretaceous to Mid-Jurassic extension (km) | Percentage (%) of individual rift phases | Early Triassic to mid-Permian extension (km) | Percentage (%) of individual rift phases |
|---|---|---|---|---|---|---|
| | SW Barents Sea and Northern NE Greenland conjugate margin profiles | | | | | |
| H-SW Barents Sea | 43 | 17 | 155 | 60 | 59 | 23 |
| H'-Northern NE Greenland | 52 | 31 | 55 | 33 | 58 | 35 |
| **Average** | 47 | 24 | 105 | 47 | 58 | 29 |
| | NE Atlantic conjugate margin profiles | | | | | |
| G'-NE Greenland thetis | 65 | 32 | 66 | 32 | 74 | 36 |
| G-Northern Lofoten Andøya | 4 | 22 | 13 | 63 | 3 | 16 |
| F'-NE Greenland | 30 | 19 | 76 | 47 | 54 | 34 |
| F-Northern Lofoten | 18 | 25 | 36 | 51 | 17 | 24 |
| E'-NE Greenland Shannon | 8 | 12 | 29 | 45 | 28 | 43 |
| E-Southern Lofoten | 27 | 27 | 43 | 44 | 28 | 29 |
| D'-NE Greenland Foster | 6 | 17 | 9 | 24 | 21 | 59 |
| D-Northern Vøring | 69 | 27 | 119 | 47 | 68 | 26 |
| C'-Trail Ø | 12 | 35 | 11 | 29 | 13 | 36 |
| C-Central Vøring | 61 | 22 | 112 | 40 | 102 | 36 |
| B'- Jameson Land/Jan Mayen | 15 | 26 | 13 | 22 | 31 | 52 |
| B-Central Møre | 47 | 22 | 114 | 53 | 53 | 25 |
| A' Blosseville-Jan Mayen | 72 | 59 | 37 | 30 | 13 | 11 |
| A-Southern Møre | 58 | 28 | 101 | 50 | 45 | 22 |
| Average | 35 | 27 | 56 | 41 | 39 | 32 |

*Note.* For simplification we consider the mid Jurassic-earliest to mid-Cretaceous rift phase as one single phase.

rifting phase represents ~43% of the total extension of the NE Atlantic area. The mid-Jurassic–mid-Cretaceous rifting phase is characterized by considerable crustal extension and thinning (Faleide et al., 1993, 2008; Roberts et al., 1999; Skogseid, 1994), setting the stage for the development of the major Cretaceous basins on the Norwegian continental shelf, SW Barents Sea and Greenland shelf. This rifting phase led to major fault activity with reactivation of older fault zones, which generally created slightly rotated fault blocks and caused subsequent subsidence along major rift systems. The Cretaceous deposits were not uniformly distributed in the conjugate margins. For the Møre/Vøring and their conjugate margin segments, most of the Cretaceous depocenters were located on the Norwegian side while they were situated on the NE Greenland side to the north of the Vøring margin segment (Figure 17C). From the basin modeling result, the total extension in the Møre and Vøring margin segments is larger that farther north. This implies a counterclockwise rotation component when restoring Greenland (Figure 17).

#### 5.4.4. Late Cretaceous-Paleocene

The late Cretaceous-Paleocene rifting phase was dominated by a NNW-SSE extensional direction (Figure 17D). The late Cretaceous (~80 Ma) plate restoration compensates for the amount of extension derived for the rifting phase between 80 and 56 Ma. This extensional episode represents ~25% of the total extension of the NE Atlantic area (Table 4). During the late Cretaceous-Paleocene time (80–56 Ma), most of the deformation is focused toward the location of the COB (Figure 16). At the onset of the late Cretaceous rifting, the area between NW Europe and Greenland was an epicontinental sea covering a region in which the crust had been extensively thinned by previous rift episodes.

#### 5.4.5. Breakup

The breakup and continental separation between Norway and Greenland in the earliest Eocene (56–55 Ma) are characterized by the occurrence of large-scale magmatic activity and volcanism, uplift, erosion and regional low-angle detachment faults (Abdelmalak et al., 2015; Polteau et al., 2020). The distribution of flood basalts, as shown in Figure 1, presumably outlines the regions that both had a high potential for melt generation (e.g., thinnest lithosphere) and had dominantly a subaerial depositional environment during breakup (Abdelmalak, Planke, et al., 2016). Moreover, the orientation of the breakup axis is oblique to the pre-existing Paleozoic/Mesozoic rift structures (Figures 17E and 17F), thus creating a margin asymmetry that does not necessarily reflect the configuration of the pre-breakup rift system (e.g., Gernigon et al., 2020).

## 6. Conclusions

We have quantified the pre-drift extension of the NE Atlantic margins from the mid-Permian to breakup times at early Eocene by utilizing a set of eight 2D conjugate crustal transects that were constructed using an integrated analysis of relevant geophysical and geological data. For each crustal transect we calculated the crustal stretching factors, defined as the ratio between the measured present-day crustal thickness at a given location and an initial reference crustal thickness defining the UCC assumed to be around 35 km. Uncertainties with respect to the exact location of the COB and the contribution from breakup-related igneous intrusions to the observed crustal thicknesses are taken into consideration when calculating the crustal stretching factors. The average stretching factor calculated from observed crustal thickness is used to quantify total pre-drift extension until the mid-Permian time. Along the conjugate transects the total extension is ranging between 180 and 330–390 km with an average of 265–286 km.

For forward basin modeling, we constrained a stratigraphic model for each transect based on 2D/3D seismic interpretation and well data. The corresponding stretching factors derived from forward modeling along each transect provide a total extension ranging between 173 and 312 km with an average of 254 km. The cumulative stretching factors and the pre-drift extension estimates, inferred from the present-day crustal structure, successfully compare to the forward basin modeling values. This allows forward basin modeling to be used as a base to reconstruct the geometrical evolution and the isostatic response of the margin through time.

The basin modeling approach was used to calculate the crustal stretching for each extensional episode where the mid-Permian–early Triassic, the mid-Jurassic–earliest to mid-Cretaceous and the late Cretaceous-Paleocene

extensional episodes account for an average of 32%, 43%, and 25%, respectively, of the cumulative crustal extension in the NE Atlantic margins. These values were used, at first, to establish manual full-fit palinspastic plate kinematic models for the NE Atlantic down to the mid-Permian time taking into consideration the changes of extensional directions through time.

The restoration of the NE Atlantic back to the mid-Permian time shows an alignment of the salt diapirs along the NE Greenland area and the SW Barents Sea which belongs to the same Permian salt basin prior to the initiation of the lithospheric extension. This result supports the validity of our approach. Furthermore, forward basin modeling provides good constraints for the lithospheric extension processes and, hence, on the sedimentary basin configuration since the mid-Permian time which will be the base of more elaborated plate reconstruction models and will be the base for building accurate paleogeographic and tectonic maps.

## Data Availability Statement

All details regarding the seismic reflection/refraction data are provided in Table 1.

**Acknowledgments**

The present work is part of the project titled "the North Atlantic-Arctic tectonics related to the wider Barents Sea paleogeography and basin evolution" funded by the Norwegian Petroleum Directorate (NPD) and Research Centre for Arctic Petroleum Exploration (ARCEx) which was funded by the Research Council of Norway (funding scheme project 228107). The work is also part of CEED-MOD project funded by AkerBP, Lundin and Vår Energi. TecMod 2D is used for the basin modeling purpose. Seismic interpretation was done using the HS Kingdom software. Grid interpolations and map compilations were established using the Geosoft Oasis Montaj and ArcGis software. We acknowledge the support from the Research Council of Norway through its Center of Excellence funding scheme, project 223272 (CEED). G.E.S acknowledges support from the Research Council of Norway's Young Research Talent project scheme (Project number 326238—POLARIS, Evolution of the Arctic in deep time), and The Norwegian Academy of Science and Letters VISTA project 6268 (DEFormation MODelling in the North Atlantic and Arctic). Stéphane Polteau is partly funded by NCS2030 the National Centre for Sustainable Subsurface Utilization of the Norwegian Continental Shelf (Research Council of Norway project 331644). We thank the Editor/associate Editor and anonymous reviewers for their useful comments and suggestions that improved the paper.

## References

Abdelmalak, M. M., Andersen, T. B., Planke, S., Faleide, J. I., Corfu, F., Tegner, C., et al. (2015). The ocean-continent transition in the mid-Norwegian margin: Insight from seismic data and an onshore Caledonian field analogue. *Geology*, *43*(11), 1011–1014. https://doi.org/10.1130/g37086.1

Abdelmalak, M. M., Faleide, J. I., Planke, S., Gernigon, L., Zastrozhnov, D., Shephard, G. E., & Myklebust, R. (2017). The T-reflection and the deep crustal structure of the Vøring Margin offshore mid-Norway. *Tectonics*, *36*(11), 2497–2523. https://doi.org/10.1002/2017tc004617

Abdelmalak, M. M., Meyer, R., Planke, S., Faleide, J. I., Gernigon, L., Frieling, J., et al. (2016). Pre-breakup magmatism on the Vøring margin: Insight from new sub-basalt imaging and results from Ocean Drilling Program Hole 642E. *Tectonophysics*, *675*, 258–274. https://doi.org/10.1016/j.tecto.2016.02.037

Abdelmalak, M. M., Planke, S., Faleide, J. I., Jerram, D. A., Zastrozhnov, D., Eide, S., & Myklebust, R. (2016). The development of volcanic sequences at rifted margins: New insights from the structure and morphology of the Vøring Escarpment, mid-Norwegian margin. *Journal of Geophysical Research: Solid Earth*, *121*(7), 5212–5236. https://doi.org/10.1002/2015jb012788

Ady, B. E., & Whittaker, R. C. (2019). *Examining the influence of tectonic inheritance on the evolution of the North Atlantic using a palinspastic deformable plate reconstruction* (Vol. 470, p. 245). Geological Society, London, Special Publications.

Andersen, T. B., Osmundsen, P. T., & Jolivet, L. (1994). Deep crustal fabrics and a model for the extensional collapse of the southwest Norwegian Caledonides. *Journal of Structural Geology*, *16*(9), 1191–1203. https://doi.org/10.1016/0191-8141(94)90063-9

Barnett-Moore, N., Müller, D. R., Williams, S., Skogseid, J., & Seton, M. (2018). A reconstruction of the North Atlantic since the earliest Jurassic. *Basin Research*, *30*, 160–185. https://doi.org/10.1111/bre.12214

Bergh, S. G., Eig, K., Kløvjan, O. S., Henningsen, T., Olesen, O., & Hansen, J.-A. (2007). The Lofoten-Vesterålen continental margin: A multiphase mesozoic-Palaeogene rifted shelf as shown by offshore-onshore brittle fault-fracture analysis. *Norwegian Journal of Geology/Norsk Geologisk Forening*, *87*, 29– 58.

Berndt, C., Mjelde, R., Planke, S., Shimamura, H., & Faleide, J. I. (2001). Controls on the tectono-magmatic evolution of a volcanic transform margin: The Vøring transform margin, NE-Atlantic. *Marine Geophysical Researches*, *22*(3), 133–152. https://doi.org/10.1023/a:1012089532282

Blischke, A., Gaina, C., Hopper, J. R., Péron-Pinvidic, G., Brandsdóttir, B., Guarnieri, P., et al. (2017). *The Jan Mayen microcontinent: An update of its architecture, structural development and role during the transition from the Ægir ridge to the mid-oceanic Kolbeinsey ridge* (Vol. 447, pp. 299–337). Geological Society, London, Special Publications.

Blischke, A., Stoker, M. S., Brandsdóttir, B., Hopper, J. R., Peron-Pinvidic, G., Ólavsdóttir, J., & Japsen, P. (2019). The Jan Mayen microcontinent's Cenozoic stratigraphic succession and structural evolution within the NE-Atlantic. *Marine and Petroleum Geology*, *103*, 702–737. https://doi.org/10.1016/j.marpetgeo.2019.02.008

Blystad, P., Brekke, H., Færseth, R. B., Larsen, B. T., Skogseid, J., & Tørudbakken, B. (1995). *Structural elements of the Norwegian continental shelf part II: The Norwegian sea region: NPD-bulletin* (Vol. 8). The Norwegian Petroleum Directorate.

Braathen, A., Osmundsen, P. T., Nordgulen, Ø., Roberts, D., & Meyer, G. (2002). Orogen-parallel extension of the Caledonides in northern Central Norway: An overview. *Norsk Geologisk Tidsskrift*, *82*, 225–241.

Brandsdóttir, B., Hooft, E. E. E., Mjelde, R., & Murai, Y. (2015). Origin and evolution of the Kolbeinsey ridge and Iceland plateau, N-Atlantic. *Geochemistry, Geophysics, Geosystems*, *16*(3), 612–634. https://doi.org/10.1002/2014gc005540

Braun, J., & Beaumont, C. (1989). A physical explanation of the relation between flank up lifts and the breakup unconformity at rifted continental margin. *Geology*, *17*(8), 760–764. https://doi.org/10.1130/0091-7613(1989)017<0760:apeotr>2.3.co;2

Breivik, A., Faleide, J. I., Mjelde, R., Flueh, E., & Murai, Y. (2014). Magmatic development of the outer Vøring margin from seismic data. *Journal of Geophysical Research: Solid Earth*, *119*(9), 6733–6755. https://doi.org/10.1002/2014jb011040

Breivik, A. J., Faleide, J. I., Mjelde, R., & Flueh, E. R. (2009). Magma productivity and early seafloor spreading rate correlation on the northern Vøring Margin, Norway—Constraints on mantle melting. *Tectonophysics*, *468*(1–4), 206–223. https://doi.org/10.1016/j.tecto.2008.09.020

Breivik, A. J., Faleide, J. I., Mjelde, R., Flueh, E. R., & Murai, Y. (2017). A new tectono-magmatic model for the Lofoten/Vesterålen Margin at the outer limit of the Iceland Plume influence. *Tectonophysics*, *718*, 25–44. https://doi.org/10.1016/j.tecto.2017.07.002

Breivik, A. J., Mjelde, R., Faleide, J. I., & Murai, Y. (2006). Rates of continental breakup magmatism and seafloor spreading in the Norway Basin–Iceland plume interaction. *Journal of Geophysical Research*, *111*(B7), B07102. https://doi.org/10.1029/2005jb004004

Breivik, A. J., Mjelde, R., Faleide, J. I., & Murai, Y. (2012). The eastern Jan Mayen microcontinent volcanic margin. *Geophysical Journal International*, *188*(3), 798–818. https://doi.org/10.1111/j.1365-246x.2011.05307.x

Breivik, A. J., Mjelde, R., Grogan, P., Shimamura, H., Murai, Y., & Nishimura, Y. (2005). Caledonide development offshore–onshore Svalbard based on ocean bottom seismometer, conventional seismic, and potential field data. *Tectonophysics*, *401*(1), 79–117. https://doi.org/10.1016/j.tecto.2005.03.009

Breivik, A. J., Mjelde, R., Raum, T., Faleide, J. I., Murai, Y., & Flueh, E. R. (2011). Crustal structure beneath the Trøndelag Platform and adjacent areas of the mid-Norwegian margin, as derived from wide-angle seismic and potential field data. *Norweian Journal of Geology*, *90*, 141–161.
Breivik, A. J., Verhoef, J., & Faleide, J. I. (1999). Effect of thermal contrasts on gravity modeling at passive margins: Results from the western Barents Sea. *Journal of Geophysical Research*, *104*(B7), 15293–15311. https://doi.org/10.1029/1998jb900022
Brekke, H. (2000). *The tectonic evolution of the Norwegian Sea continental margin with emphasis on the Vøring and Møre basins* (Vol. 167, pp. 327–378). Geological Society, London, Special Publications.
Brekke, H., Sjulstad, H. I., Magnus, C., & Williams, R. W. (2001). Sedimentary environments offshore Norway—An overview. In J. M. Ole & D. Tom (Eds.), *Norwegian petroleum society special publications* (Vol. 10, pp. 7–37). Elsevier.
Brun, J. P. (1999). Narrow rifts versus wides rifts: Inference for the mechanics of rifting from laboratory experiments. *Philosophical Transactions of the Royal Society of London Series A*, *357*(1753), 695–712. https://doi.org/10.1098/rsta.1999.0349
Brune, S., Heine, C., Clift, P. D., & Pérez-Gussinyé, M. (2017). Rifted margin architecture and crustal rheology: Reviewing Iberia-Newfoundland, central South Atlantic, and South China Sea. *Marine and Petroleum Geology*, *79*, 257–281. https://doi.org/10.1016/j.marpetgeo.2016.10.018
Buck, R. W. (1991). Modes of continental lithospheric extension. *Journal of Geophysical Research*, *96*(B12), 20161–120178. https://doi.org/10.1029/91jb01485
Bullard, E., Everett, J. E., & Smith, A. G. (1965). The fit of the continents around the Atlantic. *Philosophical Transactions of the Royal Society of London Series A: Mathematical and Physical Sciences*, *258*(1088), 41–51.
Bunkholt, H. S. S., Oftedal, B. T., Hansen, J. A., Løseth, H., & Kløvjan, O. S. (2021). *Trøndelag platform and Halten–Dønna Terraces composite tectono-sedimentary element, Norwegian rifted margin, Norwegian sea* (Vol. 57, p. M57-2017-2013). Geological Society, London, Memoirs.
Clark, S. A., Faleide, J. I., Hauser, J., Ritzmann, O., Mjelde, R., Ebbing, J., et al. (2013). Stochastic velocity inversion of seismic reflection/refraction traveltime data for rift structure of the southwest Barents Sea. *Tectonophysics*, *593*, 135–150. https://doi.org/10.1016/j.tecto.2013.02.033
Clark, S. A., Glorstad-Clark, E., Faleide, J. I., Schmid, D., Hartz, E. H., & Fjeldskaar, W. (2014). Southwest Barents Sea rift basin evolution: Comparing results from backstripping and time-forward modelling. *Basin Research*, *26*(4), 550–566. https://doi.org/10.1111/bre.12039
Czuba, W., Ritzmann, O., Nishimura, Y., Grad, M., Mjelde, R., Guterch, A., & Jokat, W. (2005). Crustal structure of northern Spitsbergen along the deep seismic transect between the Molloy Deep and Nordaustlandet. *Geophysical Journal International*, *161*(2), 347–364. https://doi.org/10.1111/j.1365-246x.2005.02593.x
Dinkelman, M. G., Granath, J. W., & Whittaker, J. M. (2010). The NE Greenland continental margin, GEOEXPRO (Vol. *6*).
Domeier, M., & Torsvik, T. H. (2014). Plate tectonics in the late Paleozoic. *Geoscience Frontiers*, *5*(3), 303–350. https://doi.org/10.1016/j.gsf.2014.01.002
Doré, A. G., Lundin, E. R., Fichler, C., & Olesen, O. (1997). Patterns of basement structure and reactivation along the NE Atlantic margin. *Journal of the Geological Society*, *154*, 85–92. https://doi.org/10.1144/gsjgs.154.1.0085
Doré, A. G., Lundin, E. R., Jensen, L. N., Birklamd, Ø., Eliassen, P. E., & Fichler, C. (1999). Principal tectonic events in the evolution of the northwest European Atlantic margin. In *Geological Society, London, Petroleum Geology conference series* (Vol. *5*, pp. 41–61).
Doré, A. G., Lundin, E. R., Kusznir, N. J., & Pascal, C. (2008). *Potential mechanisms for the genesis of Cenozoic domal structures on the NE Atlantic margin: Pros, cons and some new ideas* (Vol. 306, p. 1). Geological Society, London, Special Publications.
Doré, T., & Lundin, E. (2015). Hyperextended continental margins—Knowns and unknowns. *Geology*, *43*(1), 95–96. https://doi.org/10.1130/focus012015.1
Eidvin, T., Bugge, T., & Smelror, M. (2007). The molo formation, deposited by coastal progradation on the inner mid-Norwegian continental shelf, coeval with the Kai formation to the west and the Utsira formation in the North Sea. *Norwegian Journal of Geology*, *87*, 75–142.
Eldholm, O., Gladczenko, T. P., Skogseid, J., & Planke, S. (2000). Atlantic volcanic margins: A comparative study. In A. E. A. NOTTVEDT (Ed.), *Dynamics of the Norwegian margin, volume 167* (pp. 411–428). Geological Society, London, Special Publications.
Eldholm, O., & Grue, K. (1994). North Atlantic volcanic margins: Dimensions and production rates. *Journal of Geophysical Research*, *99*(B2), 2955–2968. https://doi.org/10.1029/93jb02879
Eldhom, O., & Coffin, M. F. (2000). Large igneous provinces and plate tectonics, the history and dynamics of global plate motions (pp. 309–326).
Faleide, J. I., Tsikalas, F., Breivik, A. J., Mjelde, R., Ritzmann, O., Engen, Ø., et al. (2008). Structure and evolution of the continental margin off Norway and the Barents Sea. *Episodes*, *31*(1), 82–91. https://doi.org/10.18814/epiiugs/2008/v31i1/012
Faleide, J. I., Vågnes, E., & Gudlaugsson, S. T. (1993). Late Mesozoic-Cenozoic evolution of the south-western Barents Sea in a regional rift-shear tectonic setting. *Marine and Petroleum Geology*, *10*(3), 186–214. https://doi.org/10.1016/0264-8172(93)90104-z
Fjeldskaar, W., Grunnaleite, I., Zweigel, J., Mjelde, R., Faleide, J. I., & Wilson, J. (2009). Modelled palaeo-temperature on Vøring, offshore mid-Norway—The effect of the lower crustal body. *Tectonophysics*, *474*(3–4), 544–558. https://doi.org/10.1016/j.tecto.2009.04.036
Fossen, H. (2010). *Extensional tectonics in the North Atlantic Caledonides: A regional view* (Vol. 335, pp. 767–793). Geological Society Special Publication.
Fossen, H., Cavalcante, G. C., & de Almeida, R. P. (2017). Hot versus cold orogenic behavior: Comparing the Araçuaí-West Congo and the Caledonian Orogens. *Tectonics*, *36*(10), 2159–2178. https://doi.org/10.1002/2017tc004743
Franke, D., Klitzke, P., Barckhausen, U., Berglar, K., Berndt, C., Damm, V., et al. (2019). Polyphase magmatism during the formation of the northern East Greenland continental margin. *Tectonics*, *38*(8), 2961–2982. https://doi.org/10.1029/2019tc005552
Funck, T., Erlendsson, Ö., Geissler, W. H., Gradmann, S., Kimbell, G. S., McDermott, K., & Petersen, U. K. (2017). *A review of the NE Atlantic conjugate margins based on seismic refraction data* (Vol. 447, pp. 171–205). Geological Society, London, Special Publications.
Funck, T., Geissler, W. H., Kimbell, G. S., Gradmann, S., Erlendsson, Ö., McDermott, K., & Petersen, U. K. (2017). *Moho and basement depth in the NE Atlantic Ocean based on seismic refraction data and receiver functions* (Vol. 447, pp. 207–231). Geological Society, London, Special Publications.
Fyhn, M. B. W., & Hopper, J. R. (2021). *NE Greenland composite tectono-sedimentary element, northern Greenland Sea and Fram strait* (Vol. 57, p. M57-2017-2012). Geological Society, London, Memoirs.
Fyhn, M. B. W., Hopper, J. R., Sandrin, A., Lauridsen, B. W., Heincke, B. H., Nøhr-Hansen, H., et al. (2021). Three-phased latest Jurassic–Eocene rifting and mild mid-Cenozoic compression offshore NE Greenland. *Tectonophysics*, *815*, 228990. https://doi.org/10.1016/j.tecto.2021.228990
Gac, S., Abdelmalak, M. M., Faleide, J. I., Schmid, D. W., & Zastrozhnov, D. (2021). Basin modelling of a complex rift system: The northern Vøring volcanic margin case example. *Basin Research*, *34*(2), 702–726. https://doi.org/10.1111/bre.12637
Gac, S., Klitzke, P., Minakov, A., Faleide, J. I., & Scheck-Wenderoth, M. (2016). Lithospheric strength and elastic thickness of the Barents Sea and Kara Sea region. *Tectonophysics*, *691*, 120–132. https://doi.org/10.1016/j.tecto.2016.04.028
Gaina, C., Blischke, A., Geissler, W. H., Kimbell, G. S., & Erlendsson, Ö. (2017). Seamounts and oceanic igneous features in the NE Atlantic: A link between plate motions and mantle dynamics. In G. Péron-Pinvidic, J. R. Hopper, T. Funck, M. S. Stoker, C. Gaina, J. C. Doornenbal, et al. (Eds.), *The NE Atlantic region. A reappraisal of crustal structure, tectonostratigraphy and magmatic evolution, volume 447*. Geological Society of London.

Gaina, C., Gernigon, L., & Ball, P. (2009). Palaeocene-recent plate boundaries in NE Atlantic and formation of the Jan Mayen microcontinent. *Journal of Geological Society, London*, *166*(4), 601–616. https://doi.org/10.1144/0016-76492008-112

Geissler, W. H., Gaina, C., Hopper, J. R., Funck, T., Blischke, A., Arting, U., et al. (2016). *Seismic volcanostratigraphy of the NE Greenland continental margin* (p. 447) Geological Society, London, Special Publications.

Geoffroy, L. (2005). Volcanic passive margins. *Comptes Rendus Geoscience*, *337*(16), 1395–1408. https://doi.org/10.1016/j.crte.2005.10.006

Gernigon, L., Blischke, A., Nasuti, A., & Sand, M. (2015). Conjugate volcanic rifted margins, sea-floor spreading and microcontinent: Insights from new high-resolution aeromagnetic surveys in the Norway basin. *Tectonics*, *34*, 907–933. https://doi.org/10.1002/2014TC003717

Gernigon, L., Brönner, M., Dumais, M. A., Gradmann, S., Grønlie, A., Nasuti, A., & Roberts, D. (2018). Basement inheritance and salt structures in the SE Barents Sea: Insights from new potential field data. *Journal of Geodynamics*, *119*, 82–106. https://doi.org/10.1016/j.jog.2018.03.008

Gernigon, L., Franke, D., Geoffroy, L., Schiffer, C., Foulger, G. R., & Stoker, M. (2020). Crustal fragmentation, magmatism, and the diachronous opening of the Norwegian-Greenland Sea. *Earth-Science Reviews*, *206*, 102839. https://doi.org/10.1016/j.earscirev.2019.04.011

Gernigon, L., Olesen, O., Ebbing, J., Wienecke, S., Gaina, C., Mogaard, J. O., et al. (2009). Geophysical insights and early spreading history in the vicinity of the Jan Mayen Fracture Zone, Norwegian-Greenland Sea. *Tectonophysics*, *468*(1–4), 185–205. https://doi.org/10.1016/j.tecto.2008.04.025

Gernigon, L., Ringenbach, J.-C., Planke, S., & Jonquet-Kolsto, H. (2003). Extension, crustal structure and magmatism at the outer Vøring Basin, Norwegian margin. *Journal of Geological Society, London*, *160*(2), 197–208. https://doi.org/10.1144/0016-764902-055

Gernigon, L., Ringenbach, J.-C., Planke, S., & Le Gall, B. (2004). Deep structures and breakup along volcanic rifted margins: Insights from integrated studies along the outer Vøring Basin (Norway). *Marine and Petroleum Geology*, *21*(3), 363–372. https://doi.org/10.1016/j.marpetgeo.2004.01.005

Gernigon, L., Zastrozhnov, D., Planke, S., Manton, B., Abdelmalak, M. M., Olesen, O., et al. (2021). A digital compilation of structural and magmatic elements of the mid-Norwegian continental margin (Version 1.0). *Norsk Geologisk Tidsskrift*, *101*(1), 202112. https://doi.org/10.1785/njg101-3-2

Granath, J. W., Whittaker, R. C., Singh, V., Bird, D. E., & Dinkelman, M. G. (2010). Full crustal seismic imaging in northeast Greenland. *Petroleum Geology and Basins*, *28*(11), 79–83. https://doi.org/10.3997/1365-2397.28.11.42810

Granath, J. W., Wittaker, R. G., Dinkelman, M. G., Bird, D. E., & Emmet, P. A. (2011). Long offset seismic refelction data and the crustal structure of the NE Greenland margin. In *Proceedings AGU fall meeting*.

Gresseth, J. L. S., Braathen, A., Serck, C. S., Faleide, J. I., & Osmundsen, P. T. (2022). Late Paleozoic supradetachment basin configuration in the southwestern Barents Sea—Intrabasement seismic facies of the Fingerdjupet Subbasin. *Basin Research*, *34*(2), 570–589. https://doi.org/10.1111/bre.12631

Guarnieri, P., Brethes, A., Rasmussen, T. M., Blischke, A., Erlendsson, Ö., & Bauer, T. (2017). *CRUSMID-3D: Crustal structure and mineral deposit systems: 3D-modelling of base metal mineralization in Jameson land (East Greenland)*. Nordisk Ministerråd.

Haase, C., Ebbing, J., & Funck, T. (2017). *A 3D regional crustal model of the NE Atlantic based on seismic and gravity data* (Vol. 447, pp. 233–247). Geological Society, London, Special Publications.

Hamann, N. E., Whittaker, R. C., & Stemmmerik, L. (2005). Geological development of the northeast Greenland shelf. In A. G. Dore & B. A. Vining (Eds.), *Petroleum geology: North-West Europe and global perspectives—proceedings of the 6th petroleum geology conference, volume 5* (pp. 887–902). London, Geological Society.

Hansen, J.-A., Bergh, S. G., & Henningsen, T. (2011). Mesozoic rifting and basin evolution on the Lofoten and Vesterålen Margin, North-Norway; time constraints and regional implications. *Norwegian Journal of Geology/Norsk Geologisk Forening*, *91*(4), 203–228.

Hartz, E., & Andresen, A. (1995). Caledonian sole thrust of central East Greenland: A crustal-scale devonian extensional detachment? *Geology*, *23*(7), 637–640. https://doi.org/10.1130/0091-7613(1995)023<0637:cstoce>2.3.co;2

Hartz, E. H., Medvedev, S., & Schmid, D. W. (2017). Development of sedimentary basins: Differential stretching, phase transitions, shear heating and tectonic pressure. *Basin Research*, *29*(5), 591–604. https://doi.org/10.1111/bre.12189

Hassaan, M., Inge Faleide, J., Helge Gabrielsen, R., & Tsikalas, F. (2021). Effects of basement structures and Carboniferous basin configuration on evaporite distribution and the development of salt structures in Nordkapp Basin. Barents Sea—Part I. *Basin Research*, *33*(4), 2474–2499. https://doi.org/10.1111/bre.12565

Haupert, I., Manatschal, G., Decarlis, A., & Unternehr, P. (2016). Upper-plate magma-poor rifted margins: Stratigraphic architecture and structural evolution. *Marine and Petroleum Geology*, *69*, 241–261. https://doi.org/10.1016/j.marpetgeo.2015.10.020

Helwig, J., Whittaker, R. C., Dinkelman, M. G., Emmet, P. A., & Bird, D. E. (2012). Interpretation of tectonics of passive margin of NE Greenland from new seismic reflection data and geological—Geophysical constraints. In *Proceedings third central & North Atlantic conjugate margins conference, Trinity College Dublin*.

Henstra, G. A., Gawthorpe, R. L., Helland-Hansen, W., Ravnås, R., & Rotevatn, A. (2017). Depositional systems in multiphase rifts: Seismic case study from the Lofoten margin, Norway. *Basin Research*, *29*(4), 447–469. https://doi.org/10.1111/bre.12183

Hermann, T. (2013). The Northeast Greenland margin tectonic evolution: Vorgelegt dem Rat der Chemisch-Geowissenschaftlichen Fakultät der Friedrich-Schiller-Universität Jena (p. 170).

Holbrook, W. S., Larsen, H. C., Korenaga, J., Dahl-Jensen, T., Reid, I. D., Kelemen, P. B., et al. (2001). Mantle thermal structure and active upwelling during continental breakup in the North Atlantic. *Earth and Planetary Science Letters*, *190*(3–4), 251–266. https://doi.org/10.1016/s0012-821x(01)00392-2

Hosseinpour, M., Müller, R. D., Williams, S. E., & Whittaker, J. M. (2013). Full-fit reconstruction of the Labrador Sea and Baffin Bay. *Solid Earth*, *4*(2), 461–479. https://doi.org/10.5194/se-4-461-2013

Hosseinpour, M., Williams, S., Seton, M., Barnett-Moore, N., & Müller, R. D. (2016). Tectonic evolution of Western Tethys from Jurassic to present day: Coupling geological and geophysical data with seismic tomography models. *International Geology Review*, *58*(13), 1616–1645. https://doi.org/10.1080/00206814.2016.1183146

Jackson, D., Protacio, A., Silva, M., Helwig, J. A., & Dinkelman, M. G. (2013). The North East Greenland Danmarkshavn Basin, GEOEXPRO (Vol. *9*, pp. 60–62).

Jakobsson, M., Mayer, L. A., Bringensparr, C., Castro, C. F., Mohammad, R., Johnson, P., et al. (2020). The International bathymetric chart of the Arctic Ocean version 4.0. *Scientific Data*, *7*(1), 176. https://doi.org/10.1038/s41597-020-0520-9

Kandilarov, A., Mjelde, R., Pedersen, R.-B., Hellevang, B., Papenberg, C., Petersen, C.-J., et al. (2012). The northern boundary of the Jan Mayen microcontinent, North Atlantic determined from ocean bottom seismic, multichannel seismic, and gravity data. *Marine Geophysical Researches*, *33*(1), 55–76. https://doi.org/10.1007/s11001-012-9146-4

Kaus, B. J. P., Connolly, J. A. D., Podladchikov, Y. Y., & Schmalholz, S. M. (2005). Effect of mineral phase transitions on sedimentary basin subsidence and uplift. *Earth and Planetary Science Letters*, *233*(1), 213–228. https://doi.org/10.1016/j.epsl.2005.01.032

Klitzke, P., Faleide, J. I., Scheck-Wenderoth, M., & Sippel, J. (2015). A lithosphere-scale structural model of the Barents Sea and Kara Sea region. *Solid Earth*, *6*(1), 153–172. https://doi.org/10.5194/se-6-153-2015

Kodaira, S., Mjelde, R., Gunnarsson, K., Shiobara, H., & Shimamura, H. (1998). Structure of the Jan Mayen microcontinent and implications for its evolution. *Geophysical Journal International*, *132*(2), 383–400. https://doi.org/10.1046/j.1365-246x.1998.00444.x

Kusznir, N. J., & Park, R. G. (1987). *The extensional strength of the continental lithosphere: Its dependence on geothermal gradient, and crustal composition and thickness* (Vol. 28, pp. 35–52). Geological Society Special Publication.

Kvarven, T., Mjelde, R., Hjelstuen, B. O., Faleide, J. I., Thybo, H., Flueh, E. R., & Murai, Y. (2016). Crustal composition of the Møre Margin and compilation of a conjugate Atlantic margin transect. *Tectonophysics*, *666*, 144–157. https://doi.org/10.1016/j.tecto.2015.11.002

Lebedeva-Ivanova, N., Gaina, C., Minakov, A., & Kashubin, S. (2019). ArcCRUST: Arctic crustal thickness from 3-D gravity inversion. *Geochemistry, Geophysics, Geosystems*, *20*(7), 3225–3247. https://doi.org/10.1029/2018gc008098

Libak, A., Mjelde, R., Keers, H., Faleide, J. I., & Murai, Y. (2012). An integrated geophysical study of Vestbakken Volcanic Province, western Barents Sea continental margin, and adjacent oceanic crust. *Marine Geophysical Researches*, *33*(2), 185–207. https://doi.org/10.1007/s11001-012-9155-3

Lister, J. R., & Kerr, R. C. (1991). Fluid-mechanical models of crack propagation and their application to magma transport in dykes. *Journal of Geophysical Research*, *96*(B6), 10049–10077. https://doi.org/10.1029/91jb00600

Løseth, H., Kyrkjebø, R., Hilde, E., Wild, R. J., & Bunkholt, H. (2017). 500 m of rapid base level rise along an inner passive margin—Seismic observations from the Pliocene Molo Formation, mid Norway. *Marine and Petroleum Geology*, *86*, 268–287. https://doi.org/10.1016/j.marpetgeo.2017.05.039

Lundin, E., & Doré, A. G. (2002). Mid-Cenozoic post-breakup deformation in 'passive' margin bordering the Norwegian-Greenland Sea. *Marine and Petroleum Geology*, *19*(1), 79–93. https://doi.org/10.1016/s0264-8172(01)00046-0

Lundin, E. R., & Doré, A. G. (1997). A tectonic model for the Norwegian passive margin with implications for the NE Atlantic: Early Cretaceous to break-up. *Journal of the Geological Society*, *154*(3), 545–550. https://doi.org/10.1144/gsjgs.154.3.0545

Lundin, E. R., & Doré, A. G. (2005). NE Atlantic break-up: A re-examination of the Iceland mantle plume model and the Atlantic–Arctic linkage. In: *Geological society, petroleum geology conference series* (Vol. *6*, pp. 739–754). https://doi.org/10.1144/0060739

Lundin, E. R., & Doré, A. G. (2011). Hyperextension, serpentinization, and weakening: A new paradigm for rifted margin compressional deformation. *Geology*, *39*(4), 347–350. https://doi.org/10.1130/g31499.1

Mandler, H. A. F., & Jokat, W. (1998). The crustal structure of Central East Greenland: Results from combined land–sea seismic refraction experiments. *Geophysical Journal International*, *135*(1), 63–76. https://doi.org/10.1046/j.1365-246x.1998.00586.x

Maus, S., Barckhausen, U., Berkenbosch, H., Bournas, N., Brozena, J., Childers, V., et al. (2009). EMAG2: A 2-arc min resolution Earth Magnetic Anomaly Grid compiled from satellite, airborne, and marine magnetic measurements. *Geochemistry, Geophysics, Geosystems*, *10*(8), Q08005. https://doi.org/10.1029/2009gc002471

McKenzie, D. P. (1978). Some remarks on the development of sedimentary basins. *Earth and Planetary Science Letters*, *40*(1), 25–32. https://doi.org/10.1016/0012-821x(78)90071-7

Menzies, M. A., Klemperer, S. L., Ebinger, C. J., & Baker, J. (2002). *Characteristics of volcanic rifted margins* (pp. 1–14). Geological Society of America.

Meza-Cala, J. C., Tsikalas, F., Faleide, J. I., & Abdelmalak, M. M. (2021). New insights into the late Mesozoic-Cenozoic tectono-stratigraphic evolution of the northern Lofoten-Vesterålen margin, offshore Norway. *Marine and Petroleum Geology*, *134*, 105370. https://doi.org/10.1016/j.marpetgeo.2021.105370

Mjelde, R., Faleide, J. I., Breivik, A. J., & Raum, T. (2009). Lower crustal composition and crustal lineaments on the Vøring margin, NE Atlantic: A review. *Tectonophysics*, *472*(1–4), 183–193. https://doi.org/10.1016/j.tecto.2008.04.018

Mjelde, R., Kodaira, S., Hassan, R. K., Goldschmidt-Rokita, A., Tomita, N., Sellevoll, M. A., et al. (1996). The continent/ocean transition of the Lofoten volcanic margin, N. Norway. *Journal of Geodynamics*, *22*(3–4), 189–206. https://doi.org/10.1016/0264-3707(96)00016-6

Mjelde, R., Raum, T., Breivik, A., Shimamura, H., Murai, Y., Takanami, T., & Faleide, J. I. (2005). Crustal structure of the Vøring margin, NE Atlantic: A review of geological implications based on recent OBS data. In *Geological Society, London, petroleum geology conference series* (Vol. *6*, pp. 803–813).

Mjelde, R., Raum, T., Digranes, P., Shimamura, H., Shiobara, H., & Kodaira, S. (2003). Vp/vs ratio along the Vøring margin, NE Atlantic, derived from OBS data: Implications on lithology and stress field. *Tectonophysics*, *369*(3–4), 175–197. https://doi.org/10.1016/s0040-1951(03)00198-7

Mjelde, R., Raum, T., Kandilarov, A., Murai, Y., & Takanami, T. (2009). Crustal structure and evolution of the outer Møre Margin, NE Atlantic. *Tectonophysics*, *468*(1–4), 224–243. https://doi.org/10.1016/j.tecto.2008.06.003

Mjelde, R., Raum, T., Murai, Y., & Takanami, T. (2007). Continent-ocean-transitions: Review, and a new tectono-magmatic model of the Vøring plateau, NE Atlantic. *Journal of Geodynamics*, *43*(3), 374–392. https://doi.org/10.1016/j.jog.2006.09.013

Mjelde, R., Sellevoll, M., Shimamura, H., Iwasaki, T., & Kanazawa, T. (1993). Crustal structure beneath Lofoten, N. Norway, from vertical incidence and wide-angle seismic data. *Geophysical Journal International*, *114*(1), 116–126. https://doi.org/10.1111/j.1365-246x.1993.tb01471.x

Mosar, J., Eide, E. A., Osmundsen, P. T., Sommaruga, A., & Torsvik, T. H. (2002). Greenland-Norway separation: A geodynamic model for the North Atlantic. *Norweian Journal of Geology*, *82*, 282–299.

Neres, M., Miranda, J. M., & Font, E. (2013). Testing Iberian kinematics at Jurassic-Cretaceous times. *Tectonics*, *32*(5), 1312–1319. https://doi.org/10.1002/tect.20074

Neumann, E.-R., Svensen, H., Tegner, C., Planke, S., Thirlwall, M., & Jarvis, K. E. (2013). Sill and lava geochemistry of the mid-Norway and NE Greenland conjugate margins. *Geochemistry, Geophysics, Geosystems*, *14*(9), 3666–3690. https://doi.org/10.1002/ggge.20224

Nirrengarten, M., Manatschal, G., Tugend, J., Kusznir, N., & Sauter, D. (2018). Kinematic evolution of the Southern North Atlantic: Implications for the formation of hyperextended rift Systems. *Tectonics*, *37*(1), 89–118. https://doi.org/10.1002/2017tc004495

Osmundsen, P. T., Péron-Pinvidic, G., & Bunkholt, H. (2021). Rifting of collapsed orogens: Successive incision of continental crust in the proximal margin offshore Norway. *Tectonics*, *40*(2), e2020TC006283. https://doi.org/10.1029/2020tc006283

Osmundsen, P. T., Sommaruga, A., Skilbrei, J. R., & Olesen, O. (2002). Deep structure of the mid Norway rifted margin. *Norwegian Journal of Geology*, *82*(4), 205–224.

Ottesen, D., Dowdeswell, J. A., & Rise, L. (2005). Submarine landforms and the reconstruction of fast-flowing ice streams within a large quaternary ice sheet: The 2500-km-long Norwegian-Svalbard margin (57°–80°N). *GSA Bulletin*, *117*(7–8), 1033–1050. https://doi.org/10.1130/b25577.1

Peace, A. L., Welford, J. K., Ball, P. J., & Nirrengarten, M. (2019). Deformable plate tectonic models of the southern North Atlantic. *Journal of Geodynamics*, *128*, 11–37. https://doi.org/10.1016/j.jog.2019.05.005

Peacock, D. C. P., Price, S. P., Whitham, A. G., & Pickles, C. S. (2000). The World's biggest relay ramp: Hold with hope, NE Greenland. *Journal of Structural Geology*, *22*(7), 843–850. https://doi.org/10.1016/s0191-8141(00)00012-2

Peron-Pinvidic, G., Gernigon, L., Gaina, C., & Ball, P. (2012a). Insights from the Jan Mayen system in the Norwegian–Greenland Sea—I. Mapping of a microcontinent. *Geophysical Journal International*, *191*(2), 385–412. https://doi.org/10.1111/j.1365-246x.2012.05639.x

Peron-Pinvidic, G., Gernigon, L., Gaina, C., & Ball, P. (2012b). Insights from the Jan Mayen system in the Norwegian–Greenland Sea—II. Architecture of a microcontinent. *Geophysical Journal International*, *191*(2), 413–435. https://doi.org/10.1111/j.1365-246x.2012.05623.x

Péron-Pinvidic, G., & Manatschal, G. (2008). The final rifting evolution at deep magma-poor passive margins from Iberia-Newfoundland: A new point of view. *International Journal of Earth Sciences*, *98*, 1581–1597. https://doi.org/10.1007/s00531-008-0337-9

Peron-Pinvidic, G., Manatschal, G., & Osmundsen, P. T. (2013). Structural comparison of archetypal Atlantic rifted margins: A review of observations and concepts. *Marine and Petroleum Geology*, *43*, 21–47. https://doi.org/10.1016/j.marpetgeo.2013.02.002

Peron-Pinvidic, G., Osmundsen, P. T., & Bunkholt, H. (2020). The proximal domain of the mid-Norwegian rifted margin: The Trøndelag Platform revisited. *Tectonophysics*, *790*, 228551. https://doi.org/10.1016/j.tecto.2020.228551

Petrov, O., Morozov, A., Shokalsky, S., Kashubin, S., Artemieva, I. M., Sobolev, N., et al. (2016). Crustal structure and tectonic model of the Arctic region. *Earth-Science Reviews*, *154*, 29–71. https://doi.org/10.1016/j.earscirev.2015.11.013

Planke, S., Rasmussen, T., Rey, T., & Myklebust, R. (2005). Seismic characteristics and distribution of volcanic intrusions and hydrothermal vent complexes in the Vøring and Møre basins. In A. G. Doré & B. A. Vining (Eds.), *Petroleum geology: North-West Europe and global perspectives. Proceedings of the 6th petroleum geology conference. Petroleum Geology Conferences Ltd* (pp. 833–844). London, Geological Society.

Polteau, S., Mazzini, A., Hansen, G., Planke, S., Jerram, D. A., Millett, J. M., et al. (2019). The pre-breakup stratigraphy and petroleum system of the Southern Jan Mayen Ridge revealed by seafloor sampling. *Tectonophysics*, *760*, 152–164. https://doi.org/10.1016/j.tecto.2018.04.016

Polteau, S., Planke, S., Zastrozhnov, D., Abdelmalak, M. M., Lebedeva-Ivanova, N., Planke, E. E., et al. (2020). Upper Cretaceous-Paleogene stratigraphy and development of the Mimir High, Vøring transform margin, Norwegian Sea. *Marine and Petroleum Geology*, *122*, 104717. https://doi.org/10.1016/j.marpetgeo.2020.104717

Quirk, D. G., & Rüpke, L. H. (2018). Melt-induced buoyancy may explain the elevated rift-rapid sag paradox during breakup of continental plates. *Scientific Reports*, *8*(1), 9985. https://doi.org/10.1038/s41598-018-27981-2

Ranero, C. R., & Pérez-Gussinyé, M. (2010). Sequential faulting explains the asymmetry and extension discrepancy of conjugate margins. *Nature*, *468*(7321), 294–299. https://doi.org/10.1038/nature09520

Raum, T., Mjelde, R., Digranes, P., Shimamura, H., Shiobara, H., Kodaira, S., et al. (2002). Crustal structure of the southern part of the Vøring Basin, mid-Norway margin, from wide-angle seismic and gravity data. *Tectonophysics*, *355*(1–4), 99–126. https://doi.org/10.1016/s0040-1951(02)00136-1

Raum, T., Mjelde, R., Shimamura, H., Murai, Y., Bråstein, E., Karpuz, R. M., et al. (2006). Crustal structure and evolution of the southern Vøring Basin and Vøring transform margin, NE Atlantic. *Tectonophysics*, *415*(1–4), 167–202. https://doi.org/10.1016/j.tecto.2005.12.008

Ren, S., Faleide, J. I., Eldholm, O., Skogseid, J., & Gradstein, F. (2003). Late Cretaceous–Paleocene tectonic development of the NW Vøring Basin. *Marine and Petroleum Geology*, *20*(2), 177–206. https://doi.org/10.1016/s0264-8172(03)00005-9

Rise, L., Ottesen, D., Berg, K., & Lundin, E. (2005). Large-scale development of the mid-Norwegian margin during the last 3 million years. In A. Solheim, P. Bryn, K. Berg, H. P. Sejrup, & J. Mienert (Eds.), *Ormen Lange—An integrated study for safe field development in the Storegga submarine area* (pp. 33–44). Elsevier.

Ritzmann, O., & Faleide, J. I. (2007). Caledonian basement of the western Barents Sea. *Tectonics*, *26*, 5. https://doi.org/10.1029/2006tc002059

Ritzmann, O., Jokat, W., Czuba, W., Guterch, A., Mjelde, R., & Nishimura, Y. (2004). A deep seismic transect from Hovgård ridge to northwestern Svalbard across the continental-ocean transition: A sheared margin study. *Geophysical Journal International*, *157*(2), 683–702. https://doi.org/10.1111/j.1365-246x.2004.02204.x

Roberts, D., & Gee, D. G. (1985). An introduction to the structure of the Scandinavian Caledonides. In *The Caledonide orogen–Scandinavia and related areas* (Vol. *1*, pp. 55–68).

Roberts, D., Thompson, M., Mitchener, B., Hossack, J., Carmichael, S., & Bjørnseth, H.-M. (1999). Palaeozoic to tertiary rift and basin dynamics: Mid-Norway to the Bay of Biscay—A new context for hydrocarbon prospectivity in the deep water frontier. In *Proceedings Geological Society, London, petroleum geology conference series* (Vol. 5, pp. 7–40). Geological Society of London.

Royden, L., & Keen, C. E. (1980). Rifting process and thermal evolution of the continental margin of eastern Canada determined from subsidence curves. *Earth and Planetary Science Letters*, *51*(2), 343–361. https://doi.org/10.1016/0012-821x(80)90216-2

Rüpke, L. H., Schmalholz, S. M., Schmid, D. W., & Podladchikov, Y. Y. (2008). Automated thermotectonostratigraphic basin reconstruction: Viking Graben case study. *AAPG Bulletin*, *92*(3), 309–326. https://doi.org/10.1306/11140707009

Salomon, E., Rotevatn, A., Kristensen, T. B., Grundvåg, S. A., Henstra, G. A., Meckler, A. N., et al. (2020). Fault-controlled fluid circulation and diagenesis along basin-bounding fault systems in rifts—Insights from the East Greenland rift system. *Solid Earth*, *11*(6), 1987–2013. https://doi.org/10.5194/se-11-1987-2020

Sandwell, D. T., & Smith, W. H. F. (2009). Global marine gravity from retracked Geosat and ERS-1 altimetry: Ridge segmentation versus spreading rate. *Journal of Geophysical Research*, *114*(B1), B01411. https://doi.org/10.1029/2008jb006008

Scheck-Wenderoth, M., Raum, T., Faleide, J. I., Mjelde, R., & Horsfield, B. (2007). The transition from the continent to the ocean: A deeper view on the Norwegian margin. *Journal of the Geological Society*, *164*(4), 855–868. https://doi.org/10.1144/0016-76492006-131

Schiffer, C., Doré, A. G., Foulger, G. R., Franke, D., Geoffroy, L., Gernigon, L., et al. (2020). Structural inheritance in the North Atlantic. *Earth-Science Reviews*, *206*, 102975. https://doi.org/10.1016/j.earscirev.2019.102975

Schlindwein, V., & Jokat, W. (1999). Structure and evolution of the continental crust of northern east Greenland from integrated geophysical studies. *Journal of Geophysical Research*, *104*(B7), 15227–15245. https://doi.org/10.1029/1999jb900101

Schlindwein, V., & Jokat, W. (2000). Post-collisional extension of the East Greenland Caledonides: A geophysical perspective. *Geophysical Journal International*, *140*(3), 559–567. https://doi.org/10.1046/j.1365-246x.2000.00036.x

Schmidt-Aursch, M. C., & Jokat, W. (2005). The crustal structure of central East Greenland—I: From the Caledonian orogen to the tertiary igneous province. *Geophysical Journal International*, *160*(2), 736–752. https://doi.org/10.1111/j.1365-246x.2005.02514.x

Scott, R. A. (2000). Mesozoic-cenozoic evolution of East Greenland: Implications of a reinterpreted continent-ocean boundary location. *Polarforschung*, *68*, 83–91.

Seton, M., Müller, R. D., Zahirovic, S., Gaina, C., Torsvik, T., Shephard, G., et al. (2012). Global continental and ocean basin reconstructions since 200 Ma. *Earth-Science Reviews*, *113*(3–4), 212–270. https://doi.org/10.1016/j.earscirev.2012.03.002

Simon, N. S. C., & Podladchikov, Y. Y. (2008). The effect of mantle composition on density in the extending lithosphere. *Earth and Planetary Science Letters*, *272*(1), 148–157. https://doi.org/10.1016/j.epsl.2008.04.027

Skogseid, J. (1994). Dimensions of the late Cretaceous-Paleocene northeast Atlantic rift derived from Cenozoic subsidence: Tectonophysics. *Tectonophysics*, *240*(1–4), 225–247. https://doi.org/10.1016/0040-1951(94)90274-7

Skogseid, J., Planke, S., Faleide, J. I., Pedersen, T., Eldholm, O., & Neverdal, F. (2000). NE Atlantic continental rifting and volcanic margin formation. In A. E. A. Nøttvedt (Ed.), *Dynamics of the Norwegian margin* (Vol. 167, pp. 295–326). Geological Society, London, Special Publications.

Surlyk, F. (1991). Sequence stratigraphy of the Jurassic-lowermost Cretaceous of East Greenland. *AAPG Bulletin*, *75*(9), 1468–1488.

Theissen, S., & Rüpke, L. H. (2010). Feedbacks of sedimentation on crustal heat flow: New insights from the Vøring Basin, Norwegian Sea. *Basin Research*, *22*(6), 976–990.

Theissen-Krah, S., Zastrozhnov, D., Abdelmalak, M. M., Schmid, D. W., Faleide, J. I., & Gernigon, L. (2017). Tectonic evolution and extension at the Møre Margin—Offshore mid-Norway. *Tectonophysics*, *721*, 227–238. https://doi.org/10.1016/j.tecto.2017.09.009

Torsvik, T. H., Amundsen, H. E. F., Trønnes, R. G., Doubrovine, P. V., Gaina, C., Kusznir, N. J., et al. (2015). Continental crust beneath southeast Iceland. *Proceedings of the National Academy of Sciences*, *112*(15), E1818–E1827. https://doi.org/10.1073/pnas.1423099112

Torsvik, T. H., & Cocks, L. R. M. (2016). *Earth history and palaeogeography*. Cambridge University Press.

Tsikalas, F., Eldholm, O., & Faleide, J. I. (2005). Crustal structure of the Lofoten–Vesterålen continental margin, off Norway. *Tectonophysics*, *404*(3–4), 151–174. https://doi.org/10.1016/j.tecto.2005.04.002

Tsikalas, F., Faleide, J. I., & Eldholm, O. (2001). Lateral variations in tectono-magmatic style along the Lofoten-Vesterålen volcanic margin off Norway. *Marine and Petroleum Geology*, *18*(7), 807–832. https://doi.org/10.1016/s0264-8172(01)00030-7

Tsikalas, F., Faleide, J. I., Eldholm, O., & Antonio Blaich, O. (2012). The NE Atlantic conjugate margins. In D. G. R. W. Bally (Ed.), *Regional geology and tectonics: Phanerozoic passive margins, cratonic basins and global tectonic maps* (pp. 140–201). Elsevier.

Tsikalas, F., Faleide, J. I., Eldholm, O., & Wilson, J. T. (2005). Late Mesozoic-Cenozoic structural and stratigraphic correlation between the conjugate mid-Norway and NE Greenland continental margins. In A. G. Doré, & B. A. Vining (Eds.), *Petroleum geology: North-West Europe and global perspective. Proceedings of the 6th petroleum geology conference* (pp. 785–801). Geological Society, London.

Tsikalas, F., Faleide, J. I., & Kalač, A. (2019). New insights into the Cretaceous-Cenozoic tectono-stratigraphic evolution of the southern Lofoten margin, offshore Norway. *Marine and Petroleum Geology*, *110*, 832–855. https://doi.org/10.1016/j.marpetgeo.2019.07.025

Tsikalas, F., Meza-Cala, J. C., Abdelmalak, M. M., Faleide, J. I., & Brekke, H. (2022). *Lofoten composite tectono-sedimentary element, Norwegian rifted margin, Norwegian sea*. (Vol. 57(1), pp. M57-2021-2043. Geological Society, London, Memoirs.

Tugend, J., Gillard, M., Manatschal, G., Nirrengarten, M., Harkin, C., Epin, M.-E., et al. (2018). *Reappraisal of the magma-rich versus magma-poor rifted margin archetypes* (Vol. 476, pp. SP476–SP479). Geological Society, London, Special Publications.

Turcotte, D. L., & Schubert, G. (2002). *Geodynamics*. Cambridge University Press.

Van Wijk, J. W., & Cloetingh, S. (2002). Basin migration caused by slow lithospheric extension. *Earth and Planetary Science Letters*, *198*(3–4), 275–288. https://doi.org/10.1016/s0012-821x(02)00560-5

Van Wijk, J. W., Huismans, S. R., Ter Voorde, M., & Cloetingh, S. (2001). Melt generation at volcanic continental margin: No need for a mantle plume? *Geophysical Research Letters*, *28*(20), 3995–3998. https://doi.org/10.1029/2000gl012848

Verhoef, J., MacNab, R., Roest, W., & Arkani-Hamed, J. (1996). Magnetic anomalies of the Arctic and North Atlantic oceans and adjacent land areas (GAMM-AA5: Gridded Aeromagnetic and marine magnetics of the North Atlantic and Arctic, 5 km). In *Geological survey of Canada, open file report* (Vol. *3125a*).3125.

Voss, M., & Jokat, W. (2007). Continent–ocean transition and voluminous magmatic underplating derived from *P*-wave velocity modelling of the East Greenland continental margin. *Geophysical Journal International*, *170*(2), 580–604. https://doi.org/10.1111/j.1365-246x.2007.03438.x

Voss, M., & Jokat, W. (2009). From devonian extensional collapse to early Eocene continental break-up: An extended transect of the Kejser Franz Joseph Fjord of the East Greenland margin. *Geophysical Journal International*, *177*(2), 743–754. https://doi.org/10.1111/j.1365-246x.2008.04076.x

Voss, M., Schmidt-Aursch, M. C., & Wilfried, J. (2009). Variations in magmatic processes along the East Greenland volcanic margin. *Geophysical Journal International*, *177*(2), 755–782. https://doi.org/10.1111/j.1365-246x.2009.04077.x

Wangen, M., Mjelde, R., & Faleide, J. I. (2011). The extension of the Vøring margin (NE Atlantic) in case of different degrees of magmatic underplating. *Basin Research*, *23*(1), 83–100. https://doi.org/10.1111/j.1365-2117.2010.00467.x

Watts, A. B., Karner, G. D., & Steckler, M. S. (1982). Lithospheric flexure and the evolution of Sedimentary basins. *Philosophical Transactions of the Royal Society of London Series A: Mathematical and Physical Sciences*, *305*(1489), 249–281.

Weigel, W., Flüh, E. R., Miller, H., Butzke, A., Dehghani, G. A., Gebhardt, V., et al. (1995). Investigations of the East Greenland continental margin between 70° and 72°N by deep seismic sounding and gravity studies. *Marine Geophysical Researches*, *17*(2), 167–199. https://doi.org/10.1007/bf01203425

White, R. S., & Smith, L. K. (2009). Crustal structure of the Hatton and the conjugate east Greenland rifted volcanic margins, NE Atlantic. *Journal of Geophysical Research*, *114*, 1–28. https://doi.org/10.1029/2008JB005856

White, R. S., Smith, L. K., Roberts, A. W., Christie, P. A. F., Kusznir, N. J., & Kusznir, N. J. (2008). Lower-crustal intrusion on the North Atlantic continental margin. *Nature*, *452*(7186), 460–465. https://doi.org/10.1038/nature06687

White, R. S., Spence, G. D., Fowler, S. R., McKenzie, D. P., Westbrook, G. K., & Bowen, A. N. (1987). Magmatism at rifted continental margins. *Nature*, *330*(6147), 439–444. https://doi.org/10.1038/330439a0

Wilson, J. T. (1966). Did the Atlantic close and then re-open? *Nature*, *211*(5050), 676–681. https://doi.org/10.1038/211676a0

Zastrozhnov, D., Gernigon, L., Gogin, I., Abdelmalak, M. M., Faleide, J. I., Planke, S., et al. (2018). Cretaceous-Paleocene evolution and crustal structure of the northern Vøring margin (offshore mid-Norway): Results from Integrated Geological and Geophysical Study. *Tectonics*, *37*(2), 497–528. https://doi.org/10.1002/2017tc004655

Zastrozhnov, D., Gernigon, L., Gogin, I., Planke, S., Abdelmalak, M. M., Polteau, S., et al. (2020). Regional structure and polyphased Cretaceous-Paleocene rift and basin development of the mid-Norwegian volcanic passive margin. *Marine and Petroleum Geology*, *115*, 104269. https://doi.org/10.1016/j.marpetgeo.2020.104269